

A STANDARD TENSILE TESTING PROCEDURE FOR FIBER-REINFORCED
CONCRETE (FRC) AND ULTRA-HIGH-PERFORMANCE
FIBER-REINFORCED CONCRETE (UHP-FRC)
BASED ON DOUBLE PUNCH TEST (DPT)

by

SHUVEKSHA TULADHAR

Presented to the Faculty of the Graduate School of
The University of Texas at Arlington in Partial Fulfillment
of the Requirements
for the Degree of

MASTER OF SCIENCE IN CIVIL ENGINEERING

THE UNIVERSITY OF TEXAS AT ARLINGTON

DECEMBER 2017

Copyright © by Shuveksha Tuladhar 2017

All Rights Reserved



Acknowledgements

I would like to express my sincere gratitude to my advisor, Dr. Shih-Ho Chao for his continuous support, motivation, and guidance for driving me into research for my thesis throughout my Master's program in the University of Texas at Arlington. It would not have been possible without his guidance and priceless advice. I would also like to thank Dr. Suyun Ham and Dr. Xinbao Yu for spending their valuable time serving on my committee.

I would like to thank Bekaert Company for providing steel fibers and Extensometer needed for this research and Mr. Varthan Babakhanian, Technical Services Lab Manager at Forterra Pipe & Precast in Grand Prairie, TX, for providing cement, fly ash and construction materials. I am truly grateful to Ashish Karmacharya for helping me in this research with all the experimental works. I am very much thankful to graduate students Santosh Gurjar, Santosh Maney, Akshay Suryawanshi, Nisarg Patel and Venkata Rahul Chandra for their help in casting and specimen preparation. I would also like to thank all the members of Dr. Chao's research group Venkatesh Babu Kaka, Nga Thuy Phan, Carlos Leyva, Dr. Kyoung-Sub Park, Dr. Hyunsu Seo, Chatchai Jiansinlapadamrong, Young-Jae Choi, Ghassan Almasabha, Ra'ed Al-Mazaidh and Seyed Missagh Shamshiri Guilvayi for the support. I would also like to acknowledge the UTA CELB technician, Mr. Timothy Andrew Kruzic, for the technical support in the lab.

I am greatly indebted to my father Amrit Man Tuladhar, my mother Ramila Tuladhar and my sister Lasata Tuladhar for their cooperation, understanding and moral support during my stay in UTA. My special thanks to Ashish Tamrakar for his unconditional love, support, and encouragement throughout my study. Last but not the least, I would like to extend my deepest gratitude to all my friends for their constant encouragement.

November 20, 2017

Abstract

A STANDARD TENSILE TESTING PROCEDURE FOR FIBER-REINFORCED CONCRETE (FRC) AND ULTRA-HIGH-PERFORMANCE FIBER-REINFORCED CONCRETE (UHP-FRC) BASED ON DOUBLE PUNCH TEST (DPT)

Shuveksha Tuladhar, MS

The University of Texas at Arlington, 2017

Supervising Professor: Shih-Ho Chao

Current test methods such as ASTM 1609, ASTM 1550 and direct tensile test are used for evaluating the mechanical properties of Fiber Reinforced Concrete (FRC) and to determine the quality of mixture in design and construction practice. These test methods show high variability in the results, requires large specimen and complicated test setup. An ideal material test method for FRC should give consistent results in determining mechanical properties such as peak strength and residual strengths. Moreover, current test methods are expensive and time-consuming as more specimens are needed to acquire reliable test results. Double Punch Test (DPT) is a simple, reliable and consistent test method for evaluating the post-cracking behavior of FRC. DPT originally developed to determine the tensile strength of plain concrete, can also be used for evaluation of peak load and post-peak behavior of FRC and Ultra-High-Performance Fiber Reinforced Concrete (UHP-FRC). This method has a simple test setup and is easier to conduct in comparison to other test methods. DPT experimental test results are seen to be more consistent than the other test methods currently in practice. The simplicity of test setup, reliability of results (low scatter due to the higher cracking surface) and smaller specimens (fewer materials used) are the major advantages of using DPT method for evaluation of

post cracking response of FRC and UHP-FRC. In this research, the application of double punch test is validated for FRC and the same method has been used and developed to confirm the suitability for UHP-FRC material in determining tensile strength and behavior in post cracking phase.

However, there still exist some potential issue in the DPT method that needs to be resolved. The circumferential extensometer that is used to determine the total crack opening displacement in DPT is an expensive instrument. This limits the use of DPT method in most of the industrial and research laboratories. The measurement of crack width and inspection of a number of cracks are the important parameter for evaluating the characteristics of any concrete material. It is time-consuming to measure the crack width in a test by conventional visual inspection and automated crack width measurement is indispensable. This research mainly focuses on the deriving a simple formula for estimating average and maximum crack width using the axial deformation data and optimize the time taken for each DPT test. The relation would remove the need of using the expensive circumferential extensometer for the test. Thus, DPT could be used to evaluate and compare the quality of mixture for FRC and UHP-FRC by using a simple arrangement of LVDTs.

Table of Contents

Acknowledgements.....	iii
Abstract	iv
List of Illustrations	x
Chapter 1 Introduction.....	1
1.1 Background	1
1.2 Scope and Objectives	2
1.3 Thesis Organization	3
Chapter 2 Literature Review.....	4
2.1 Overview of FRC	4
2.1.1 Effects of Fiber in Concrete	4
2.1.2 Fiber geometry, distribution, and orientation	5
2.2 UHP-FRC Definition.....	5
2.3 Compressive Properties of UHP-FRC	7
2.4 Tensile Properties FRC and UHP-FRC	9
2.5 Existing Standard Material Test Method for FRC.....	12
2.5.1 ASTM C496 - 2017: Standard Test Method for Splitting Tensile Strength of Cylindrical Concrete Specimens.....	14
2.5.2 ASTM C1609 - 2012 Standard Test Method for Flexural Performance of Fiber-Reinforced Concrete (Using Beam with Third-Point Loading)	15
2.5.3 ASTM C1550 – 2012 Standard Test Method for Flexural Toughness of Fiber Reinforced Concrete (Using Centrally Loaded Round Panel)	20
2.5.4 Uniaxial Direct Tensile Test.....	23

2.6	Comparison of Existing Test Method.....	27
2.7	Introduction to Double Punch Test (DPT)	28
2.8	Theory of Double Punch Test.....	29
2.9	Fracture Mechanics of DPT.....	36
2.10	FEM analysis for DPT	38
2.11	Comparison between DPT and existing test methods.....	42
2.12	Potential issue in DPT.....	45
2.13	Research Objectives.....	46
Chapter 3 Double Punch Test – Experimental Program.....		47
3.1	Experimental Program Overview.....	47
	Phase 1.....	47
	Phase 2.....	50
3.2	Fiber Type and geometry	51
	3.2.1 Phase 1: SFRC.....	51
	3.2.2 Phase 2: UHP-FRC.....	52
3.3	Mix Design.....	53
	3.3.1 SFRC Mix Design	53
	3.3.2 UHP-FRC Mix Design	54
3.4	Formwork for the specimen.....	55
3.5	Mixing of concrete, casting and curing of the specimen.....	56
3.6	Specimen Preparation	59
3.7	Material test and instrumentation	59
	3.7.1 Compressive strength test.....	59
	3.7.2 Direct Tensile Test	64
	3.7.3 Double punch test setup.....	66

3.8	Test procedure of Double Punch Test	69
Chapter 4	Experimental Results	71
4.1	General	71
4.2	Double Punch Test with FRC (Phase 1)	71
4.2.1	Different fiber dosage for FRC.....	72
4.2.2	Determination of relation between deformation and circumferential strain	78
4.2.3	Computation of average crack width:.....	83
4.2.4	Verification from measured maximum crack width	85
4.2.5	Effects of displacement rate	89
4.2.6	Effects of specimen sizes	96
4.2.7	Comparison with Direct Tensile Test	102
4.3	Double Punch Test with UHP-FRC (Phase 2).....	104
4.3.1	Effects of displacement rates and influence of fiber type.....	104
4.3.2	Effects of specimen height	110
4.3.3	Determination of relation between deformation and circumferential strain	114
4.3.4	Computation of average crack width.....	119
4.3.5	Verification from measured maximum crack width	121
4.3.6	Comparison with Direct Tensile Test	124
4.4	Comparison between Double Punch Test (DPT) and Direct Tensile Test (DTT) for FRC and UHP-FRC	125
4.5	Comparison between formula in DPT	127
Chapter 5	Summary and conclusion	130
	Recommendation for DPT:.....	132

Appendix A Detail calculation and graphs for Phase 1	134
Appendix B Detail calculation and graphs for Phase 2	155
Appendix C ASTM Draft Ballot for Standardization of Double Punch Test.....	169
References	184
Biographical Information.....	189

List of Illustrations

Figure 2-1: Compressive stress-strain of UHPC without fibers (Fehling et.al. 2004)	7
Figure 2-2 Compressive stress-strain curve for UHP-FRC (Parham et. al 2016)	8
Figure 2-3 Stress-strain curve for steel fiber reinforced concrete with various type of steel fibers (Shah et. al 1978, ACI Committee 544 [1988])	9
Figure 2-4 Idealized tensile response for UHP-FRC (Greybeal 2014)	10
Figure 2-5: Tensile stress-strain curve of UHP-FRC and multiple cracking (Wille et. al 2011)	11
Figure 2-6: Tensile stress-strain curve of UHP-FRC (Parham et. al 2016).....	11
Figure 2-7 Split Cylinder Test [ASTM C496]	14
Figure 2-8 Three-Point Loading Test Setup (ASTM C1609)	16
Figure 2-9 Typical load vs mid-span deflection relationships for FRC specimen under third-point loading test (first peak load matching the peak load) [ASTM 1609-2012].....	18
Figure 2-10 Typical load vs mid-span deflection relationships for FRC specimen under third-point loading test (first peak load lower than the peak load) [ASTM 1609-2012].....	18
Figure 2-11 (a) Test setup and (b) Specimen (ASTM C1550 - 2012).....	20
Figure 2-12 (a) Specimen (b) Setup (d) Location of major cracks for ASTM C1550 Round Panel Test (Chao 2011)	22
Figure 2-13 Uniaxial Direct Tensile Test	25
Figure 2-14 Formation of crack beyond gauge length and at gripping position	26
Figure 2-15 Double punch test layout	29
Figure 2-16 Bearing Capacity of Double Punch Test (Chen 1970)	30

Figure 2-17 (a) Front view of specimen after cracking (b) Top view of specimen after cracking (Blanco et. al 2014)	33
Figure 2-18 (a) Details of forces at conical block (b) balance of forces at conical block (c) details of forces at the specimen (d) balance of forces at the specimen.	34
Figure 2-19 Simplified σ - ϵ diagram (Blanco et.al 2014)	36
Figure 2-20 (a) DPT with three radial fracture plane (b) DPT with four radial fracture planes (Pros et. al 2011)	38
Figure 2-21 Plan view for principal stress in tension (a) at mid height (b) 1.5 inch above mid-height (Karki 2011).....	39
Figure 2-22 Elevation view for principal stresses in tension (a) at centerline (b) 1.5 inch from center along height (Karki 2011)	39
Figure 2-23 Distribution of stress at various distance from centerline along height of specimen (Karki 2011)	40
Figure 2-24 Distribution of stress at various distance from top of specimen along the diameter of cylinder	41
Figure 2-25 Damage profile for DPT on plain concrete (Pros et. al 2011) (a) Top view (b) Bottom view (c) Inside view.....	42
Figure 3-1: Experimental program	47
Figure 3-2: Experimental program for Phase 1 (FRC).....	48
Figure 3-3: Experimental program for Phase 2 (UHP-FRC)	50
Figure 3-4 Dramix® 5D steel fibers.....	52
Figure 3-5 (a) Micro-straight steel fibers (b) Polyethylene (PE) fibers.....	52
Figure 3-6: Mold for DPT specimens (a) 6 x 12 cylinder (b) 8 x 16 cylinder	55
Figure 3-7 Formwork for Direct Tensile Testing specimen	55
Figure 3-8: Concrete mixing using (a) drum mixer (b) pan mixer	56

Figure 3-9: Mixer used for UHP-FRC (a) Rotating pan mixer (b) Self-loading concrete mixer	57
Figure 3-10: DPT cylinders after casting (a) 6in. x 12in. cylinder (b) 8in. x 16in. cylinder	58
Figure 3-11: DTT specimen (a) During casting (b) After casting	58
Figure 3-12 Preparation of DPT specimen using a concrete saw	59
Figure 3-13: Preparation of 2.78 in. cube for UHP-FRC mix.....	60
Figure 3-14 Compressive strength test of UHP-FRC (2.78 in. cube)	61
Figure 3-15 (a) 4 x 8 in. cylinder after testing for FRC (b) Typical 2.78 in. cube after testing for UHP-FRC (steel fiber) (c) 2.78 in. cube after testing for UHP-FRC (PE fiber).....	61
Figure 3-16 Flow table apparatus in accordance to ASTM C230 (2014).....	62
Figure 3-17 Determination of spread value (flow diameter) in accordance to ASTM C230 (2014) (a) UHP-FRC with steel fiber (b) UHP-FRC with PE fiber.....	62
Figure 3-18: Compressive stress-strain curve for UHP-FRC (at 14 days from Trial mix).....	63
Figure 3-19: Compressive stress-strain curve for UHP-FRC (after 28 days from DPT casting).....	63
Figure 3-20: Dimension of DTT specimen.....	64
Figure 3-21 Direct tensile test (a) UHP-FRC with steel fibers (b) UHP-FRC with PE fibers.....	65
Figure 3-22: Crack location in direct tensile test.....	65
Figure 3-23: Specimen after testing (a) FRC (b) UHP-FRC.....	66
Figure 3-24: DPT test setup for (a) SFRC (b) UHP-FRC	67

Figure 3-25: Dimensions of centering disk and steel punch for 6 inch diameter DPT.....	68
Figure 3-26 (a) Centering disk on specimen (b) centering disk and two punches.	68
Figure 3-27: DPT preparation and testing process.....	70
Figure 4-1 Load vs deformation for different fiber volume fraction	74
Figure 4-2 Tensile stress versus circumferential strain for different fiber volume fraction	74
Figure 4-3: (a) A bottom sample (Set 4) (b) A top sample (Set 1).....	75
Figure 4-4: (a) Crack pattern (Set 2) (b) Crack along the length (Set 4).....	76
Figure 4-5: Bottom and Top specimen (Set 4)	76
Figure 4-6: Load vs. deformation for bottom samples with 0.35% V_f (Set 1)	77
Figure 4-7: Load vs. deformation for top samples with 0.35% V_f (Set 1)	77
Figure 4-8 (a) Typical load vs deformation for FRC (b) Typical tensile stress vs circumferential strain for FRC	78
Figure 4-9: Total Deformation vs circumferential strain	79
Figure 4-10: Post-peak Deformation vs circumferential strain (after peak only)	80
Figure 4-11: δ vs ϵ (before and after peak)	81
Figure 4-12 δ_p vs ϵ_p (after peak only)	81
Figure 4-13: Distribution of values for different fiber dosage	83
Figure 4-14: Post-peak deformation vs maximum crack width (48 samples).....	89
Figure 4-15 Load vs deformation for comparing various displacement rate (0.55% V_f)	91
Figure 4-16 Tensile stress vs circumferential strain for comparing various displacement rate (0.55% V_f).....	92

Figure 4-17 Load vs deformation with V_f of 0.35% for 0.02 in/min and 0.04 in/min rates	94
Figure 4-18 Tensile stress vs circumferential strain with V_f of 0.35% for 0.02 in/min and 0.04 in/min rates	95
Figure 4-19: (a) Crack pattern (b) Specimen (Set 5)	95
Figure 4-20 Load vs deformation for comparing specimen height (0.55% V_f)	99
Figure 4-21 Tensile stress vs circumferential strain for comparing specimen height (0.55% V_f).....	99
Figure 4-22 Load vs deformation for comparing specimen diameter (0.55% V_f)	100
Figure 4-23 Tensile stress vs circumferential strain for comparing specimen diameter (0.55% V_f).....	100
Figure 4-24 Plan view (a) 6 x 6 in. bottom (b) 6 x 4 in. bottom (c) 8 x 8 in. bottom	101
Figure 4-25 Side view (a) 6 x 6 in. bottom (b) 6 x 4 in. bottom (c) 8 x 8 in. bottom	102
Figure 4-26: 6 x 6 in., 6 x 4in. and 8x 8 in. specimen	102
Figure 4-27 Comparison between double punch test and direct tensile test for FRC.....	103
Figure 4-28: Plan view (a) 6x6 in. with steel fiber (b) 6x6 in. with PE fiber	107
Figure 4-29: Side view (a) 6x6 in. with steel fiber (b) 6x6 in. with PE fiber	107
Figure 4-30: Crack pattern (a) UHP-FRC with steel fibers (b) UHP-FRC with PE fibers.....	108
Figure 4-31 Load vs deformation for UHP-FRC with 3% Steel and 0.75% PE fiber and 6x6 specimen.....	109

Figure 4-32 Tensile stress vs circumferential strain for UHP-FRC with 3% Steel and 0.75% PE fiber and 6x6 specimen	109
Figure 4-33 Tested specimen (UHP-FRC)	110
Figure 4-34: Load vs deformation for UHP-FRC with 3% Steel and 0.75% PE fiber for 6x6 and 6x4 specimen	113
Figure 4-35: Tensile stress vs circumferential strain for UHP-FRC with 3% Steel and 0.75% PE fiber for 6x6 and 6x4 specimen	113
Figure 4-36: Plan view (a) 6 x 4 in. (UHP-FRC with steel fibers (b) 6 x 4 in. (UHP-FRC with PE fibers)	114
Figure 4-37: Side view (a) 6 x 4 in. (UHP-FRC with steel fibers (b) 6 x 4 in. (UHP-FRC with PE fibers)	114
Figure 4-38 Typical load vs deformation for UHP-FRC (b) Typical tensile stress vs circumferential strain for FRC	115
Figure 4-39 Typical tensile stress vs circumferential strain for UHP-FRC	115
Figure 4-40: Total Deformation vs circumferential strain (UHP-FRC)	116
Figure 4-41 Post-peak Deformation vs circumferential strain for UHP-FRC (after peak only)	116
Figure 4-42: Post-peak Deformation vs circumferential strain for UHP-FRC with steel and PE fiber (after peak only)	117
Figure 4-43: Determination of α values for UHP-FRC	119
Figure 4-44: Comparison between DPT and DTT for UHP-FRC	124
Figure 4-45: Comparison between peak tensile strength obtained from DPT and DTT	125
Figure 4-46: Tensile stress vs. circumferential strain from DPT for FRC and UHP-FRC	126

Figure 4-47: Comparison between available expression in the literature	128
Figure 4-48: Tensile stress vs. circumferential strain (UHP-FRC with steel fibers) with different stress formulas	128
Figure 4-49: Tensile stress vs. circumferential strain (UHP-FRC with PE fibers) with different stress formulas	129
Figure A-1: Load vs. Deformation - Set 1 (With 0.35% Bottom and Top Cylinders).....	136
Figure A-2:Tensile Stress vs. Circumferential Strain – Set 1 (With 0.35% Bottom and Top Cylinders).....	136
Figure A-3: Post-peak deformation vs. Circumferential Strain – Set 1 (With 0.35% Bottom and Top Cylinders)	137
Figure A-4: Load vs. Deformation – Set 2 (With 0.45% Bottom and Top Cylinders)	139
Figure A-5:Tensile Stress vs. Circumferential Strain – Set 2 (With 0.45% Bottom and Top Cylinders).....	139
Figure A-6: Post-peak deformation vs. Circumferential Strain – Set 2 (With 0.45% Bottom and Top Cylinders)	140
Figure A-7: Load vs. Deformation – Set 3 (With 0.55% Bottom and Top Cylinders)	142
Figure A-8:Tensile Stress vs. Circumferential Strain – Set 3 (With 0.55% Bottom and Top Cylinders).....	142
Figure A-9: Post-peak deformation vs. Circumferential Strain – Set 3 (With 0.55% Bottom and Top Cylinders)	143
Figure A-10: Load vs. Deformation – Set 4 (With 0.75% Bottom and Top Cylinders)	145

Figure A-11: Tensile Stress vs. Circumferential Strain – Set 4 (With 0.75% Bottom and Top Cylinders).....	145
Figure A-12: Post-peak deformation vs. Circumferential Strain – Set 4 (With 0.75% Bottom and Top Cylinders).....	146
Figure A-13: Load vs. Deformation – Set 6 (With 0.35% Bottom and Top Cylinders)	148
Figure A-14: Tensile Stress vs. Circumferential Strain – Set 6 (With 0.35% Bottom and Top Cylinders).....	148
Figure A-15: Load vs. Deformation – Set 7 (With 0.55% Bottom and Top Cylinders and 6x6 in.)	150
Figure A-16: Tensile Stress vs. Circumferential Strain – Set 7 (With 0.55% Bottom and Top Cylinders and 6x6 in.).....	150
Figure A-17: Load vs. Deformation – Set 8 (With 0.55% Bottom and Top Cylinders and 6x4 in.)	152
Figure A-18: Tensile Stress vs. Circumferential Strain – Set 8 (With 0.55% Bottom and Top Cylinders and 6x4 in.).....	152
Figure A-19: Load vs. Deformation- Set 9 (With 0.55% Bottom and Top Cylinders and 8x8 in.)	154
Figure A-20: Tensile Stress vs. Circumferential Strain – Set 9 (With 0.55% Bottom and Top Cylinders and 8x8 in.).....	154
Figure B-1: Load vs. Deformation – Set 10 (With 3% Steel fibers Bottom and Top Cylinders).....	157
Figure B-2: Tensile Stress vs. Circumferential Strain – Set 10 (With 3% steel fibers Bottom and Top Cylinders).....	157

Figure B-3: Load vs. Deformation – Set 11 (With 3% Steel fibers Bottom and Top Cylinders).....	159
Figure B-4:Tensile Stress vs. Circumferential Strain – Set 11 (With 3% steel fibers Bottom and Top Cylinders)	159
Figure B-5: Load vs. Deformation – Set 12 (With 3% Steel fibers Bottom and Top Cylinders)	161
Figure B-6:Tensile Stress vs. Circumferential Strain and Post-peak deformation vs. Circumferential Strain – Set 12 (With 3% steel fibers Bottom and Top Cylinders)	161
Figure B-7: Load vs. Deformation – Set 13 (With 0.75% PE fibers Bottom and Top Cylinders).....	163
Figure B-8:Tensile Stress vs. Circumferential Strain – Set 13 (With 0.75% PE fibers Bottom and Top Cylinders).....	163
Figure B-9: Post-peak deformation vs. Circumferential Strain – Set 13 (With 0.75% PE fiber and 6x6 in.).....	164
Figure B-10: Load vs. Deformation – Set 14 (With 3% Steel fibers 6x4 in. Bottom, Middle and Top Cylinders).....	166
Figure B-11:Tensile Stress vs. Circumferential Strain – Set 14 (With 3% steel fibers 6 x4 in. Bottom, Middle and Top Cylinders).....	166
Figure B-12: Load vs. Deformation – Set 15 (With 0.75% PE fibers 6x4 in. Bottom, Middle and Top Cylinders).....	168
Figure B-13:Tensile Stress vs. Circumferential Strain – Set 15 (With 0.75% PE fibers 6x4 in. Bottom, Middle and Top Cylinders).....	168

List of Tables

Table 2-1: Comparison of typical conventional concrete and UHP-FRC	12
Table 2-2 Net Deflection testing rates (ASTM 1609 - 2012)	16
Table 2-3 Comparison between existing standard test methods (Woods 2012).....	27
Table 2-4 Parameters for simplified model using DPT (Blanco et. al 2014)	35
Table 2-5 Comparison between existing standard test methods with DPT (Woods 2012)	44
Table 2-6 Simplicity, Reliability, and Reproducibility of Current FRC Testing Procedures vs. Double-Punch Test (Woods 2012)	45
Table 3-1 Summary of Specimens for the experimental program for Phase 1.	49
Table 3-2 Experimental program details for Phase 2.....	51
Table 3-3: Fiber type and geometry.....	53
Table 3-4: Mix Proportion by weight for SFRC	53
Table 3-5 : Mix Proportions by weight for UHP-FRC (developed at UTA).....	54
Table 3-6: Test results from direct tensile test.....	64
Table 4-1: Test parameter for FRC with various fiber dosages.....	72
Table 4-2: Comparison of peak load, peak tensile strength and residual tensile strength at 0.3%, 1%, 2.5% and 5% circumferential strain for various fiber volume fraction.....	73
Table 4-3 Comparison of COV for Set 1, 2, 3 and 4 (including top and bottom samples).....	75
Table 4-4: Determination of α	82
Table 4-5: Percentage of samples with respective crack number	85
Table 4-6: Measurement of crack width during experiments for one randomly selected sample from sets of 0.35% and 0.45% V_f	86

Table 4-7: Measurement of crack width during experiments for one selected sample from sets of 0.55% and 0.75% V_f	86
Table 4-8: Relation between deformation and measured maximum crack width (48 samples)	87
Table 4-9: Average values of coefficient λ and β	87
Table 4-10 Comparison for various displacement rate with 0.55% V_f	91
Table 4-11 : Test parameter for FRC with 0.35% fiber volume fraction for rate 0.02 in./min and 0.04 in./min	92
Table 4-12 Comparison of peak load, peak tensile strength and residual tensile strength with 0.35% fiber volume fraction for rate 0.02 in./min and 0.04 in./min	93
Table 4-13 Comparison of COV for Set 1 and Set 6.	94
Table 4-14 Ratio of b/a for 6 in. and 8 in. specimen	96
Table 4-15: Test parameter for FRC with different specimen size	97
Table 4-16 Comparison of peak load, peak tensile strength and residual tensile strength at 0.3% , 1%, 2.5% and 5% circumferential strain for 6 x 6 , 6 x 4 and 8 x 8 specimen.....	98
Table 4-17: Comparison of COV for Set 7, 8 and 9.....	101
Table 4-18 Comparison between double punch test (DPT) and direct tensile test (DTT)	103
Table 4-19 Comparison of testing time for UHP-FRC.....	105
Table 4-20: Test parameter for UHP-FRC with different fiber type	105
Table 4-21: Comparison of peak load, peak tensile strength and residual tensile strength at 0.3%, 1%, 2.5% and 5% circumferential strain for set 10, set 11, set 12 and set 13.	106
Table 4-22 Comparison of COV for set 10, set 11, set 12 and set 13.	106

Table 4-23 Test parameter for UHP-FRC with different specimen size and fiber type	111
Table 4-24: Comparison of peak load, peak tensile strength and residual tensile strength at 0.3% , 1%, 2.5% and 5% circumferential strain for UHP-FRC with 6 x 6 and 6 x 4 specimen.	111
Table 4-25 Comparison of COV for set 11, set 12, set 13 and set 14.	112
Table 4-26: Determination of α for UHP-FRC	118
Table 4-27: Percentage of samples with respective crack number (UHP-FRC with steel and PE fiber).....	121
Table 4-28: Measurement of crack width during experiments for one selected sample from sets of UHP-FRC with steel and PE fibers.	122
Table 4-29: Relation between deformation and measured maximum crack width.....	123
Table 4-30: Average values of coefficient λ and β for the 6x6 specimen and rate 0.04 in./min.	123
Table 4-31 Comparison between double punch test (DPT) and direct tensile test (DTT) for UHP-FRC.....	124
Table 4-32: Difference in peak tensile strength from DPT and DTT.....	126
Table 4-33 Expression for tensile strength using DPT.....	127
Table A-1 Calculation of Coefficient of Variation for set 1 (0.35% V_f).....	135
Table A-2 Calculation of Coefficient of Variation for set 2 (0.45% V_f).....	138
Table A-3 Calculation of Coefficient of Variation for set 3 (0.55% V_f).....	141
Table A-4 Calculation of Coefficient of Variation for set 4 (0.75% V_f)	144
Table A-5 Calculation of Coefficient of Variation for set 6 (0.35% V_f and 0.04 in./min displacement rate).....	147

Table A-6 Calculation of Coefficient of Variation for set 7 (0.55% V_f , 0.04 in./min displacement rate and 6x6 in. size)	149
Table A-7 Calculation of Coefficient of Variation for set 8 (0.55% V_f , 0.04 in./min displacement rate and 6x4 in. size)	151
Table A-8 Calculation of Coefficient of Variation for set 9 (0.55% V_f , 0.04 in./min displacement rate and 8x8 in. size)	153
Table B-1 Calculation of Coefficient of Variation for set 10 (UHP-FRC with 3% steel fiber and 6 x 6 in. size).....	156
Table B-2 Calculation of Coefficient of Variation for set 11 (UHP-FRC with 3% steel fiber and 6 x 6 in. size).....	158
Table B-3 Calculation of Coefficient of Variation for set 12 (UHP-FRC with 3% steel fiber, 0.04 in./min and 6 x 6 in. size)	160
Table B-4 Calculation of Coefficient of Variation for set 13 ((UHP-FRC with 0.75% PE fiber, 0.04 in./min and 6 x 6 in. size).....	162
Table B-5 Calculation of Coefficient of Variation for set 14 (UHP-FRC with 3% steel fiber and 6 x 4 in. size).....	165
Table B-6: Calculation of Coefficient of Variation for set 15 (UHP-FRC with 0.75% PE fiber and 6 x 4 in. size).....	167

Chapter 1

Introduction

1.1 Background

Several methods have been developed to determine the tensile strength of concrete and analyze the post-cracking stage of Fiber Reinforced Concrete (FRC). As of now, there is no standard method to determine tensile strength and characterization of the tensile behavior of Ultra-High-Performance Fiber Reinforced Concrete (UHP-FRC). The various standard methods for the tensile test such as the split cylinder, round panel, third point bending and the customized uniaxial tensile test, are being used for FRC. Non-standard tests for tensile strength of UHP-FRC such as direct tensile test (DTT), notched cylinder or dog-bone shaped specimen, and modified pull off test are being used in the research fields and commercial industry. Among these, the uniaxial direct tension method can more realistically predict the tensile strength and ductile behavior of UHP-FRC. However, there are some limitations and difficulties in performing direct tension test with dog bone specimens which include difficulty in gripping the specimen, complicated test setup, a localized crack formed beyond the gauge length and the inconsistency in crack formation which causes the higher variability in post cracking stages. Moreover, in DTT with notches, the fractures do not always occur at the notch and cannot accurately predict the tensile strength due to local stress concentration caused by the notch.

UHP-FRC is an extrinsic concrete material, the material properties depend on the geometry of its components, methods of casting and alignment, type, distribution and orientation of fiber. Considering these factors, a new easy and candid method is essential for systematic characterization of tensile behavior that is suitable for both SFRC and UHP-FRC. The double punch test has proven to be simple, effective and reliable to determine the tensile strength of SFRC which was originally developed by Chen in 1970. In this

research, the application of double punch test is validated for SFRC and the same method has been used and developed to confirm the suitability for UHP-FRC material in determining tensile strength and behavior in post cracking phase.

Circumferential extensometer, an expensive equipment, limits the application of double punch test as it is not common in most of the laboratories. To make the test simpler, an alternative measuring procedure was proposed by Malatesta et.al (2012) by determining the theoretical relationship between axial displacement and total crack opening displacement (TCOD) to evaluate the FRC toughness. However, the correlations proposed are only valid for axial displacement ranging from 1 mm to 4 mm and are empirical. Blanco et. al (2014) proposed another formulation to estimate the stress and associated strain using physical mechanism involved in the tensile failure. The analytical formulation requires a reliable value of kinetic friction coefficient and the strain values are predefined. A simpler form of the relationship between axial displacement and strain is of prime importance.

1.2 Scope and Objectives

Double-Punch Test characterizes the elastic and inelastic behavior (toughness) of fiber-reinforced concrete composites better than current testing procedures for FRC. It has been proved that this method is very suitable for the systematic control of the tensile behavior of FRC (Mollins et.al. 2009, Chao et. al 2011, Pujadas et.al. 2012, Blanco et.al 2014). The main objectives of this study are:

1. To develop simple and reliable test protocols by comparing the influence of fiber volume fractions for FRC and UHP-FRC.
2. To assess the suitability of DPT method for UHP-FRC material in determining tensile strength and behavior in post cracking phase.

3. To determine the relation between axial deformation and circumferential strain using double punch test method applicable to FRC and UHP-FRC.
4. To derive a simple formula to estimate the average crack width.

1.3 Thesis Organization

The thesis is divided into six chapters that are summarized below

Chapter 1 provides an introduction, presents the research scope and objectives of the study.

Chapter 2 presents the literature review on the importance of tensile testing and the different existing standard tensile testing methods for FRC. This chapter also describes the details of double punch method that includes theory, fracture mechanics, and test procedure.

Chapter 3 mainly focuses on the details of the experiment for developing a simple and reliable test method for FRC and UHP-FRC. This chapter also describes the mix design used, preparation of specimen, instrumentation, test setup and the potential issue of the DPT method.

Chapter 4 summarizes the test results obtained from the study. The results have been used to formulate an equation to calculate the average crack width.

Chapter 5 includes the summary of this experimental investigation and conclusion are presented in this chapter.

Chapter 2

Literature Review

2.1 Overview of FRC

The plain concrete is relatively brittle and has tensile strength typically only about one-tenth of its compressive strength. It is alluring to reinforce the concrete with randomly distributed small fibers instead of normally reinforced with steel reinforcing bars for different applications. However, fiber reinforcement is not a substitute for conventional steel reinforcement as fibers and reinforcing bars play different roles in concrete. Reinforcing bars are used to increase the load-bearing capacity of structural concrete elements while fibers are more effective for crack control. The various types of fiber are used in the commercial industry such as steel, glass, synthetic, polypropylene, asbestos, organic and carbon. The steel fibers are the most commonly used for various structural and nonstructural applications. It has been observed that the steel fibers can improve the structural strength, reduce the reinforcement requirements and can improve explosive spalling of concrete.

2.1.1 Effects of Fiber in Concrete

The fibers are mainly used in concrete to control crack and shrinkage that enhances the durability of concrete. They are also used to increase the energy absorption capacity (toughness) of the material, and also increase the tensile and flexural strength of concrete. There is considerable improvement in the mechanical properties of the concrete mix in terms of post-cracking strength, toughness, and ductility compared to plain concrete due to the addition of steel fibers.

2.1.2 *Fiber geometry, distribution, and orientation*

The geometry, type, and distribution are the key parameters for the evaluation of performance and efficiency of FRC. The efficiency of fiber reinforcement is based on the enhancement of strength and toughness of composite matrix. The effects depend upon the fiber length, the orientation of fibers and fiber-matrix bond strength. It is assumed that the fibers are uniformly distributed throughout the concrete matrix and are randomly oriented. The orientation of fiber relative to the plane of a crack in concrete influences the reinforcing capacity of the fiber.

2.2 UHP-FRC Definition

Ultra-high performance fiber-reinforced concrete (UHP-FRC) is an advanced reinforced cementitious material, with improved mechanical properties, fractural toughness, and durability properties compared to normal or high-performance concrete. According to Rossi (2000, 2008), UHPC can be defined as a concrete or cementitious composite with a relatively high binder ratio, a water to the cementitious ratio (w/c) less than 0.2, and compressive strength of more than 21.8 ksi (150 MPa). The ACI Concrete Terminology defines UHPC as “*concrete that has a minimum specified the compressive strength of 22 ksi (150 MPa) with specified durability, tensile ductility, and toughness requirements; fibers are generally included to achieve specified requirements*” (ACI Committee 239).

According to the French Recommendations on UHP-FRC (AFGC 2013), UHP-FRC is a material with a cement matrix having

- A characteristic compressive strength more than 21.8 ksi (150 MPa) and a maximum of 36.3 ksi (250 Mpa).

- Sufficient fiber content to achieve ductile behavior under tension, with high post-cracking tensile strength.
- Highbinder content which decreases capillary porosity that improves the durability of the fibers inside UHP-FRC.

The *main characteristics* of UHP-FRC are achieved through the following three principles (Richard and Cheyrezy 1995):

- i. *Homogeneity enhancement* by eliminating coarse aggregates in the matrix,
- ii. *Density enhancement* by optimizing the packing density of the matrix. This is achieved by optimizing gradation and mix proportions between the main matrix constituents.
- iii. *Ductility enhancement* by the introduction of fibers. As the matrix is very brittle, fiber reinforcement is added to obtain elastic-plastic or strain-hardening behavior in tension.

Typically, UHP-FRC has fiber contents of more than 2-3 % by volume. The maximum fiber content is a function of the fiber aspect ratio and fiber shape as well as production issues such as workability.

The UHP-FRC mixture design used in this research is a proprietary product developed at the University of Texas at Arlington (Aghdasi et al., 2015). The UHP-FRC mix design was developed using a dense particle-packing concept without any special material, mixing, or treatment and has a compressive strength of 25-30 ksi (207 MPa). All the materials used are locally available in the U.S. market. The research has proven a much higher strength and ductility than conventional concrete or ultra-high-performance concrete.

2.3 Compressive Properties of UHP-FRC

UHPC without fibers: Unlike conventional concrete and high-performance concrete, UHPC does not have a distinctive mix proportion so the mechanical properties of UHPC depend on the composition of the mix. The increase in compressive strength can be attributed to selection of specific components and dense particle packing concept. Typically, UHPC mix without fibers has a characteristic compressive strength of higher than 22 ksi (150 MPa), with a high modulus of elasticity in the range of 6,500 ksi to 8,000 ksi (45 GPa to 55 GPa) and exhibiting extremely brittle failure after peak strength. Due to the explosive failure after peak compressive strength, the descending curve cannot be recorded. It has been observed with the increase in compressive strength in UHPC, brittleness in UHPC increases as well. This has already been experimental observed in conventional and high-strength concretes. The higher modulus of elasticity of UHPC is due to increased density of the hardened cement paste. Figure 2-1 shows the compressive stress-strain curve of UHPC without fibers. (Fehling et.al 2004)

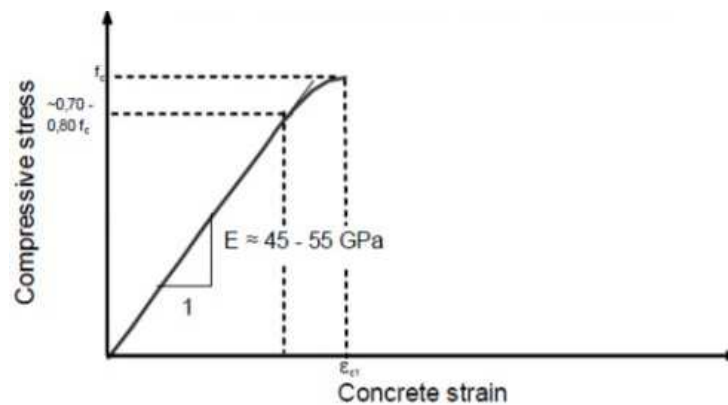


Figure 2-1: Compressive stress-strain of UHPC without fibers (Fehling et.al. 2004)

UHPC with fibers: Addition of fibers to the matrix decreases the brittleness and increases the maximum useable compressive strain. Addition of fibers slightly increases the compressive strength. With the addition of fibers up to 4% by volume fraction

compressive strength increased by 5 – 10% [Nielson, 1995 and Behloul, 1996]. Compared to UHPC without fibers, a matrix with fibers have more noticeable non-linear behavior before the peak compressive strength. Compressive stress-strain relations presented by different researchers in Figure 2-2 has shown that the compressive strength is attained at a compressive strain of 0.35 – 0.5%. Whereas mix presented by Parham et al., 2016 reached an ultimate compressive strength at a strain range of approximately 1.2 – 1.4%. Post-peak behavior is affected by several reasons attributing to fiber content, fiber type and distribution and size of the specimen. Figure 2-2 shows compressive stress-strain behavior of different UHP-FRC mixes and mix developed at UTA research (Parham et al., 2016).

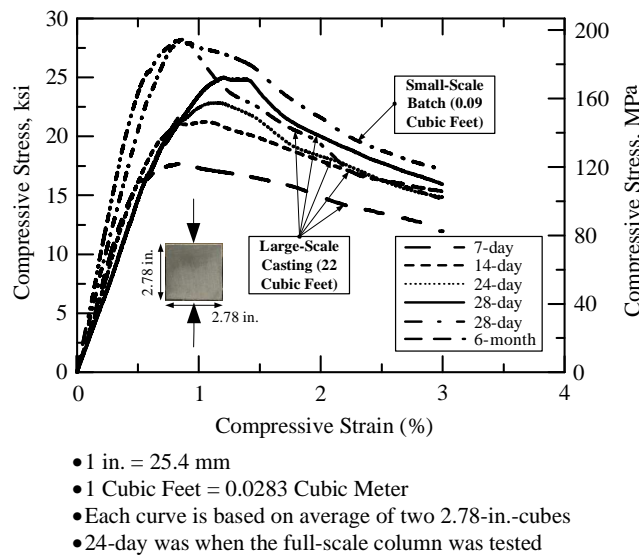


Figure 2-2 Compressive stress-strain curve for UHP-FRC (Parham et. al 2016)

2.4 Tensile Properties FRC and UHP-FRC

The tensile properties of concrete are an important parameter for understanding the behavior of the concrete member. These properties are utilized in analysis and design of structural member. It is generally known that conventional concrete is weak in tension, and the tensile strength of conventional concrete is generally about 1/10 to 1/12 of their compressive strength. Hence, the tensile strength of conventional concrete is considerably influenced by the fracture strength of the matrix. It is very difficult to assess the tensile behavior of FRC as standard test methods are not available to date and in order to evaluate the fiber distribution in real structures, sufficiently large specimen should be assessed. From the Direct Tensile Test (DTT), the results obtained are scattered and it is difficult to grip the large specimen. Figure 2-3 shows an example of a stress-strain curve for steel fiber reinforced concrete with a straight, hooked and enlarged type of steel fibers resulted from the Direct Tensile Test (Shah et.al. 1978, ACI Committee 544 [1988]).

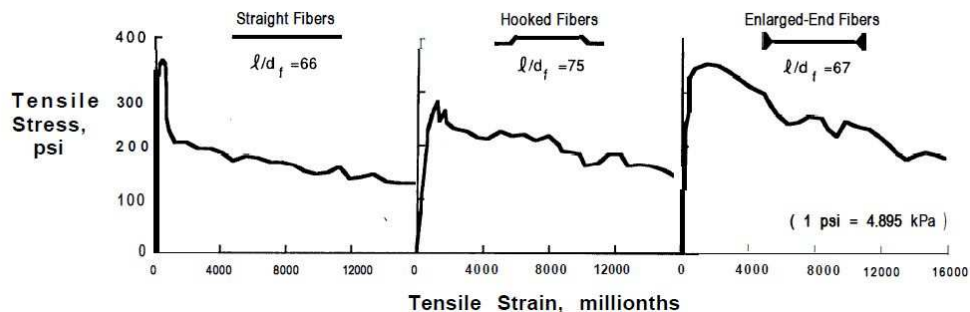


Figure 2-3 Stress-strain curve for steel fiber reinforced concrete with various type of steel fibers (Shah et. al 1978, ACI Committee 544 [1988])

Since the UHP-FRC mixes have very high compressive strengths compared to conventional concrete (nearly 5 times), the tensile strength of UHP-FRC matrix is also presumed to be higher. The addition of fibers in UHP-FRC mix helps in redistribution of tensile stresses after the initial cracking, resulting in strain hardening after the first cracking.

The idealized tensile mechanical response for UHP-FRC based on tensile responses observed during the development of direct tension method (Greybeal 2014) is shown in Figure 2-4. The multiple cracking may occur before the pullout of fiber reinforcement bridging in an individual crack.

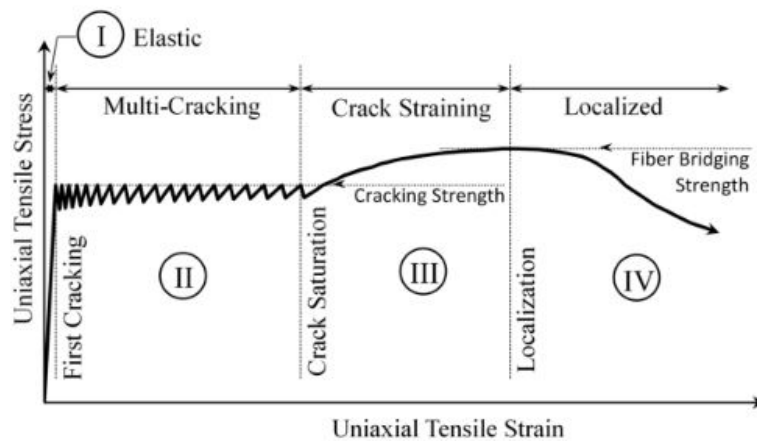


Figure 2-4 Idealized tensile response for UHP-FRC (Greybeal 2014)

Tensile behavior of UHP-FRC investigated by other researchers was based on small-scale specimens with cross-sectional area of 2.0 in.² (1,290 mm²) [Wille et al., 2011, 2012], 0.59 in.² (381 mm²) [Ranade et al., 2013] and 16.0 in.² (10,323 mm²) [Parham et al., 2016]. Wille et al. (2011) reported a tensile strength of 2.9 ksi (20 MPa) at a strain value at peak tensile stress of 0.6% with a 3% volume fraction of straight steel fibers. Ranade et al. (2013) reported a tensile strength of 2.1 ksi (14.5 MPa) at a strain value at peak tensile stress of 3.4% with a 2% volume fraction of ultra-high-molecular-weight poly-ethylene fibers. Furthermore, Parham et al. (2016) reported a tensile strength of 1.21 ksi (8.3 MPa) at a strain value with a peak stress of 0.17% with a 3% volume fraction of micro-short steel fibers. Figure 2-5 and Figure 2-6 are the tensile stress strain curve UHP-FRC (Wille et. al. 2011 and Parham et.al. 2016 respectively).

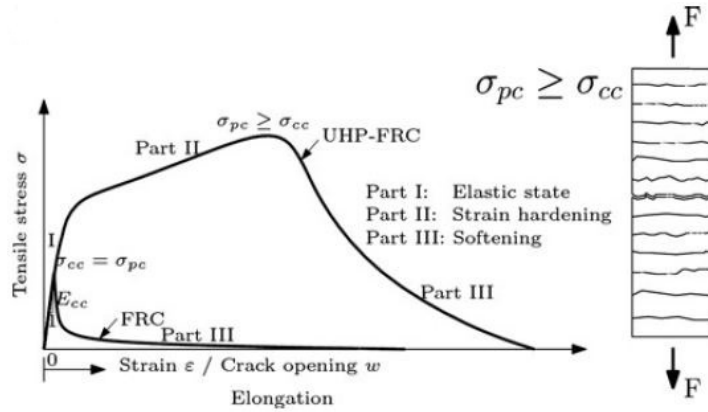


Figure 2-5: Tensile stress-strain curve of UHP-FRC and multiple cracking (Wille et. al 2011)

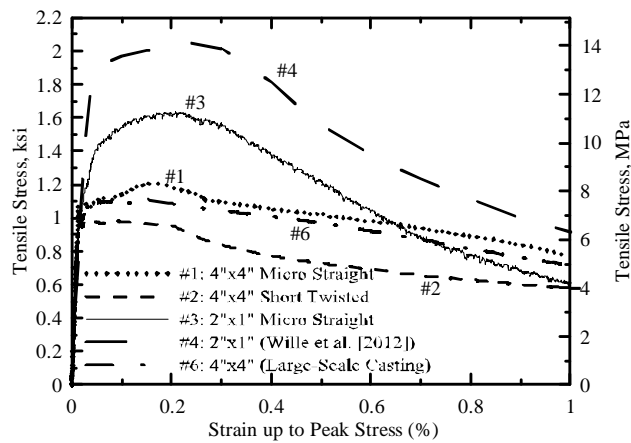


Figure 2-6: Tensile stress-strain curve of UHP-FRC (Parham et. al 2016)

The comparison of typical conventional concrete and UHP-FRC are presented in Table 2-1. UHP-FRC has very high compressive strength about 18 to 30 ksi which 5 times higher than conventional concrete. UHP-FRC also has higher early compressive strength. UHP-FRC is more better in comparison to conventional concrete in terms of flexural strength, shear strength and also in direct tension. UHP-FRC has very high ductility and has high confining capability.

Table 2-1: Comparison of typical conventional concrete and UHP-FRC

Properties of Concrete	Conventional Concrete	UHP-FRC
Ultimate Compressive Strength	< 8,000 psi (55 MPa)	18,000 to 30,000 psi (124 to 207 MPa)
Early (24-hour) compressive strength	< 3000 psi (21 MPa)	10,000 – 12,000 psi (69 to 83 MPa)
Flexural Strength	< 670 psi (4.6 MPa)	2,500 to 6,000 psi (17 to 41 MPa)
Shear strength	< 180 psi (1.2 MPa)	> 600 psi (4.1 MPa)
Direct Tension	< 450 psi (3 MPa)	up to 1,450 psi (10 MPa)
Rapid Chloride Penetration Test	2000-4000 Coulombs passed	Negligible (< 100 Coulombs passed)
Ductility	Negligible	High ductility
Ultimate Compressive Strain, ϵ_{cu}	0.003	0.015 to 0.03
Confining	Negligible	High confining capability

2.5 Existing Standard Material Test Method for FRC

The fiber-reinforced concrete (FRC) composites can be produced using the same equipment and procedures as for plain concrete. The evaluation of the mechanical properties of FRC is essential to determine the effectiveness and the economical use in design and construction practice. However, the properties of the composite are much more dependent on the presence, proportion, distribution, and properties of the fiber phase as well as the fiber matrix interactions. These characteristics must be evaluated by test methods sensitive to the addition of fibers and capable of reflecting the composite behavior which is generally undetectable by methods intended for standard concrete mix designs. An ideal material test method for FRC needs to account for many factors. According to Mindess, Young and Darwin (2003), it has been recommended that the toughness or residual strength parameters should satisfy the following criteria obtained from FRC material tests as:

1. It should have a physical meaning that is both readily understandable and of fundamental significance if it is to be used in the specification or quality control.
2. The “end-point” used in the calculation of the toughness parameters should reflect the most severe serviceability conditions anticipated in the particular application.
3. The variability inherent in any measurement of concrete properties should be low enough to give acceptable levels of both within-batch and between-laboratory precision.
4. It should be able to quantify at least one important aspect of FRC behavior (e.g. strength, toughness, or crack resistance) and should reflect some characteristics of the load vs. deflection curve itself.
5. It should be as independent as possible of the specimen size and geometry.

The various test methods have been developed to evaluate the performance characteristics of FRC in a way that satisfies the above criteria. A few have been refined and published by national and international agencies such as the American Society for Testing and Materials (ASTM), the European Federation of National Associations of Specialist Representing Concrete (EFNARC), the International Union of Laboratories and Experts in Construction Materials, Systems, and Structures (RILEM) and the Japan Society of Civil Engineers (JSCE) and some of the test methods are privately used by fiber producers or in research fields only.

2.5.1 ASTM C496 - 2017: Standard Test Method for Splitting Tensile Strength of Cylindrical Concrete Specimens

The splitting tensile test method is used for the determination of the splitting tensile strength of cylindrical concrete specimens, such as molded cylinders and drilled cores (ASTM C496-2017). A compressive force along the diametrical length of a 4 x 8-in. [100 x 200-mm] cylindrical concrete specimen until failure occurs in which cylinder splits across the vertical diameter. This failure occurs in tension instead of compression as the load application is in a state of triaxial compression. A thin plywood bearing strips are used to distribute the applied load along the length of the cylinder as shown in Figure 2-7.

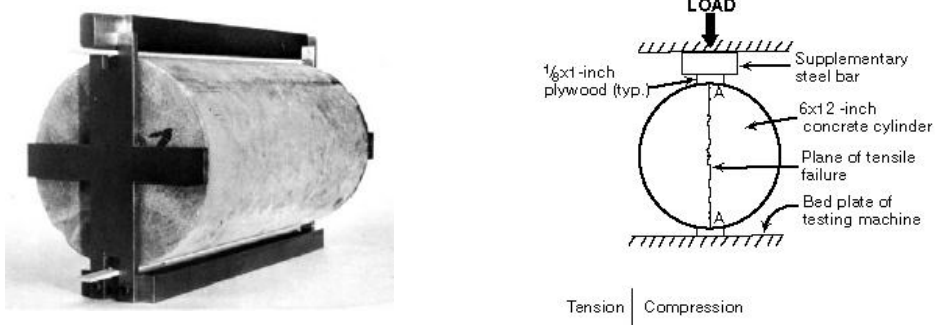


Figure 2-7 Split Cylinder Test [ASTM C496]

The splitting tensile strength of specimen (ASTM C496 2017) can be calculated as:

$$T = \frac{2P}{\pi ld}$$

where,

T = splitting tensile strength, psi [MPa]

P = maximum applied load measured by the testing machine, lbf [N]

l = length, in. [mm]

d = diameter, in. [mm]

The splitting tensile strength is a good indicator of tensile capacity and correlates well with the performance of conventional concrete structures stressed in tension (ASTM C496 2017). However, the major drawback of this test is as the cylinder is loaded in a predetermined position, failure occurs at that predetermined plane. This method is not suitable for FRC as fibers are randomly oriented and distributed within a given concrete specimen. The probability that crack plane will coincide with the plane of a sample of fiber content is very low. Moreover, there is no guarantee that the fibers will be oriented perpendicular to the crack plane and consequently, the true properties of the material obtained may not be accurate. ASTM C496 does not provide the means of obtaining load-deflection curve and cannot be used comparing post tensile behavior for the different types of fibers and volume fractions except only for ultimate tensile capacity.

2.5.2 ASTM C1609 - 2012 Standard Test Method for Flexural Performance of Fiber-Reinforced Concrete (Using Beam with Third-Point Loading)

This test method is used to evaluate the flexural performance of FRC using parameters derived from the load-deflection curve obtained by testing a simply supported beam using a closed-loop, servo-controlled testing system. The specimen size of 4 x 4 x 14-in. [100 x 100 x 350-mm] beam tested on a 12-in. [300-mm] span, or 6 x 6 x 20-in. [150 x 150 x 500-mm] beam tested on an 18-in. [450-mm] span is preferred in this method. Figure 2-8 shows a third point loading test setup consisting of two hinged support and two loading points on the top. To ensure an actual reading of the deflection at the mid-span, a rectangular jig is used which is placed on the neutral axis of the beam directly over the supports and surrounds the beam. For measuring the deflection of the beam at the mid-span, LVDTs are placed on both sides of the beam as in Figure 2-8. This test setup helps

in minimizing the errors which are caused by twisting or seating in the supports to the concrete specimen.

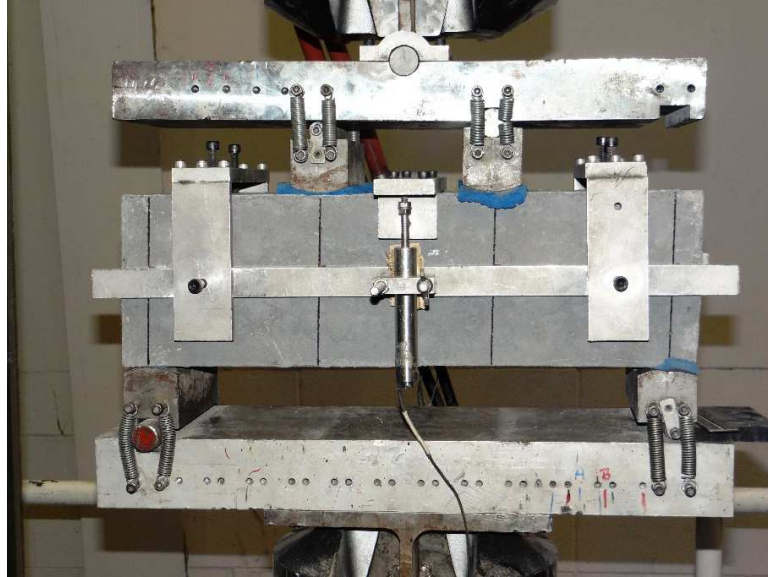


Figure 2-8 Three-Point Loading Test Setup (ASTM C1609)

The test is operated at a specified net deflection rate and run until a net deflection reaches $L/600$ (considering L to be the span distance between supports). After that net deflection, it can be operated at a higher specified net deflection rate until the test's specified endpoint (Table 2-2).

Table 2-2 Net Deflection testing rates (ASTM 1609 - 2012)

Beam Size	Up to net deflection of $L/900$	Beyond net deflection of $L/900$
100 x 100 x 350 mm [4 x 4 x 14 in.]	0.025 to 0.075 mm/min [0.001 to 0.002 in./min]	0.05 to 0.20 mm/min [0.002 to 0.008 in./min]
150 x 150 x 500 mm [6 x 6 x 20 in.]	0.035 to 0.10 mm/min [0.0015 to 0.004 in./min]	0.05 to 0.30 mm/min [0.002 to 0.012 in./min]

The data from ASTM C1609 can be obtained as the first peak strength, the peak strength, the residual strength at L/600, the residual strength at L/150, and the toughness, which is the area under the load versus net deflection curve from 0 to L/150 (Figure 2-9). The flexural strengths of the tested specimens at various stages; first peak load, the peak load, and the residual load (at deflections of L/600 and L/150); can be calculated as follows;

$$f = \frac{PL}{bd^2}$$

Where,

f = the flexural strength, psi

P= the load, lbf.

L= the span length, inches

b= the average width of the specimen at fracture, as oriented for testing,
inches

d= the average depth of the specimen at the fracture, as oriented for testing,
inches

In Figure 2-10, the first peak load (P_1) corresponds to the first point at which the load-deflection curve has a zero slope. For the load-deflection curve shown in Figure 2-9, P_1 and P_p lie at the same point. Similarly, the peak load (P_p) is the largest load on the load-deflection curve. When there is an existence of both first peak load and peak load, the first curve is used and when first peak load and second peak load is same, the second curve is used.

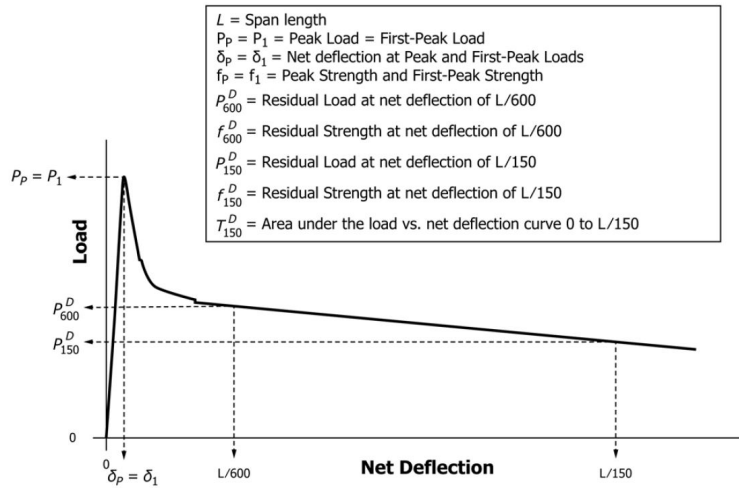


Figure 2-9 Typical load vs mid-span deflection relationships for FRC specimen under third-point loading test (first peak load matching the peak load) [ASTM 1609-2012]

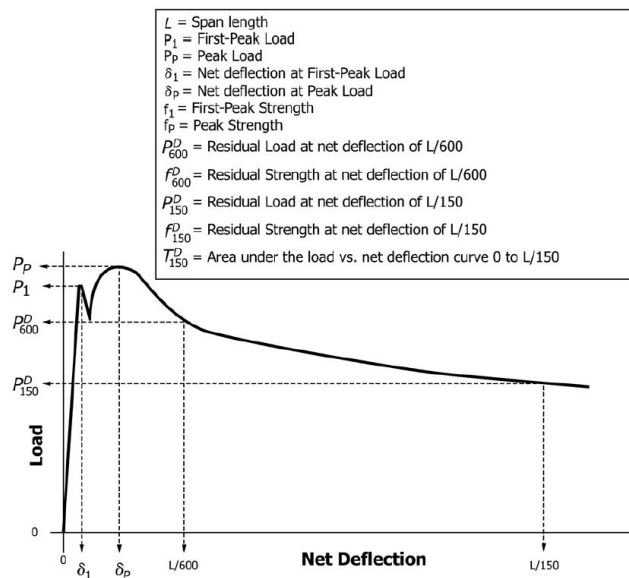


Figure 2-10 Typical load vs mid-span deflection relationships for FRC specimen under third-point loading test (first peak load lower than the peak load) [ASTM 1609-2012]

This test method can be used for comparing the various FRC mixtures by evaluating the performance of post-peak behavior of FRC, quality of concrete and flexural strength on concrete member subjected to pure bending. In ASTM C1609, failure of the

specimen is dominated by a single large crack in a well-defined plane. In fact, if the fracture occurs outside of the middle third of the span, the results are required to be discarded (ASTM C1609 2012). As the fibers are randomly distributed and oriented, the effects that they produce are not well represented by a test in which the failure location is constrained. The calculated toughness parameters greatly depend on how the point of “first crack” is defined. Thus it is important to determine the load vs. deflection curve very precisely. As a result, a number of difficulties arise (Bentur and Mindess 2007):

1. It is essential to correct for the “extraneous” deflections that occur due to the seating of the specimen on the supports and machine deformations. Different laboratories may make these corrections differently and hence may report different results (Chen and Mindess 1995, ASTM C1609 2012).

2. Because some micro-cracking begins almost immediately upon loading, it is difficult to define the point of first cracking unambiguously.

3. An instability often occurs in the measured load vs. deflection curve immediately after the first significant crack, particularly for low toughness FRC, and a servo-controlled operation is required to control the rate of increase of deflection. Closed-loop testing equipment is not always available, and different loading systems can result in quite different calculated toughness values.

4. Due to the uncertainty in determining the point of first cracking and difficulties introduced by the instability previously mentioned, toughness and residual strength parameters are sometimes insensitive to different fiber types or geometries.

Due to these factors, toughness and residual strength parameters show considerable scatter. The within-batch coefficient of variation (COV) has been reported from 15% to greater than 20% (ASTM C1609 2012, Bernard 2002, Chao 2011). The high variability is due to the lack of control over the position of the cracks, as well as fiber

orientation relative to the major crack plane (Chao 2011). Despite the considerable improvements that have been made in ASTM C1609 over the years, this testing procedure still presents major difficulties in accurately describing the behavior of FRC.

2.5.3 ASTM C1550 – 2012 Standard Test Method for Flexural Toughness of Fiber Reinforced Concrete (Using Centrally Loaded Round Panel)

ASTM C1550 is used for determination of the flexural toughness of FRC, expressed as energy absorption in the post-cracking range. Molded round panels of cast fiber-reinforced concrete or fiber-reinforced shotcrete supported on three symmetrically arranged pivots are subjected to a central-point load. The load is applied through a hemispherical-ended steel piston advanced at a prescribed rate of displacement. Load and deflection are recorded simultaneously up to a specified central deflection. The suggested panel support fixture and test arrangement are shown in Figure 2-11 and Figure 2-12. The nominal dimensions of the panel are 3-in. [75-mm] in thickness and 31.5-in. [800-mm] in diameter.

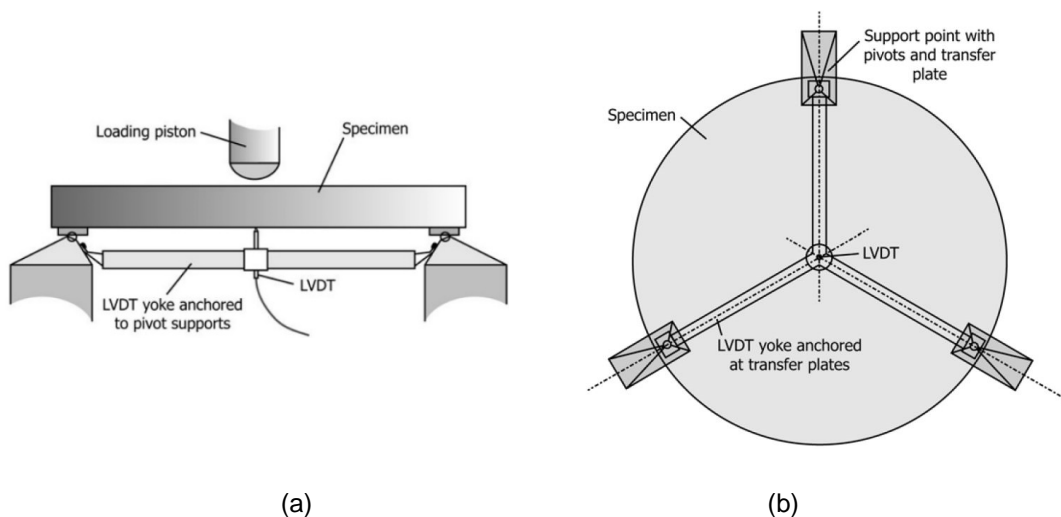


Figure 2-11 (a) Test setup and (b) Specimen (ASTM C1550 - 2012)

The performance of specimens tested by ASTM C1555 is quantified in terms of two factors. One is based on the energy absorbed between the onset of loading and another is based on the selected values of central deflection of the fiber-reinforced concrete panel. When the central point load is applied, test panels experience bi-axial bending and exhibit a mode of failure that can be related to the in-situ behavior of structures. The energy absorbed is taken to represent the ability of an FRC to redistribute stress following cracking (ASTM C1550 2012). Bernard et. al (2007) suggested performance-based specification as

1. The absorption of energy up to a deflection of 0.2 inches that indicates the performance of applications in which crack control is important;
2. The absorption of energy up to a deflection of 1.6 inches that evaluates the performance of applications in which large cracks can be tolerated.

The single-operator coefficient of variation for peak load and energy absorption is reported as 6.2% and 10.1%, respectively; the multi-laboratory precision is approximately 9% for the same test parameters (ASTM C1550 2012).



(a)



(b)



(c)



(d)

Figure 2-12 (a) Specimen (b) Setup (d) Location of major cracks for ASTM C1550 Round Panel Test (Chao 2011)

The main advantage of ASTM C1550 over other test methods for FRC is that it can discriminate between different fiber types and volumes with more precision. Past research indicated that the variation in peak load, cracking load, or energy absorbed up to a specified central deflection from this test is generally lower than bending tests, with a COV between 5% and 13% (Bernard 2002, Chao 2011). The reduced scatter in the results could be attributed to the following (Chao 2011):

- 1) Location of cracks as well as crack patterns can be controlled: As seen in Figure 2-12 (d) panels tested by this method almost always split into three segments upon failure, at angles of about 120°.
- 2) Increased cracked area: the three major cracks give a somewhat average mechanical behavior of the reinforcement that minimizes the influence of non-uniform fiber distribution as well as random fiber orientation.

The major disadvantage of ASTM C1550 is that it uses heavy steel support and difficulty in carrying out the experiments due to large specimen sizes (Figure 2-12). Moreover, in this test when a crack occurs at the location of LVDT and crack opening exceeds the probe width of LVDT, the deflection measurement is not accurate as a probe can slip into the crack. In ASTM C1550, it is suggested that using an LVDT with a maximum probe width of 0.8-in. [20-mm] can alleviate this problem. Greater probe widths are not recommended because off-center cracks may induce exaggerated apparent deflections if they occur adjacent to a wide probe (ASTM C1550 2012). However, even if the maximum probe width is used, the opening at the center could be greater than 0.8-in. [20-mm] at large deflections, which may lead to incorrect measurements of displacement (Chao 2011). This test method is less attractive for a quality control test and performance evaluation of FRC due to the complicated procedure, large specimen size, and intricate support fixtures.

2.5.4 *Uniaxial Direct Tensile Test*

A uniaxial direct tensile test is used to identify the important properties of FRC, such as strain hardening or strain-softening, elastic modulus, and tensile stress-strain relationships, and these are used to model and design of the FRC structural members (Naaman 2007). Currently, there is no standard method for this test in the United States.,

as there is difficulty in providing a gripping arrangement that precludes specimen cracking at the grips (Chao 2011). The specimens were specifically designed so that a pin-pin loading condition is created at the ends as shown in Figure 2-14 (b) (Chao 2011). Both ends have double dog-bone geometry and are strengthened by the steel mesh to ensure that cracking would only occur in the central portion of the specimen, within the gauge length. The double dog-bone shape was used to provide a better transition to avoid stress concentration which resulted from the reduction of the cross-section. The central portion has a square cross-section with a dimension of 4 x 4 inches. This dimension was selected to ensure more uniformly distributed fibers while maintaining a suitable weight for laboratory handling. The strains were measured by a pair of linear variable differential transformers (LVDTs) with a gauge length of approximately 6 inches.

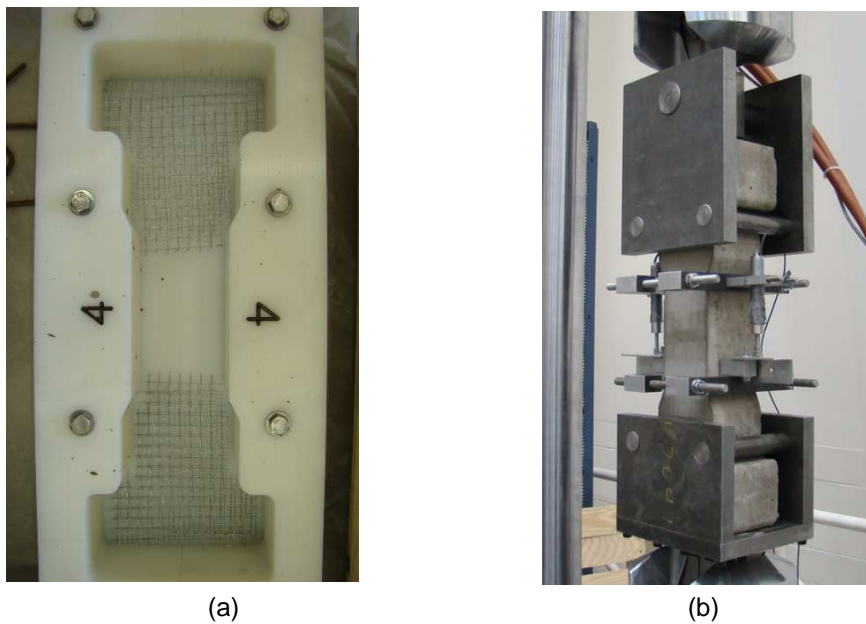
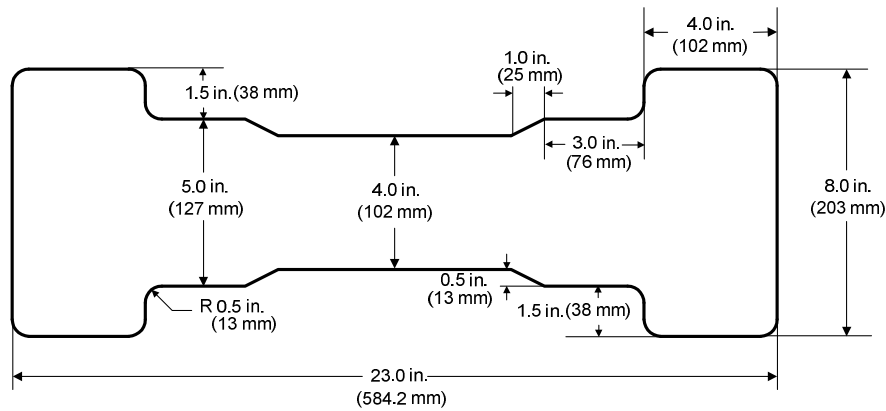


Figure 2-13 Uniaxial Direct Tensile Test

(a) Mold (b) Test Setup



(c)

Figure 2-14 Uniaxial Direct Tensile Test

(c) Test specimen dimension (Chao 2011)

This unique shaped specimen (Figure 2-14(c)) are specifically designed to create a pin-pin loading condition at the ends. The advantages of this end condition and specimen geometry are (Chao 2011) are

1. A pure axial load is applied in tension;
2. Specific treatment such as adhesives is not required to fix the ends to the test setup;
3. Both ends of the specimen are strengthened by steel meshes to ensure that cracking will occur only within the central portion.

The major drawback of the direct tensile test is the inconsistency in crack formation which causes the higher variability in post cracking stages. Currently there is no standard method for this test in US because it is difficult to provide a gripping arrangement. It is also difficult to eliminate eccentricity of the line of action of load. This method has complicated test setup and localized crack may form beyond the gauge length as shown in Figure 2-15 Formation of crack beyond gauge length and at gripping position due to higher stress

concentration near the gripping device and support ends. Moreover, the location of cracks is inconsistent, however, and crack-propagation paths are not controlled. Only one large major crack is formed that could be largely affected by fiber distribution.

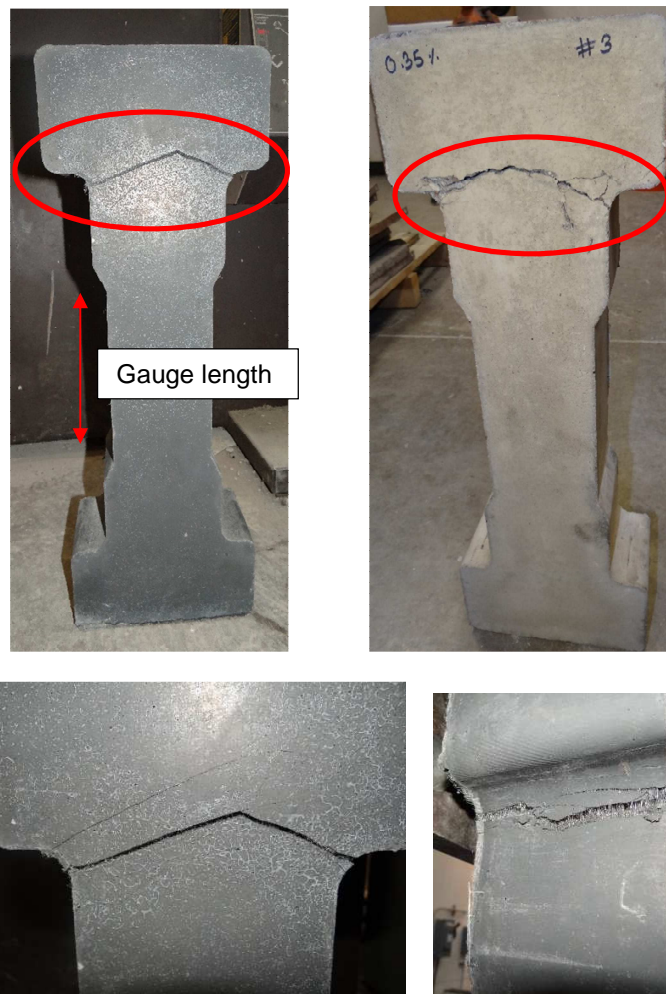
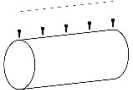
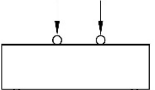
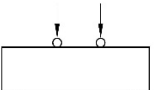
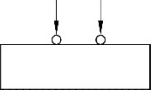
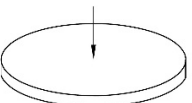
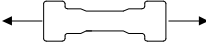


Figure 2-15 Formation of crack beyond gauge length and at gripping position

2.6 Comparison of Existing Test Method

The above-mentioned test methods fail to meet one or more recommended criteria for testing of FRC as listed earlier in this chapter (Bentur and Mindess 2007). Table 2-3 shows the comparison between existing test method based on specimen geometry, dimension, volume, and weight. ASTM 1609 is mostly used for SFRC and uniaxial direct tensile test method is common for UHP-FRC by researchers and in the commercial industry. However, most of the current testing procedure requires specimens heavier than 25 lbs that are difficult to transport and place in testing position.

Table 2-3 Comparison between existing standard test methods (Woods 2012)

Test Information ¹		Test Specimen ²			
Designation	Layout	Geometry	Dimension (in.)	Volume (in. ³)	Weight (lbs)
ASTM C496		Cylinder	4" ϕ x 8	101	9
ASTM C1609		Rectangular Prism	6 x 6 x 20	720	63
ASTM C1609		Rectangular Prism	4 x 4 x 14	224	19
ASTM C1399		Rectangular Prism	4 x 4 x 14	224	19
ASTM C1550		Circular Panel	31.5" ϕ x 3	2338	203
Uniaxial Direct Tensile Test		Dog bone	Various	524	45

¹ Test Layout modified from (Mollins 2006)

² Weight calculated using unit weight of FRC = 150 lb/ft³

Most of the test method listed in Table 2-3 shows scatter test results, has a complicated test setup with large test specimen. Besides, tensile properties of any concrete material are a significant constraint for understanding the behavior of concrete member and utilized in analysis and design of structural member. The standard test methods present major difficulties in accurately describing the behavior of FRC. Hence, a simple and reliable tensile test method is obligatory and in this situation, double punch test (DPT) can be an alternative technique. DPT provides an average tensile strength considering all the possible failure planes.

2.7 Introduction to Double Punch Test (DPT)

The Double Punch Test (DPT) was originally developed by Chen (1970) to determine the tensile strength of plain concrete which is based on the theory of perfect plasticity using the limit analysis technique. It was introduced as an alternative method to split-cylinder test for determination of the tensile strength of plain concrete, rocks, and soil. In the double punch test, the failure can occur on any one of the radial planes in contrast to the other method such as split-cylinder test in which the plane of failure is predetermined. As proposed by Chen (1970), a concrete cylinder is positioned vertically between loading platens of the test machine and compressed by two steel punches located concentrically on the top and bottom surfaces (Figure 2-16). Following an extensive literature review of test methods used for concrete, it has been shown that DPT could be extended to evaluate the behavior of FRC composites.

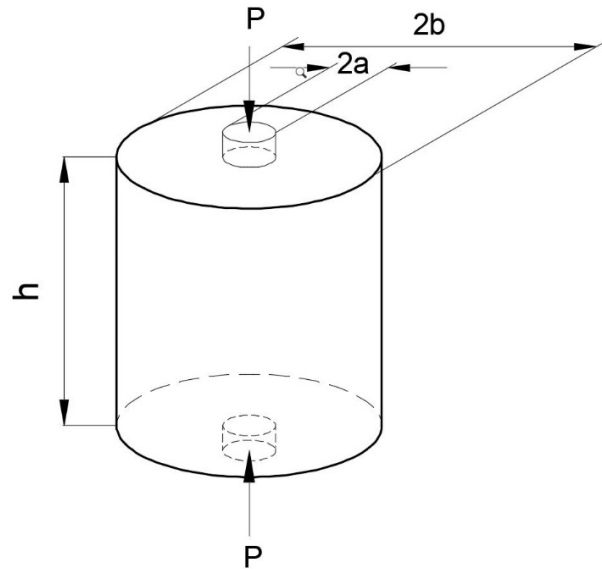


Figure 2-16 Double punch test layout

This method can also be used as an alternative method to characterize the post-cracking behavior of fiber reinforced concrete and improve the material assessment procedure. The experimental results have shown that DPT method can identify various FRC characteristics such as tensile strength, strain-hardening, toughness, and stiffness. This method can be extended to the concrete matrix containing fibers as a quality control test which is an important factor in the structural applications. The study investigates the feasibility of DPT method for UHP-FRC as this method can be carried out using a simple test setup and a compression test machine.

2.8 Theory of Double Punch Test

The basic theory of the Double-Punch Test is based on the bearing capacity of concrete blocks (Chen 1970). This approach was based on the assumption that sufficient local deformability of concrete in tension and in compression existed such that generalized theorems of limit analysis could be applied to concrete idealized as a perfectly plastic

material. The second assumption is that a modified Mohr-Coulomb failure surface in compression and a small non-zero tension cut-off is assumed as a yield surface for the concrete. The formula was determined by modifying the results from bearing capacity test. Figure 2-17 shows the failure mechanism for a double punch test as explained by Chen (1970). It consists of many simple cracks along the radial direction. The punches from top and bottom are compressed and form two cone-shaped rupture surface directly beneath the punches. As the test progresses, the cone-shaped surface move towards each other as a rigid body and displace the surrounding material horizontally sideways.

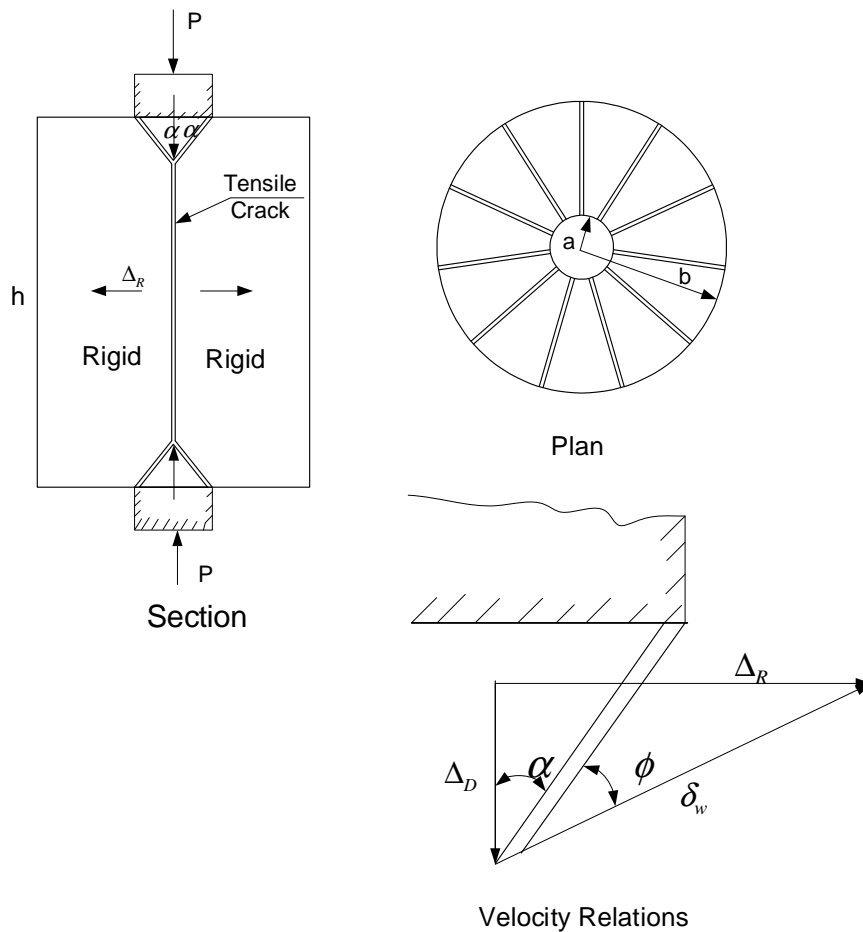


Figure 2-17 Bearing Capacity of Double Punch Test (Chen 1970)

According to upper bound computation as per Chen (Book: Limit Analysis and Soil Plasticity, 1975), equating the external rate of work to the total rate of internal dissipation gives the value of upper bound on the applied load P.

$$\frac{P^u}{\pi a^2} = f_t' \left[\frac{bh}{a^2} \tan(2\alpha + \phi) - 1 \right]$$

where, f_t = tensile strength (psi); P = Load applied (lbs.); b= radius of cylinder (in.); h = height of cylinder (in.); a = radius of punch (in.)

$$\cot \alpha = \tan \phi + \sec \phi \left[1 + \frac{\frac{bh}{a^2} \cos \phi}{\frac{f_c'}{f_t'} \left(\frac{1 - \sin \phi}{2} \right) - \sin \phi} \right]^{1/2}$$

and valid for $\alpha \geq \tan^{-1} \left(\frac{2a}{h} \right)$

The coefficient $K = \tan (2\alpha + \phi)$ is not sensitive to internal friction angle and using typical values $f_c' = 10 f_t'$; $2a = 1.5$ in.; $2b = 6$ in and $h = 6$ in., the upper bound has a minimum value at the point $\alpha = 10^\circ$ and gives:

$$P \leq P^u = \pi(1.19bh - a^2) f_t'$$

$$f_t = \frac{P}{\pi(1.2bh - a^2)} \quad \text{Equation (2-1)}$$

The working formula for computing the tensile strength in a double punch test was obtained from the theory of linear elasticity and combined with a plasticity approach for concrete as suggested by Chen (1970). The equivalent tensile strength from the working formula estimates tensile strength depending on several fractured diametric planes.

However, based on finite element analysis considering concrete as a linear elastic, plastic strain-hardening and fracture material, Chen and Yuan (1980) proposed modified equation as equation...

$$f_t = \frac{0.75 \times P}{\pi(1.2bh - a^2)} \quad \text{Equation (2-2)}$$

Equation (2-1) and Equation (2-2) are valid for $b/a \leq 4$ or $H/2a \leq 4$. For any ratio $b/a > 4$ or $H/2a > 4$, the limiting value $b = 4a$ or $H = 8a$ should be used in Equation (2-1) and Equation (2-2) for determination of tensile strength.

There are few analytical expressions available in the literature by various researchers to compute tensile strength in DPT which requires the maximum compression load and dimensions of the test as input. Based on nonlinear fracture mechanics approach Marti (1989) proposed

$$f_t = \frac{0.4P}{d^2} \cdot \sqrt{1 + \frac{d}{\lambda d_a}} \quad \text{Equation (2-3)}$$

where d_a is the maximum aggregate size and λ is an empirical constant depending on the material. In 1988, Bortolotti assumed a modified Coulomb like failure criterion for concrete and suggested a modified equation with $\alpha = 18.49$ degree considering $\alpha = \pi/2 - \phi/2$. ϕ is the shearing resistance angle in the modified Coulomb's yield.

$$f_t = \frac{P}{\pi(bh - a^2 \cot \alpha)} \quad \text{Equation (2-4)}$$

Mollins et. al (2007) developed another equation based on Strut and Tie model to calculate the unitary cracking load f_{ct} and has been standardized by AENOR in Spain.

$$\sigma_t = \frac{4P_f}{9\pi aH} \quad \text{Equation (2-5)}$$

where a is the diameter of punch and H is the height of the cylinder.

However, there is no formulation that gives the stress-strain relation and is not valid for linear-elastic and post-cracking stages. Another analytical expression to determine the tensile strength was formulated as Equation 2-6 by Blanco et.al. (2014) which is compared with the constitutive models from European codes and guidelines based on the flexural test. As crack appears, the conical concrete block slides into the cylinder in a specific displacement δ_p . This results in lateral displacement δ_L of the concrete segment as shown in Figure 2-18.

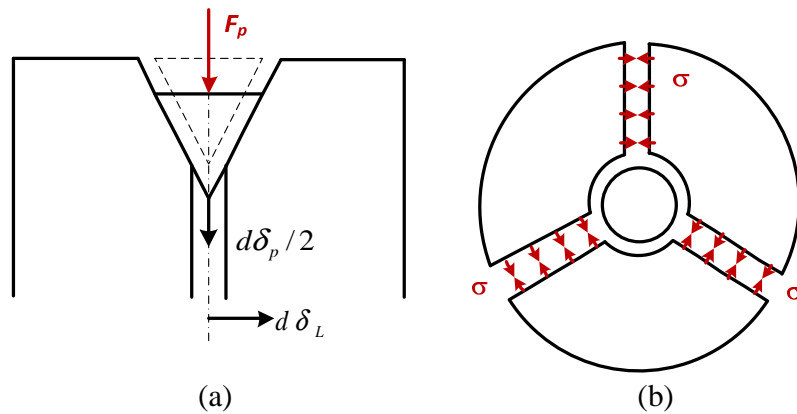


Figure 2-18 (a) Front view of specimen after cracking (b) Top view of specimen after cracking (Blanco et. al 2014)

Figure 2-19 shows the details of the interplay of forces and balance of forces at the conical wedges and the specimen during the test. The radial force (F_R) is developed due to applied vertical force (F_p) and is distributed radially around the cylinder. This radial force (F_R) from the conical block and from the specimen balances each other. The vertical components of friction force (F_{fr}) and a normal force (F_N) counterbalances the force (F_p).

The conical wedge is continuously moving downward during the test, the product of kinematic friction coefficient and normal force gives the frictional force (F_{fr}).

$$F_{fr} = \mu_k F_N$$

$$F_R = F_P \cdot \frac{\cos \beta - \mu_k \sin \beta}{\sin \beta + \mu_k \cos \beta}$$

where $\beta = 0.468$ radians (failure angle of material)

$\mu_k = 0.7$ (kinematic coefficient of friction)

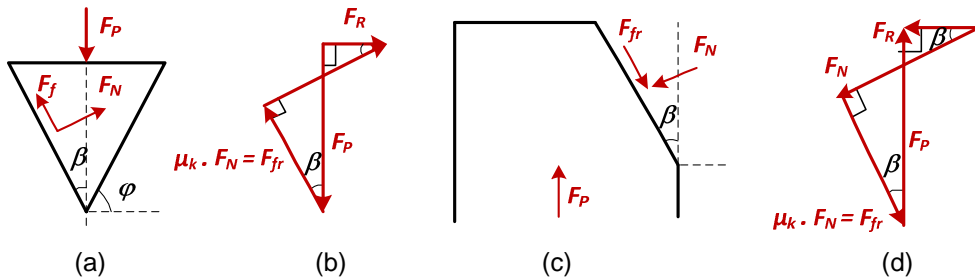


Figure 2-19 (a) Details of forces at conical block (b) balance of forces at conical block (c) details of forces at the specimen (d) balance of forces at the specimen.

The following equation has been derived by Blanco et. al (2014) analytically for estimating the tensile stress and associated strain (Equation 2-6 and Equation 2-7).

$$\sigma_t = \frac{F_p}{2\pi A} \times \frac{\cos \beta - \mu_k \sin \beta}{\sin \beta + \mu_k \cos \beta} \quad \text{Equation (2-6)}$$

$$A = \frac{d \cdot h}{4} - \frac{d'^2}{4 \cdot \tan \beta} = \text{area of cracked radial surface}$$

where, σ_t = tensile stress (MPa)

d = diameter of cylinder (mm)

H = height of cylinder (mm)

d' = diameter of plate (mm)

$$\varepsilon = \frac{N \delta_p}{\pi R} \cdot \tan \beta \cdot \sin \left(\frac{\pi}{N} \right) \quad \text{Equation (2-7)}$$

where, ε = strain (%)

R = radius of cylinder (mm)

N = number of cracks

Equation (2-6) and Equation (2-7) were used to predict a simplified σ - ε curve (Figure 2-20) in the form of a multilinear σ - ε diagram (Blanco et. al 2014). In this approach, the values of strain were defined at four points as shown in Table 2-4. The stress values were expressed as function of the load related to a specific displacement and are determined at those equivalent strains at maximum load, 0.02 mm, 0.75 mm and 4 mm displacement as shown in Table 2-4.

Table 2-4 Parameters for simplified model using DPT (Blanco et. al 2014)

Strain (%)	Stress (MPa)
$\varepsilon_1 = \frac{\sigma_1}{E_{cm}}$	$\sigma_1 = \frac{F_{\max}}{2\pi A} \times \frac{\cos \beta - \mu_k \sin \beta}{\sin \beta + \mu_k \cos \beta}$
$\varepsilon_2 = \varepsilon_1 + 0.1$	$\sigma_2 = \frac{F_{0.02mm}}{2\pi A} \times \frac{\cos \beta - \mu_k \sin \beta}{\sin \beta + \mu_k \cos \beta}$
$\varepsilon_2 = 4.0$	$\sigma_3 = \frac{F_{0.75mm}}{2\pi A} \times \frac{\cos \beta - \mu_k \sin \beta}{\sin \beta + \mu_k \cos \beta}$
$\varepsilon_2 = 20.0$	$\sigma_4 = \frac{F_{4mm}}{2\pi A} \times \frac{\cos \beta - \mu_k \sin \beta}{\sin \beta + \mu_k \cos \beta}$

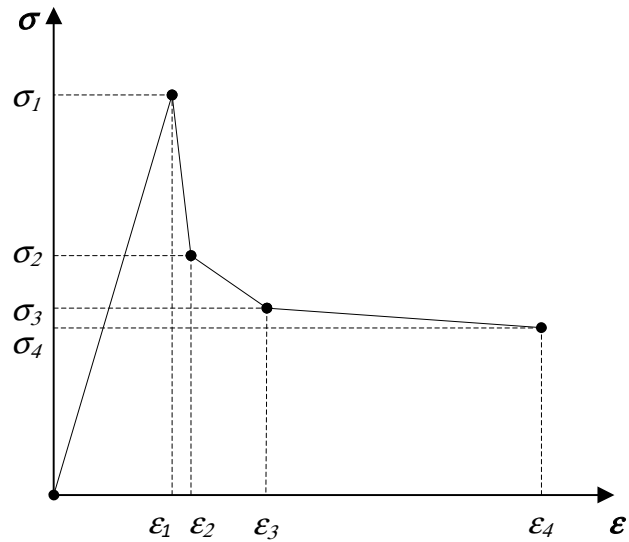


Figure 2-20 Simplified σ - ϵ diagram (Blanco et.al 2014)

In this research, the tensile strength was calculated using modified Chen's equation (Equation 2) and a sample calculation was carried for comparison of all the equation for tensile stress in a later chapter.

2.9 Fracture Mechanics of DPT

The tensile response of FRC and UHP-FRC depends on the amount of fiber in the concrete matrix. The DPT specimens experience various stages during the test that depends on the integrity of concrete matrix. Pujadas et.al (2013) provides a clear understanding of theoretical fracture mechanics for DPT which is divided into different stages and the similar stages for the idealized tensile response of UHP-FRC as explained by Greybeal (2014). Hence, DPT could show the idealized tensile behavior of FRC as well as UHPFRC similar to the direct tensile test.

Stage 1: When a compressive load is applied through the punch, the internal stresses are developed and are resisted by the concrete matrix. In FRC, the minor circumferential strain is observed until the peak load is reached. This circumferential strain is associated to the Poisson effect and the microcracking and is assumed to be zero. This stage includes the linear elastic phase to the point of first cracking which gives values of axial deformation and total crack opening displacement (TCOD), circumferential deformation as zero. In the case of UHP-FRC, a prominent circumferential deformation can be observed before reaching the peak load. The reaching of peak load marks the end of stage 1 for both FRC and UHP-FRC.

Stage 2: This stage is a multi-cracking phase for the UHP-FRC where the concrete matrix cracks repeatedly and fibers bridge the crack opening until the peak strength is reached. The conical wedges having the same base diameter as the punches are abruptly formed at the upper and lower punch. The multiple cracking may not be seen in case of SFRC due to a less ductile nature.

Stage 3: After the peak point, the crack straining and hardening behavior occur. The conical wedges slide in between concrete matrix forming radial cracks and may continue along the height of specimen. The crack opening increases gradually producing a uniform displacement radially where the number of cracks depends on the type of concrete matrix. Due to saturation in crack formation, additional cracks are less likely at this stage.

Stage 4: With the decrease in fiber bridging strength, the localization phase will begin where major cracks stabilize, and residual strength will appear. The crack opening will bring out the fragmented concrete blocks due to radial cracks and behaves as a rigid body. The

axial deformation is produced by penetration of the conical wedges into the specimen and TCOD occurs from lateral displacement of the adjacent concrete block.

Double punch test is an indirect tensile test and is not restricted to a predetermined plane (Chen 1970, Pros et. al 2011,). The load applied to the cylinder produces almost uniform tensile stress over the radial fracture planes. The experimental results have shown that an observed number of fracture plane ranges from 2 to 4. (Chen 1970, Mollins et. al 2007, Blanco et. al 2014). Figure 2-21 shows the two different fracture patterns in DPT

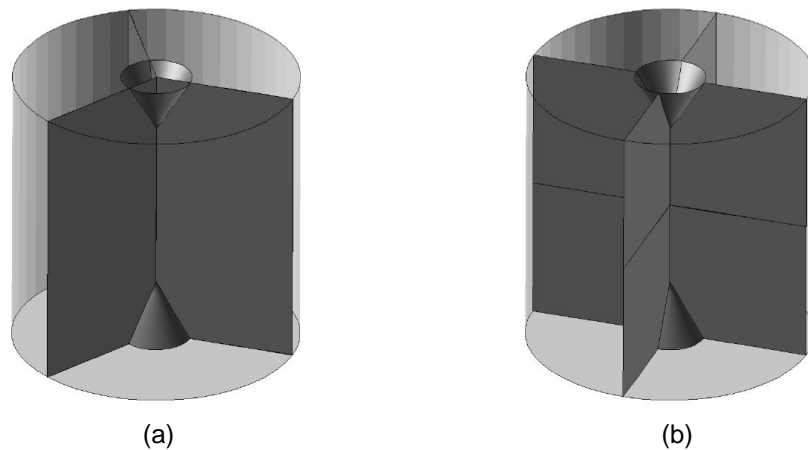


Figure 2-21 (a) DPT with three radial fracture plane (b) DPT with four radial fracture planes (Pros et. al 2011)

2.10 FEM analysis for DPT

The equation developed by Chen (1970) based on the theory of plasticity to determine the equivalent tensile stress was verified by Karki (2011) using finite element analysis. The radial principal stress at mid-height of specimen and 1.5 in. above mid-height of specimen is shown in Figure 2-22. It shows that stresses decline outward from center to edges in double punch test.

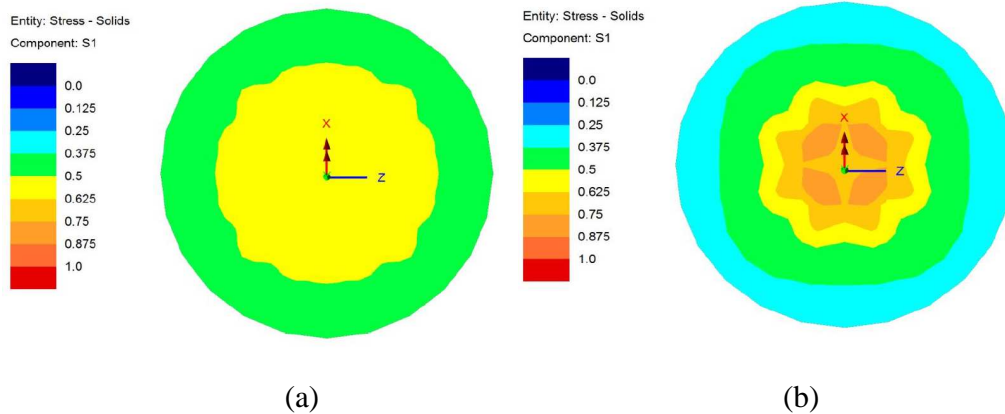


Figure 2-22 Plan view for principal stress in tension (a) at mid height (b) 1.5 inch above mid-height (Karki 2011)

From Figure 2-23, it can be seen that stresses are higher and compressive at the loading point and support while around the mid-height of the specimen principal stresses are uniform and tensile nature.

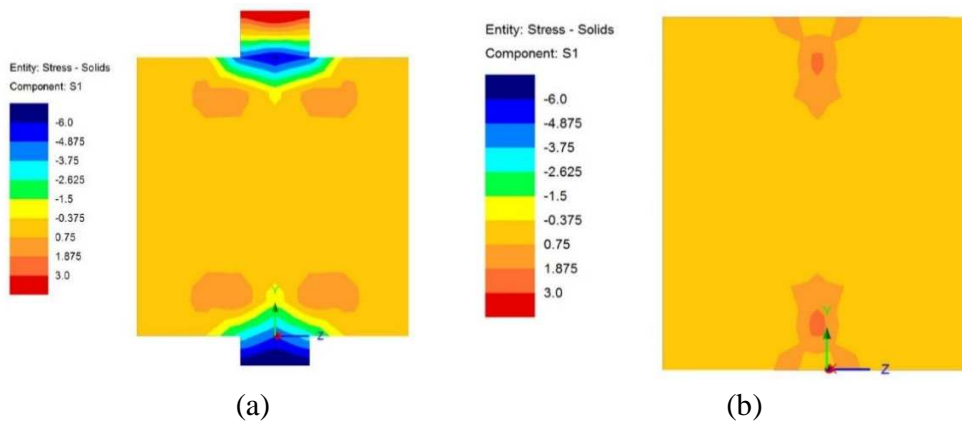


Figure 2-23 Elevation view for principal stresses in tension (a) at centerline (b) 1.5 inch from center along height (Karki 2011)

From Figure 2-24, it can be seen that tensile stresses are predominant in the central 3/4th of the depth. The compressive stresses seen just at the contact of the punch decreases rapidly after a certain depth and results in tensile stresses. Also, beyond the

vertical line touching the periphery of the punch, the tensile stress is almost uniform along the radii of the specimen.

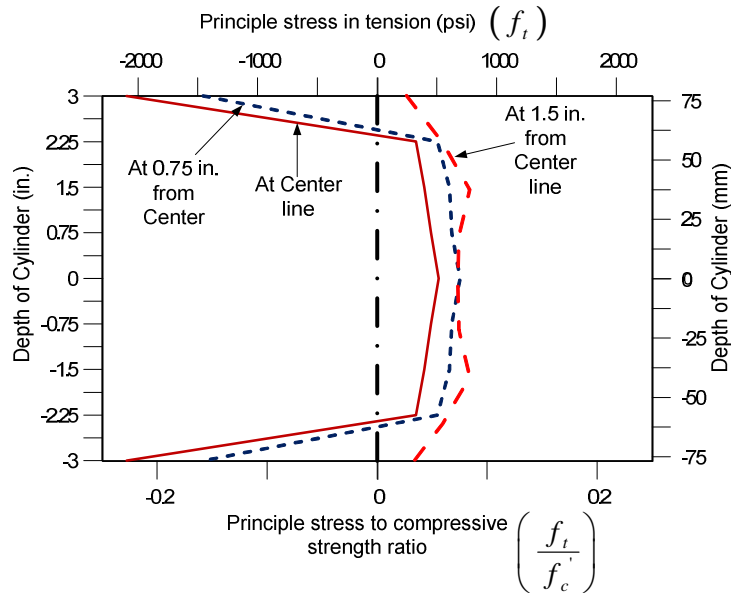


Figure 2-24 Distribution of stress at various distance from centerline along height of specimen (Karki 2011)

Figure 2-25 that at the top the cylinder, the compressive stress is highest below the punch, at the point of contact of the punch, and decreases remarkably away from the punch. However, the stress diagram at 1.5 in. from the top to the middle of the cylinder shows uniform tensile stress. From Figure 2-24 and Figure 2-25, it can be observed that the majority of the specimen in DPT is subjected to pure tension which makes it a better alternative to the direct tensile test

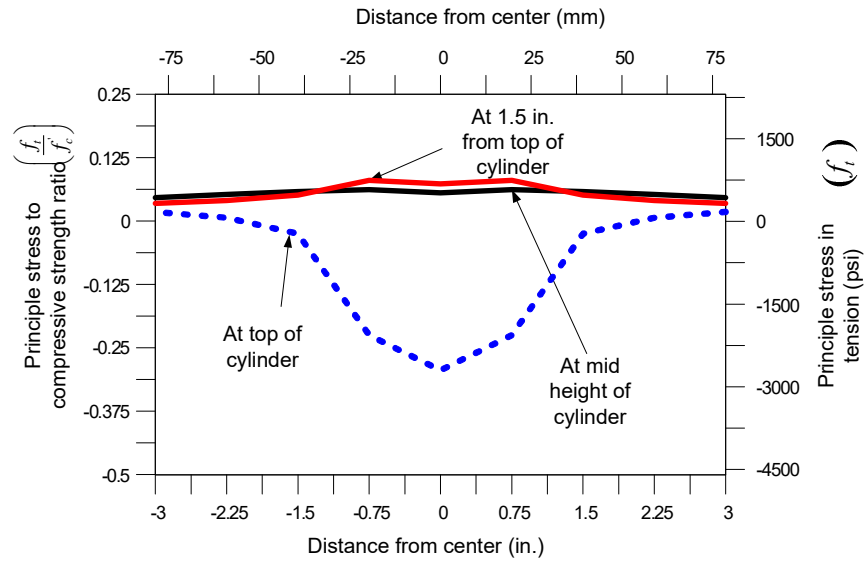
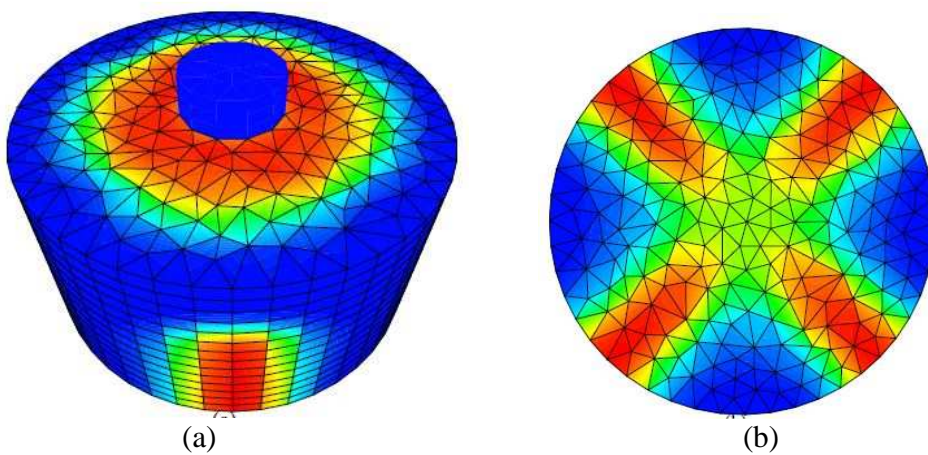


Figure 2-25 Distribution of stress at various distance from top of specimen along the diameter of cylinder

Another numerical simulation was carried by Pros et. al (2011) and presented the damage distribution that shows a cracking pattern in double punch method with plain concrete. They reported that the fracture pattern from experiments resembles the damage model and the obtained peak value is similar to other analytical expressions. Figure 2-26 shows the damage profile for DPT on plain concrete (Pros et al 2011).



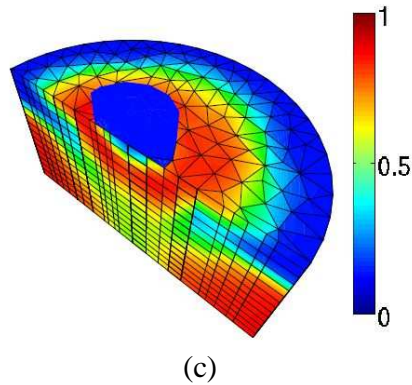


Figure 2-26 Damage profile for DPT on plain concrete (Pros et. al 2011)

(a) Top view (b) Bottom view (c) Inside view

2.11 Comparison between DPT and existing test methods.


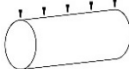
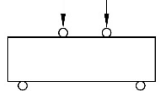
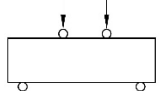
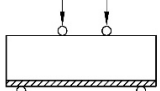
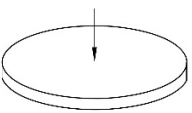
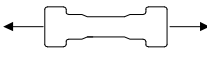
In spite of the presence of a number of tests to evaluate the tensile properties of FRC and UHP-FRC, none of them sufficiently fulfills all of the criteria mentioned Chapter 2. A simple, reliable and reproducible test to obtain the tensile behavior of FRC is still sought after (Woods 2012).

1. Simple: Complicated specimen formwork, intricate support fixtures, difficulty in specimen preparation and handling all add to the complexity of the existing tensile test methods.
2. Reliable: The theoretical basis of the test method should be sound; an actual depiction of the physical mechanism involved in the test. Some of the current test methods assume an elastic behavior for the plastic behavior observed in the test which is erroneous. For FRC, there is randomness in the fiber orientation and distribution along the specimen. This erratic nature is not adequately described by some of the tests where the failure plane is predetermined. Also, the variation in a crack location in these

- tests intensifies the disadvantage mentioned. Furthermore, an increased single operator coefficient of variation observed between batches adds to the unreliability.
3. Reproducing: A test needs be able to be reproduced between laboratories with an acceptable degree of variation. However, the current test methods have a high interlaboratory and multiple operator coefficients of variation. Also, a complicated specimen and test procedures make it difficult to conduct a number of tests to obtain sufficient data to be able to emulate the test between laboratories.

The double punch method is attractive to use for FRC due to the basic testing arrangement and straightforward technique. The same testing machine and similar instrumentation can be used for both compressive strength and tensile strength test. DPT is conducted by loading the specimen under compression. As a result, the complications seen in direct tensile tests such as eccentricity and complicated test setup can be avoided. Apart from other tensile tests, DPT specimen is small and light, a 6x6 in. specimen about 15 lbs, and the test can be conducted using a simple arrangement of LVDTs, with appropriate stroke, and a load cell for measuring the axial deformation and compressive force respectively. Moreover, results obtained from indirect tensile tests are more consistent and comparable to results from bending and tensile tests. DPT also takes advantage of the absence of predetermined failure plane in the test setup. It results in multiple possible fracture planes which help to take into account the random fiber dispersion and orientation within the specimen giving an actual depiction of the fiber-reinforcement effect which the characteristic feature of FRC. The comparison between the existing test method and double punch test are presented in Table 2-5 and Table 2-6.

Table 2-5 Comparison between existing standard test methods with DPT (Woods 2012)

Test Information ¹		Test Specimen ²				
Designation	Layout	Volume (in. ²)	Number of failure plane	Failure Surface Area	Specific failure surface (β)	β_{DPT}/β_{Test}
Double Punch Test		170	3 or 4	54	0.318	1
ASTM C496		101	1	12.6	0.125	3
ASTM C1609		720	1	36	0.05	6
ASTM C1609		224	1	16	0.071	4
ASTM C1399		224	1	16	0.071	4
ASTM C1550		2338	3	141.8	0.061	5
Uniaxial Direct Tensile Test		524	1	16	0.031	10

¹ Test Layout modified from (Mollins 2006)

Table 2-6 Simplicity, Reliability, and Reproducibility of Current FRC Testing Procedures vs. Double-Punch Test (Woods 2012)

Designation	Simplicity		Reliability ³			Reproducibility	
	Specimen and Fabrication Handling	Test Setup and Support Fixtures	Test Procedure	Test Machine	Failure Mechanism	Within-Batch Precision (COV)	Inter-Laboratory Precision (COV)
ASTM C496	Easy	Easy	Easy	Standard	Single Major Crack	± 5% PL	Not Available
ASTM C1609	Moderate	Moderate	Moderate	Closed-Loop	Single Major Crack	± 8% PL ± 20% RS	Not Available
ASTM C1399	Moderate	Difficult	Difficult	Standard	Single Major Crack	± 20% RS	± 40% RS
ASTM C1550	Difficult	Difficult	Difficult	Closed-Loop	Multiple Cracks	± 6% PL ± 10% RS	± 9% PL ± 9% RS
Uniaxial Direct Tensile Test	Difficult	Moderate	Moderate	Closed-Loop	Single Major Crack	Not Available	Not Available
Double Punch Test	Easy	Easy	Easy	Standard	Multiple Cracks	± 10% Initial Load ± 6% Peak Load ± 10% Residual Strength	Not Available

³ Reliability and reproducibility data obtained from industry standards and research literature (ASTM C496 2011, ASTM C1609 2010, ASTM C1550 2010, ASTM C1399 2010, Chao 2011, Bernard 2002). COVs for peak load and residual strength (toughness) are denoted (PL) and (RS) respectively.

2.12 Potential issue in DPT

The double punch test has many advantages over the existing test method. However, there still exist some potential issues in the DPT method. The circumferential extensometer that is used to determine the total crack opening displacement in DPT is an expensive instrument. This limits the use of DPT method in most of the industrial and research laboratories. The overall cost of the test should not be more than \$150 per test to be an affordable test method. Moreover, the total time of the test for FRC is about 25 to 30 minutes to complete the test. It is essential to optimize the time to perform the test efficiently for a quality control test in about 10-12 minutes time frame. The measurement of crack

width and inspection of a number of cracks are the important parameter for evaluating the characteristics of any concrete material. It is time-consuming to measure the crack width in a test by conventional visual inspection and automated crack width measurement is indispensable.

2.13 Research Objectives

The current standardized test methods have one or more limitations that make it unfeasible, unreliable, or inconsistent for evaluating the performance of FRC. This has negatively affected the acceptance of FRC applications into structural design codes. A more practical, reliable, and consistent test method is needed for evaluating the characteristics of FRC with different fiber types, fiber volume fractions, and mixture designs. The following are the objectives of this research:

1. To develop a standard systematic test procedure with the optimum rate for the DPT and examine consistency between accuracy, efficiency and time for the test.
2. To determine the relationship between axial deformation and circumferential strain using double punch test (DPT) method applicable to FRC and UHP-FRC.
3. To derive a simple formula to estimate the average and maximum crack widths, which allows DPT to only use LVDTs without using circumferential extensometer and other instrumentation.
4. To assess the suitability of DPT method for UHP-FRC material in determining tensile strength and behavior in post cracking phase.
5. To evaluate the qualitative and comparative assessment of the influence of fiber dosage from the nature of the cracks (number and crack width) for FRC and UHP-FRC for long fibers.
6. To investigate the effect of specimen sizes in DPT for FRC and UHP-FRC when long fibers are used.

Chapter 3

Double Punch Test – Experimental Program

The main purpose of this research is to unify and develop a tensile test method which is suitable for both FRC and UHPFRC. This Double Punch Test has been proven to be easier, more reliable and faster than the current test method for FRC. The experimental programs are divided into following stages as shown in Figure 3-1:

3.1 Experimental Program Overview

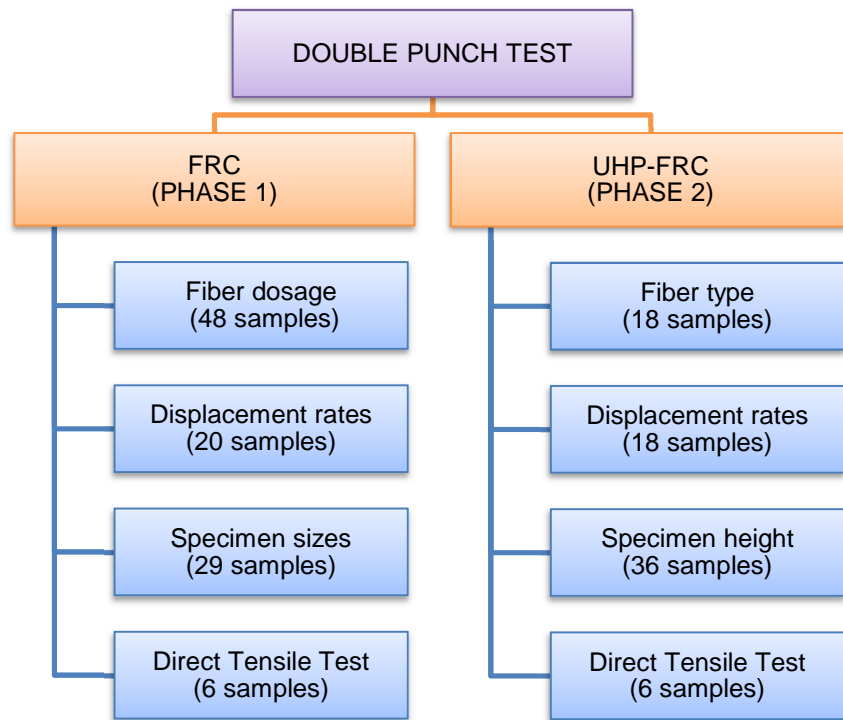


Figure 3-1: Experimental program

Phase 1

For the first phase of this research, 48 FRC samples, with six number of cylinders in each set, set 1, 2, 3, 4, were cast with 0.35%, 0.45%, 0.55% and 0.75% fiber by volume respectively to analyze the effects of fiber volume fraction on coefficient of variation and

average value of key parameters of DPT. For this, the 48 samples were tested at the displacement rate of 0.02 in./min with 12 specimens for each fiber dosage. For the next set (Set 5) eight cylinders (6x12) with 0.55% fibers by volume were cast and among them, four 6x6 specimens were tested at the displacement rate of 0.012 in./min, 0.02 in./min, 0.04 in./min and 0.05 in./min each to investigate post-cracking behavior in various displacement rate in each case. Another purpose was to explore the behavior of post-peak behavior and tensile strength by change the height and diameter of the specimen. In the next step, the post-peak behavior and tensile strength with the change in height and diameter of the specimen were studied. In the set 6, six DPT samples and three DTT samples were cast with 0.35% V_f . Figure 3-2 is the detailed experimental program for FRC.

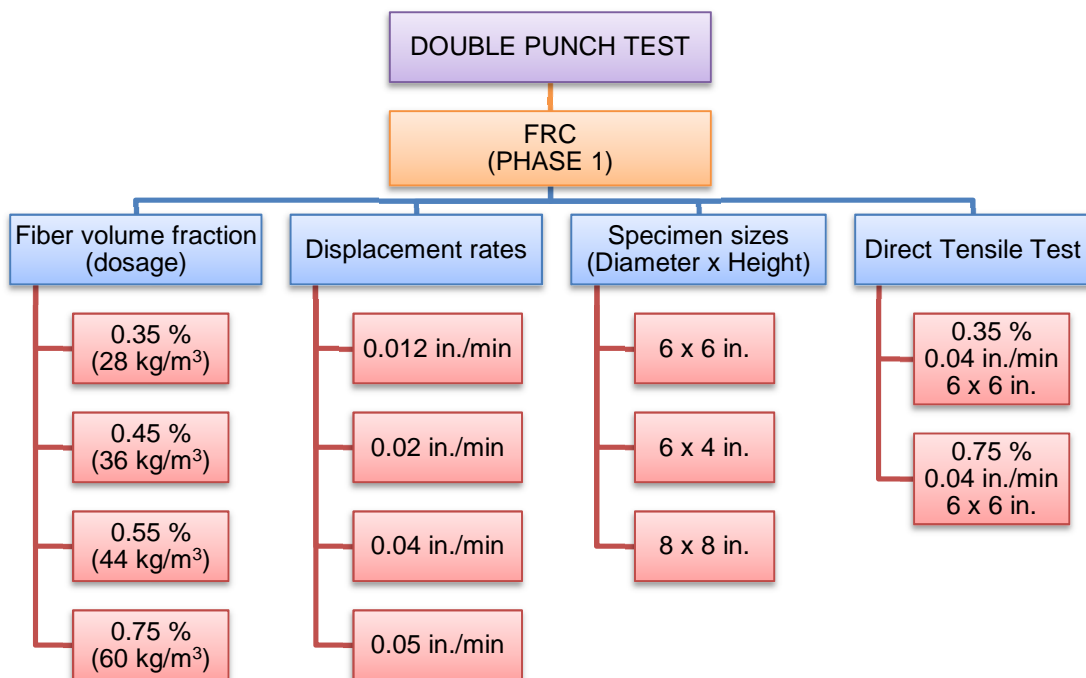


Figure 3-2: Experimental program for Phase 1 (FRC)

Then, six 6x12 cylinders (set 7 and set 8) were cast with 0.55% fibers by volume and tested with specimen sizes of 6x6 and 6x4 in at the rate of 0.04 in./min. Another set of six 6x12 cylinders were cast with 0.55% fibers and tested as a specimen size of 8x8 at the displacement rate of 0.04 in./min. The total of 95 DPT specimen was tested for Phase 1. Six DDT specimens, three each for 0.35% and 0.75% fibers (set 4 and set 6) were tested to compare the DPT result with the direct tensile test. The fiber volume of 0.35% and 0.75% were the lowest and the highest fiber content respectively in Phase 1 of this experimental program. The summary of experimental program for Phase 1 is shown in Table 3-1.

Table 3-1 Summary of Specimens for the experimental program for Phase 1.

S. N.	Volume fraction	Number – Size of specimen	Rate of displacement	Specimens	
			In. / min	No. of specimen ¹	Size of specimen
				inch	
Set 1	0.35%	6 no. of 6 x 12 for each set	0.02	12 (6B+6T)	6 x 6
Set 2	0.45%			12 (6B+6T)	6 x 6
Set 3	0.55%			12 (6B+6T)	6 x 6
Set 4	0.75%			12 (6B+6T)	6 x 6
Set 5	0.55%	8 no. of 6 x 12	0.012	2B	6 x 6
			0.02	2B	6 x 6
			0.04	2B	6 x 6
			0.05	2B	6 x 6
Set 6	0.35%	6 no. of 6 x 12	0.04	12 (6B+6T)	6 x 6
Set 7	0.55%	3 no. of 6 x 12	0.04	6 (3B+3T)	6 x 6
Set 8	0.55%	3 no. of 6 x 12	0.04	9 (3B+3M+3T)	6 x 4
Set 9	0.55%	6 no. of 8 x 16	0.04	12 (6B+6T)	8 x 8

Note:

- B, M and T represent the bottom, middle and top specimens, respectively
- All the sets were cast in different batches except for set 7 and 8. Test specimen for set 7 and 8 were cast at the same time using the same batch of concrete

Phase 2

For the second phase of this research, the UHP-FRC with six number of cylinders were cast with 3% steel fiber by volume and were tested at the displacement rate of 0.02 in./min (12 specimens) to compare with the SFRC results. For the next batches, six cylinders with 3% steel fiber were cast and were tested with 6x6 in. specimen and 6x4in. specimen. Similarly, nine cylinders were casted for UHP-FRC with 0.75% PE fiber and tested for 6x6 in. and 6x4 in. with 0.04 in./min displacement rate. Table 3-2 and Figure 3-3 summaries the experimental program for Phase 2.

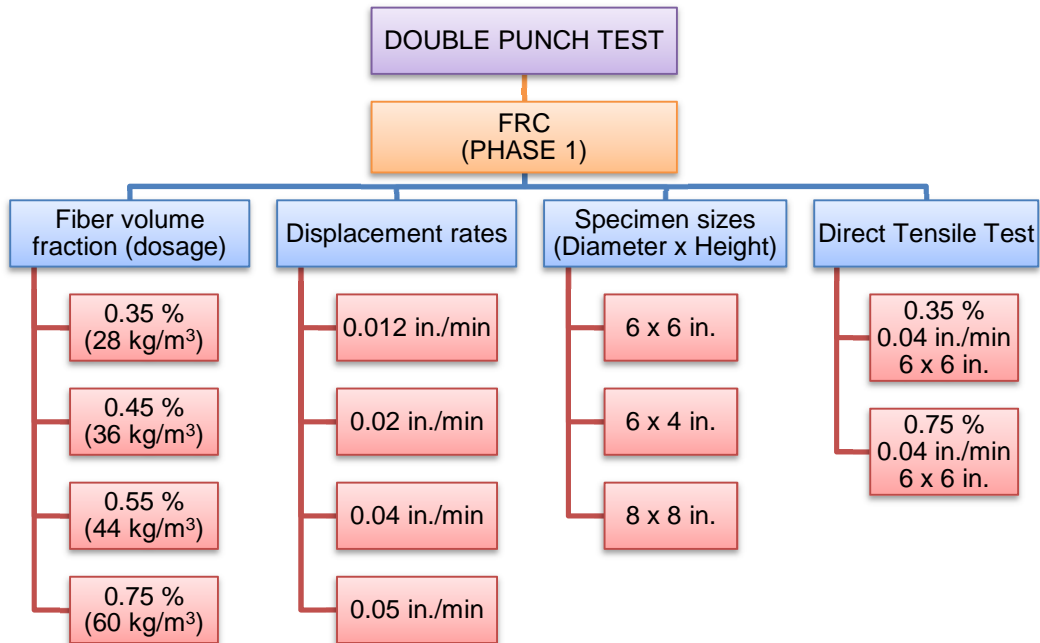


Figure 3-3: Experimental program for Phase 2 (UHP-FRC)

Table 3-2 Experimental program details for Phase 2.

S. N.	Volume fraction	Number – Size of specimen	Rate of displacement	Specimens	
			in / min	No. of specimen	Size of specimen
				inch	
Set 10	3% Steel	6 no. of 6 x 12	0.02	12 (6B+6T)	6 x 6
Set 11	3% Steel	3 no. of 6 x 12	0.04	6 (3B+3T)	6 x 6
Set 12	0.75% PE	6 no. of 6 x 12	0.04	12 (6B+6T)	6 x 6
Set 13	3% Steel	3 no. of 6 x 12	0.04	9 (3B+3M+3T)	6 x 4
Set 14	0.75% PE	3 no. of 6 x 12	0.04	9 (3B+3M+3T)	6 x 4

Note: B, M, and T represent the bottom, middle and top specimens, respectively

3.2 Fiber Type and geometry

Different types of fiber are used in the design and construction practices such as steel, glass, polypropylene, asbestos, organic and carbon. They are manufactured in different diameters, sizes, aspect ratio and forms (discrete or bundled) depending on the application and required mechanical properties of the concrete. In this research, long hooked end steel fibers are used in SFRC for phase 1 and micro-short straight steel fibers and polyethylene fibers are used in UHP-FRC for the phase 2.

3.2.1 Phase 1: SFRC

The fiber used in SFRC is Dramix® 5D steel fibers manufactured by Bekaert Corporation. The 5D fibers are bent five times at both ends that form a perfect hooked anchor inside the concrete. The fibers are glued together into bundles by a dissolvable glue for easy dosing and allowing the fibers to be uniformly distributed in the mixture as shown in Figure 3-4. The geometry and properties of an individual fiber are $L/d = 65$, $L = 2.36$ in. (60 mm), $d = 0.035$ in. (0.9 mm) and tensile strength of 334 ksi (2300MPa).



Figure 3-4 Dramix® 5D steel fibers

3.2.2 Phase 2: UHP-FRC

For UHP-FRC mix, the two types of fiber were used in two different mixes. First one is micro-short steel fibers (Dramix OL 13/0.20) with following mechanical properties: $L/d = 62$, $l = 0.51$ in. (13.0 mm), $d = 0.0083$ in. (0.21 mm), the tensile strength of 399 ksi (2750 MPa). These fibers are available in loose bundling form as shown in Figure 3-5(a). The second type of fiber were high modulus polyethylene (PE) fibers (Figure 3-5 (b)) with filament sizes = 10.0 denier per filament (dpf) (38.176 microns), $L = 0.5$ in. and breaking tenacity = 25.5 to 30.5 g/den. The details of fiber type and geometry are presented in Table 3-3.



Figure 3-5 (a) Micro-straight steel fibers (b) Polyethylene (PE) fibers

Table 3-3: Fiber type and geometry

Concrete Type	Fiber Type	Fiber Form	Length (L)	Diameter (D)	Aspect Ratio (L/D)	Tensile Strength
SFRC	Steel	Hooked-end (5-bend)	2.36 in. (60 mm)	0.035 in. (0.9 mm)	65	334 ksi (2300 MPa)
UHP-FRC	Steel	Micro-short straight	0.51 in. (13 mm)	0.0083 in. (0.21 mm)	62	399 ksi (2750 MPa)
UHP-FRC	Polyethylene (PE)	Precision cut filament	0.5 in. (12.7 mm)	10 dpf (38.176 microns)	332	breaking tenacity = 25.5 to 30.5 g/den.

3.3 Mix Design

3.3.1 SFRC Mix Design

The concrete mix design used for SFRC (Phase 1) were typically designed for varying fiber content; 0.35%, 0.45%, 0.55% and 0.75% by volume fraction to investigate the influence of fiber volume fraction in tensile strength and post-peak tensile characteristics. These are batched into 8 separate concrete mixture for this research. FRC mix proportion by weight for phase 1 is presented in Table 3-4.

Table 3-4: Mix Proportion by weight for SFRC

Mix Components	Mix proportion			
	$V_f = 0.35\%$	$V_f = 0.45\%$	$V_f = 0.55\%$	$V_f = 0.75\%$
Cement (Type 1)	1.00	1.00	1.00	1.00
Fly Ash (Class C)	0.5	0.5	0.5	0.5
Sand	2.3	2.3	2.3	2.3
Coarse aggregate ^[1]	0.5	0.5	0.5	0.5
Water ^[2]	0.53	0.53	0.53	0.53

Super-plasticizer	0.00077	0.00077	0.00077	0.00077
Steel Fiber (5D)	0.056	0.072	0.089	0.122

[1] Maximum size = 3/8in.; [2] WCM = 0.37

3.3.2 UHP-FRC Mix Design

The UHP-FRC material used in this research was developed based on the dense particle packing concept (Wille et al., 2012) at the University of Texas at Arlington (Aghdasi et al., 2015). The targeted 28-day compressive strength of the mix was 22,000 psi (150 MPa). The developed UHP-FRC is made of regular Type I cement, silica fume, Sand 1 (500 μm), Sand 2 (120 μm), glass powder (1.7 μm), and 3% by volume straight steel fibers (12.5 mm long and 0.175 mm dia.; tensile strength = 2200 MPa) or 0.75% by volume PE fibers. UHP-FRC mix proportion by weight for phase 2 is presented in Table 3-5.

Table 3-5 : Mix Proportions by weight for UHP-FRC (developed at UTA)

Mix Components	Steel (3%)	PE (0.75%)
Sand 1	0.43	0.43
Sand 2	0.37	0.37
Cement	1	1
Fly Ash	0.2	0.2
Glass Powder	0.25	0.25
Silica Fume	0.25	0.25
Water	0.29	0.29
Superplasticizer	0.021	0.021
Fibers	0.276	0.0085

3.4 Formwork for the specimen

The reusable 6in. x 12in. steel or plastic concrete cylinder molds were used to prepare the specimens for both phase 1 and phase 2 (Figure 3-6(a)). For the preparation of 8in. x16in. cylinder specimen, the formwork was made by using $\frac{3}{4}$ in. PVC pipe and $\frac{3}{4}$ in. PVC board which was glued together and made water-tight by using sealant (Figure 3-6 (b)). The formwork for dog bone specimen for the direct tensile test is as shown in Figure 3-7.

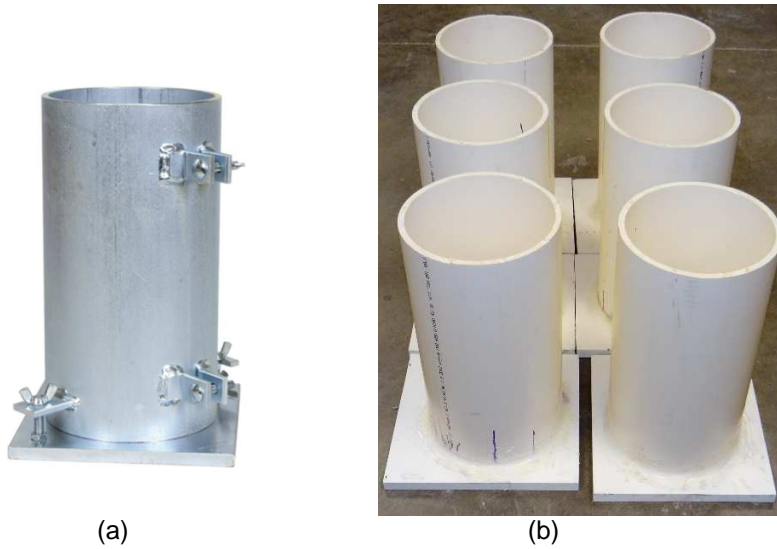


Figure 3-6: Mold for DPT specimens (a) 6 x 12 cylinder (b) 8 x 16 cylinder

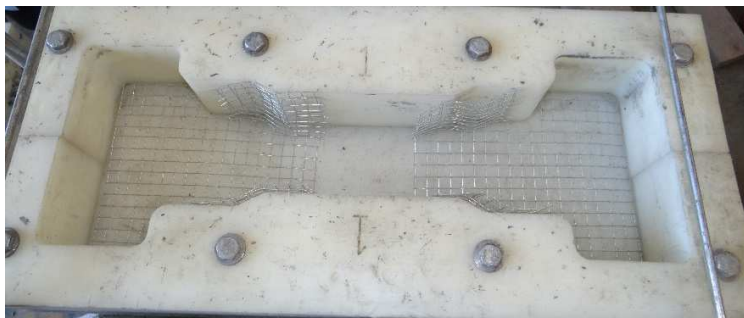


Figure 3-7 Formwork for Direct Tensile Testing specimen

3.5 Mixing of concrete, casting and curing of the specimen

The dry materials of the concrete ingredient were measured in buckets in pounds and transferred to a drum mixer /pan mixer for mixing process (Figure 3-8). The water was gradually added to get a good paste and the fibers were added when the mix was ready, then the fibers were added and mixed again for few minutes till a uniform mix was obtained. The concrete mix was poured into three layers and compacted with a table vibrator for both the 6in. x 12in. and 8in. x 16in. specimens. The market available molds of size 6in. x 12 in. cylinders and lab assembled molds of size 8in. x 16in. cylinders were made for DPT. Three 4in. x 8in. cylinders for SFRC and three 2.78in. cubes for UHP-FRC in each batch were used for the specimens to determine the 28-days compressive strength. The rotating pan mixer and self-loading concrete mixer were used to mix the UHP-FRC (Figure 3-9).



(a)



(b)

Figure 3-8: Concrete mixing using (a) drum mixer (b) pan mixer



(a)



(b)

Figure 3-9: Mixer used for UHP-FRC (a) Rotating pan mixer (b) Self-loading concrete mixer

In this research, large-scale dog bone specimens with a cross-section area of 16.0 in.² (10,323 mm²), 8 and 27 times larger than that of tested by Wille et al. (2011b) and Ranade et al. (2013), respectively, were made for the direct tensile test. After casting, all the specimens, DPT specimens, dog bone specimens, 2.78 in. cubes and 4in. x 8in. cylinders were stored in a curing room with the controlled environment at 27° C (80° F) and

100% relative humidity until the day of testing. Figure 3-10 and Figure 3-11 are the DPT samples and DTT samples after casting.



(a)



(b)

Figure 3-10: DPT cylinders after casting (a) 6in. x 12in. cylinder (b) 8in. x 16in. cylinder



(a)



(b)

Figure 3-11: DTT specimen (a) During casting (b) After casting

3.6 Specimen Preparation

The 6in. x 12in. specimen was cut into two 6in. x 6in. cylinders naming as top and bottom and 8in. x16in. specimen was cut into 8in. x 8in. cylinders by using a concrete saw (Figure 3-12). For 6 in. x 4 in. the specimen, a 6 x 12 in. cylinder was cut into three 6x4 in. specimen naming as the bottom, middle and top. The top and bottom surfaces were smoothed with sandstone or by grinding so that steel punches make uniform (flat) contact with the top and bottom faces of the specimen.



Figure 3-12 Preparation of DPT specimen using a concrete saw

3.7 Material test and instrumentation

3.7.1 Compressive strength test

The compressive strength of concrete mix is necessary to determine the quality of concrete mix which is determined by dividing the failure load by cross-sectional area resisting the load. In design and construction practice, the strength requirements are at the age of 28 days. The compressive strength is determined using three 4x8 in. cylinder for FRC in each batch/set. The load rate corresponding to a stress rate on the specimen of

0.25 ± 0.05 MPa/s [35 ± 7 psi/s] was used according to ASTM C39 (2016) for phase 1 (FRC). However, it is difficult to determine the compressive strength of very high strength concrete as it requires higher capacity machines for phase 2 (UHP-FRC). During this experimental program, 2.78 in. (70.7 mm) cubes that are acceptable alternative to standard 4 in. (102 mm) cylinders [Graybeal and Davis, 2008] are used to determine the compressive strength and to obtain the relationship between compressive strength and the uniaxial strains when loaded under compression for UHP-FRC. Trial mix was carried out before the actual cast of DPT and DTT specimen for UHP-FRC. For trial mix, three cubes were cast and were removed from molds after one day of casting, stored in curing room and tested on 14 days. The three 2.78 in. cubes (Figure 3-13) sampled from every casting were removed from molds after one day of casting, stored in curing room and tested after 28 days. No end surface preparation is required for testing these cubes and compression test machine and setup are as shown in Figure 3-14. The compression testing machine was used for the compressive strength test for 2.78-in. cubes for UHP-FRC and 4 in. x 8 in. cylinder for SFRC. The average value of two LVDTs was used to obtain the compressive stress-strain curve for UHP-FRC as shown Figure 3-14.



Figure 3-13: Preparation of 2.78 in. cube for UHP-FRC mix



Figure 3-14 Compressive strength test of UHP-FRC (2.78 in. cube)



(a)



(b)



(c)

Figure 3-15 (a) 4 x 8 in. cylinder after testing for FRC (b) Typical 2.78 in. cube after testing for UHP-FRC (steel fiber) (c) 2.78 in. cube after testing for UHP-FRC (PE fiber)

The spread value in accordance with ASTM C230 (2014) was used as a quick indicator to evaluate the flowability of trial mix. From Figure 3-17, the spread value for UHP-FRC with 3% steel fiber was found to be about 7.5 in. and UHP-FRC with 0.75% PE fiber was found to be about 7.0 in. These mixes are the proprietary product developed at UTA. (Parham et. al. 2016). The compressive stress-strain curve at 14 days for UHP-FRC are shown in Figure 3-18.



Figure 3-16 Flow table apparatus in accordance to ASTM C230 (2014)



(a)



(b)

Figure 3-17 Determination of spread value (flow diameter) in accordance to ASTM C230 (2014) (a) UHP-FRC with steel fiber (b) UHP-FRC with PE fiber

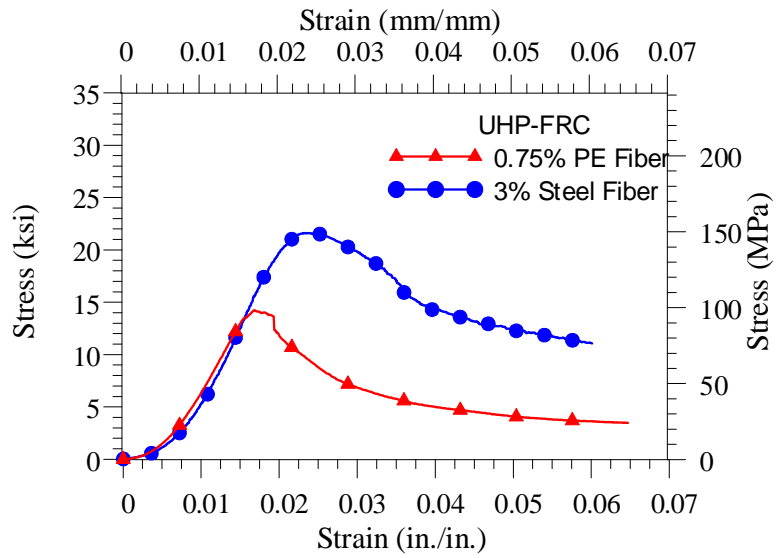


Figure 3-18: Compressive stress-strain curve for UHP-FRC (at 14 days from Trial mix)

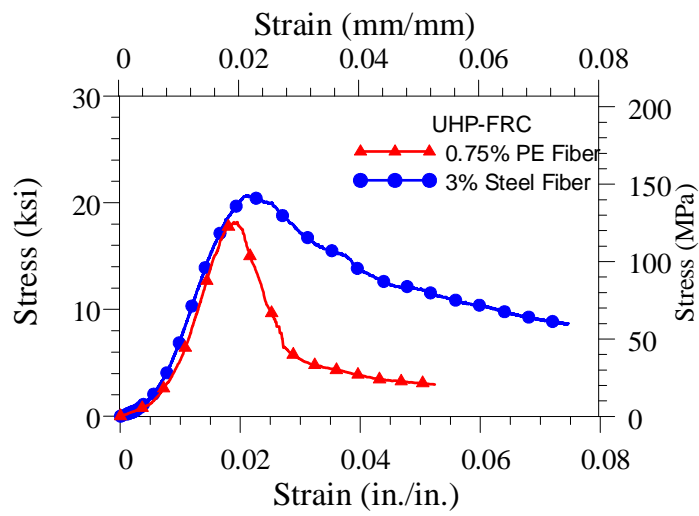


Figure 3-19: Compressive stress-strain curve for UHP-FRC (after 28 days from DPT casting)

3.7.2 Direct Tensile Test

The direct tensile test was carried in MTS Model 810 testing machine in CELB at UTA. In this research, large-scale dogbone specimens with a cross-section area of 16.0 in.² (10,323 mm²), 8 and 27 times larger than that tested by Wille et al. (2011b) and Ranade et al. (2013), respectively, were cast and tested. The tensile test setup and dimensions of this large-scale dogbone specimen are illustrated in Figure 3-20 and Figure 3-21. The test results from the direct tensile test for phase 1 and phase 2 are presented in Table 3-6.

Table 3-6: Test results from direct tensile test

S.N	Particulars	Number of DTT samples	Number of samples cracked beyond gauge length	Average Tensile Strength from DTT
Phase 1 (FRC)	0.35% (Set 6)	3	2	319.7 psi [2.2 MPa]
	0.75% (Set 4)	3	0	387.31 psi [2.67 MPa]
Phase 2 (UHP-FRC)	3% Steel (Set 10)	3	0	920.58 psi [6.35 MPa]
	3% Steel (Set 11 and 12)	3	0	1102.08 psi [7.60 MPa]
	0.75% PE (Set 13)	3	2	641.56 psi [4.43 MPa]

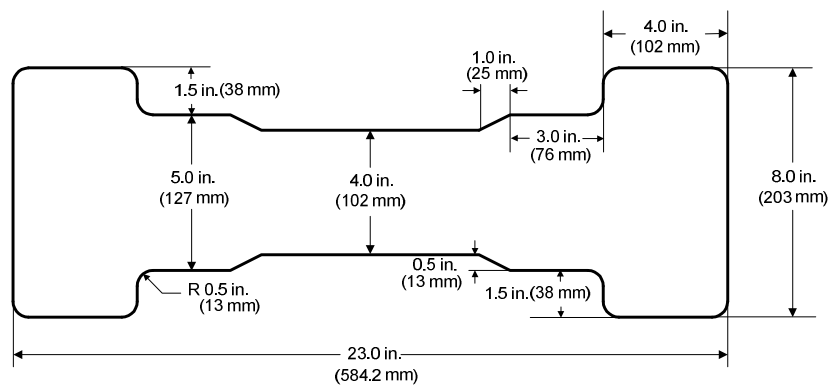
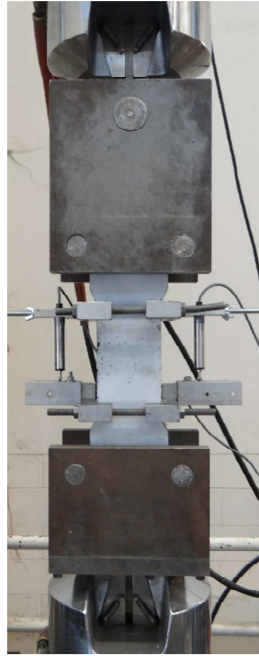
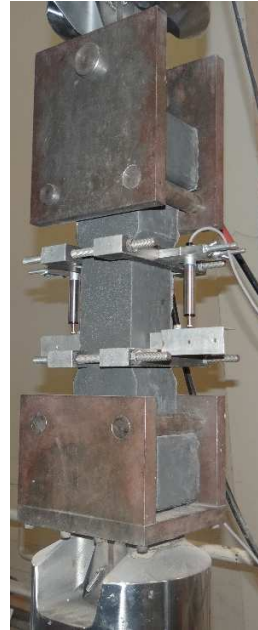


Figure 3-20: Dimension of DTT specimen



(a)



(b)

Figure 3-21 Direct tensile test (a) UHP-FRC with steel fibers (b) UHP-FRC with PE fibers



Figure 3-22: Crack location in direct tensile test

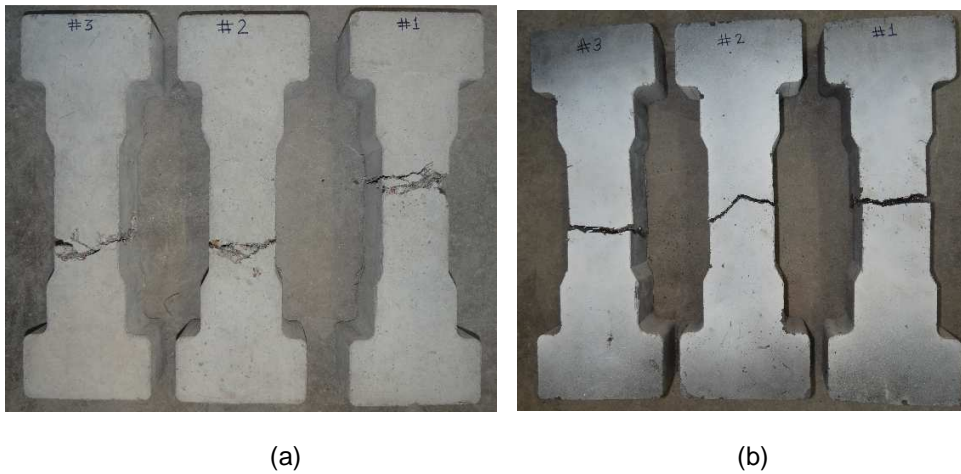


Figure 3-23: Specimen after testing (a) FRC (b) UHP-FRC

3.7.3 Double punch test setup

The double punch test has simple test setup consisting of a load cell, two Linear Variable Displacement Transducer (LVDTs), a circular extensometer and two steel punches. The tests were done in Tinius Olsen SuperL universal testing machine located in the Civil Engineering Laboratory Building (CELB) at UTA. The size of loading punches was 1.5 in. x 1 in. (diameter x height) for 6 in. x 6 in. specimens and 2 in. x 1 in. for 8 in. x 8 in. DPT specimens. These punches were centered on the top and bottom surfaces. The two LVDTs were used to measure the vertical deformation of the specimens and a circular extensometer was used to measure the total crack opening displacement. The load cell, LVDTs, and extensometer were connected to data acquisition box (DAQ) to record the data during the test. The overall view of the test setup is shown in Figure 3-24 and the dimensions of centering disk for 6 in. x 6 in. the specimen is shown in Figure 3-25.

According to Chen (1970), Equation (2-1) and Equation (2-2) are valid for $b/a \leq 4$ or $H/2a \leq 4$. For any ratio $b/a > 4$ or $H/2a > 4$, the limiting value $b = 4a$ or $H = 8a$ should be used in Equation (2-1) and Equation (2-2) for determination of tensile strength. The punch

diameter was increased to 2 inches and punch height remaining the same for testing the specimen size with height 8 in. and diameter 8 in. (Table 4-14). Hence, b/a ratio is also 4 with punch size of 2 in. x 1 in. for 8 in. x 8 in. specimen and Equation (2-2) is valid for determining tensile strength for 8 in. x 8 in. specimen.



(a)



(b)

Figure 3-24: DPT test setup for (a) SFRC (b) UHP-FRC

3.8 Test procedure of Double Punch Test

The double punch test is a simple and easy test to determine the tensile strength compared to the prevailing standard and non-standard methods. The typical test setup consists of a load cell, compression testing machine, two punches, two LVDTs (Linear Variable Differential Transducer) and a circumferential extensometer. The load cell is used to record the applied load, two LVDTs (Linear Variable Differential Transducer) are used to measure vertical axial deformation, the circumferential extensometer is used to measure the total crack opening displacement and all the instruments are connected to data acquisition system (DAQ) for recording.

The concrete cylinders of diameter 6 in. and height 12 in. are prepared and cured as per standard practice. The cylinders are cut into half and specimen size of 6 in. x 6 in. are prepared. So, there are two specimens as the bottom and a top portion of a cylinder of 6 in. x 12 in. Both top and bottom surfaces are smoothed and with sandstones. The loading punches, 1 in. height and 1.5 in. diameter for 6 in. x 6 in. and of 1 in. height and 2 in. diameter, are centered using a centering plate. At first, the bottom punch is centered and position in a compression testing machine followed by the top punch. The centering of the punch is necessary to avoid moment produced by eccentric loading. The specimens are placed in the direction of casting to make the uniformity in the test procedure.

The compressive force was applied at the rate 0.02 in./min and later changed to 0.04 in./min as explained in chapter 5. The slight modification in the testing procedure, shakedown, is suggested by Karki (2011) so that a more accurate stiffness of specimens could be gained at an early stage of the test. For this, the load is applied up to 2 kips and then unloaded down to 0.5 kips, and again reloaded to failure. The rate of the machine is kept constant for all stages i.e. from the starting of the test to the end.

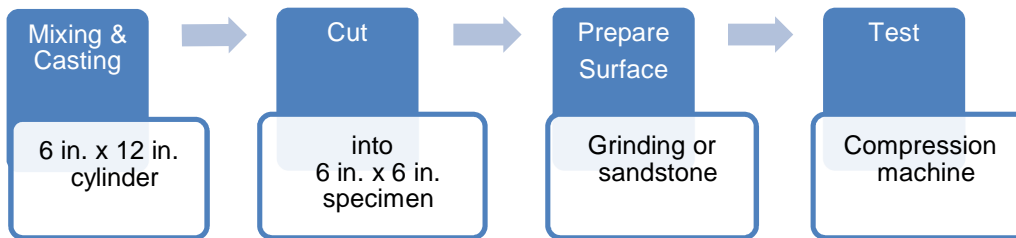


Figure 3-27: DPT preparation and testing process

The top and bottom halves of the 6-in. x 12 in. cylinders can give different curves if the fibers segregate during mixing. A good mixture generally gives much fewer variations. The load (P), deformation (δ) and total crack opening displacement (TCOD) are measured using the testing machine, LVDTs, and circumferential extensometer respectively. The tensile strength (f_t) and circumferential strain (ϵ) is calculated by

$$f_t = \frac{0.75 \times P}{\pi(1.2bh - a^2)}$$

$$\epsilon = \frac{P_1 - P_0}{P_0}$$

where $P_1 (= \pi D_1)$ is the final perimeter and $P_0 (= \pi D_0)$ is the initial perimeter of DPT specimen.

The results obtained from double punch test for FRC and UHP-FRC are included in Chapter 4.

Chapter 4

Experimental Results

4.1 General

The experimental results are used to explain the effects of test variables and to exhibit the range of characteristic behavior observed during the double punch test. The test results presented in this chapter are the average of a series of samples in a set. The typical statistical analysis results for each batch in all the phases are demonstrated and summarized to evaluate the reliability and reproducibility of the double punch test. The results, peak load, for the top and bottom specimens showed a variation of less than 15% and hence were considered alike and were grouped for simplification. The tensile strength is calculated using Equation (2-2) for all the sets.

$$f_t = \frac{0.75 \times P}{\pi(1.2bh - a^2)}$$

For comparison purpose, each test variable was analyzed based on peak load; peak tensile strength; residual strength at 0.10-inch deflection for comparison purposes; crack opening at strains 0.003, 0.01, 0.025 and 0.05; using statistical parameters such as average, standard deviation and coefficient of variation. The graphs for load versus axial deformation, stress versus circumferential strain and axial deformation versus circumferential strain are presented for each series of tests. The detail calculation and graphs for all the specimens for phase 1 and phase 2 are shown in the Appendix A and B.

4.2 Double Punch Test with FRC (Phase 1)

In this phase, the double punch test method was used to determine the equivalent tensile strength and it was compared to the results with the direct tensile test for FRC. The comparison was carried on the following criteria:

- 1) To examine the influence of fiber dosage in conventional SFRC.
- 2) To explore the effect of displacement rate for the experiment.
- 3) To investigate the effect of specimen sizes in DPT.
- 4) To compare the results obtained from DPT with the direct tensile test.

4.2.1 Different fiber dosage for FRC

6x12 in. cylinders were casted with 0.35%, 0.45%, 0.55% and 0.75% fiber volume fraction, six in each batch. The 6x12 in. specimens were cut into two 6x6 in. cylinders, named as top and bottom, by using a concrete saw. The top and bottom surfaces were smoothed with sandstone or by grinding. The test was operated at the displacement rate of 0.02 in/min (Mollins et. al. 2007, Pujadas et. al 2012 and Blanco et. al. 2014). The equivalent tensile strength was calculated using modified Chen's equation (2-2). The same procedure of DPT method as mentioned in section 3.8 was used. Table 4-1 shows the information of each batch for comparative assessment of SFRC with different fiber volume fraction.

Table 4-1: Test parameter for FRC with various fiber dosages

S.N	Set 1	Set 2	Set 3	Set 4
Fiber volume fraction (Vf)	0.35%	0.45%	0.55%	0.75%
Fiber dosage	28 kg/m ³	36 kg/m ³	44 kg/m ³	60 kg/m ³
Displacement rate	0.02 in/min [0.5 mm/min]	0.02 in/min [0.5 mm/min]	0.02 in/min [0.5 mm/min]	0.02 in/min [0.5 mm/min]
Specimen size (Diameter x Height)	6 in. x 6 in. [152 mm x 152 mm]	6 in. x 6 in. [152 mm x 152 mm]	6 in. x 6 in. [152 mm x 152 mm]	6 in. x 6 in. [152 mm x 152 mm]
Punch Size (Diameter x Height)	1.5 in. x 1 in. [38 mm x 25.4 mm]	1.5 in. x 1 in. [38 mm x 25.4 mm]	1.5 in. x 1 in. [38 mm x 25.4 mm]	1.5 in. x 1 in. [38 mm x 25.4 mm]
Total number of samples	12	12	12	12

Number of bottom samples	6	6	6	6
Number of top samples	6	6	6	6

Table 4-2 shows important characteristics for the comparative peak and post-peak evaluation of FRC with 0.35%, 0.45%, 0.55% and 0.75% fiber volume. The average peak load and average peak tensile strength were found to be highest for 0.45% fiber volume.

Table 4-2: Comparison of peak load, peak tensile strength and residual tensile strength at 0.3%, 1%, 2.5% and 5% circumferential strain for various fiber volume fraction

Parameters		Set 1 0.35%	Set 2 0.45%	Set 3 0.55%	Set 4 0.75%
Average compressive strength		5.83 ksi [40.2 MPa]	5.25 ksi [36.2 MPa]	5.40 ksi [37.2 MPa]	6.66 ksi [45.9 MPa]
Average peak load		35.6 kips [158.3 kN]	36.9 kips [164 kN]	31.8 kips [141.6 kN]	30.4 kips [135.02 kN]
Average peak tensile strength		403.7 psi [2.8 MPa]	418.5 psi [2.9 MPa]	361.2 psi [2.5 MPa]	344.4 psi [2.4 MPa]
Average residual strength at 0.1 deformation		128.9 psi [0.9 MPa]	188 psi [1.3 MPa]	124 psi [1.2 MPa]	192 psi [1.3 MPa]
Corresponding tensile stress at	0.003 in./in. [0.3%] circumferential strain	356.5 psi [2.5 MPa]	331.7 psi [2.3 MPa]	303.1 psi [2.1 MPa]	305.9 psi [2.1 MPa]
	0.01 in./in. [1%] circumferential strain	167.4 psi [1.2 MPa]	215.2 psi [1.48 MPa]	211.7 psi [1.46 MPa]	228.3 psi [1.57 MPa]
	0.025 in./in. [2.5%] circumferential strain	111.2 psi [0.8 MPa]	140.9 psi [0.97 MPa]	141.6 psi [0.98 MPa]	161.7 psi [1.1 MPa]
	0.05 in./in. [5%] circumferential strain	60.2 psi [0.41 MPa]	-	75.2 psi [0.52 MPa]	88.5 psi [0.61 MPa]

Figure 4-1 shows the load versus axial deformation curve and Figure 4-2 shows the equivalent tensile stress versus circumferential strain relation for fiber volume fractions

0.35% (28 kg/m³), 0.45% (36 kg/m³), 0.55% (44kg/m³), and 0.75% (60 kg/m³). The slopes in Figure 4-2 up to the peak loads in all cases are similar and after peak loads the variation becomes significant. With the increase in dosage of fibers, the post-cracking (or post-peak) curves drop more gradually. Note as shown in Figure 4-1 and Figure 4-2, in general, for an FRC with higher fiber dosage, it carries a higher residual load at the same circumferential strains (or average crack openings).

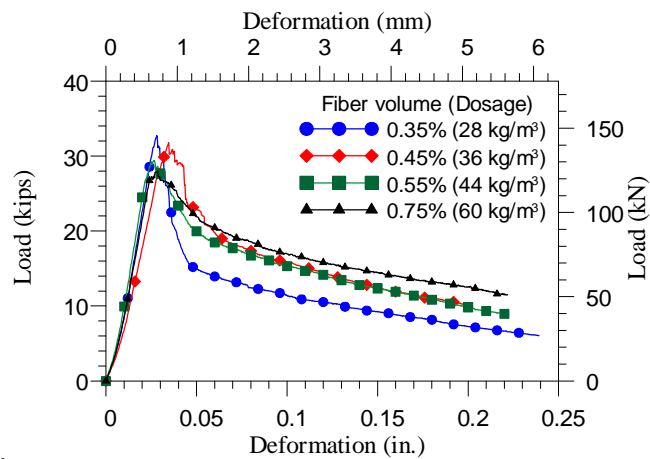


Figure 4-1 Load vs deformation for different fiber volume fraction

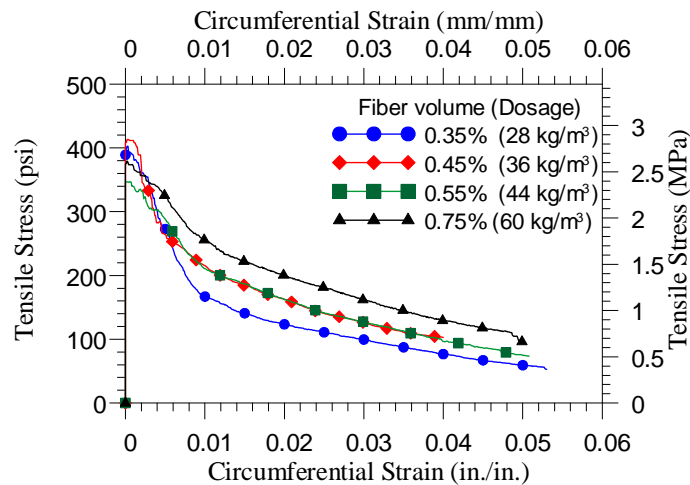


Figure 4-2 Tensile stress versus circumferential strain for different fiber volume fraction

The coefficient of variation (COV) for peak tensile strength, peak load and residual tensile strength at 0.3% (0.003 in./in.), 1% 0.01 (in./in.), 2.5% (0.025 in./in) and 5% (0.05 in./in.) was used as parameters to explain the reliability of DPT method as presented in Table 4-3. The COV for peak load of 0.45% was found to be higher among all four-fiber dosage. Figure 4-3, Figure 4-4 and Figure 4-5 are the tested samples of DPT showing crack pattern in plan view and along the length.

Table 4-3 Comparison of COV for Set 1, 2, 3 and 4 (including top and bottom samples).

S.N	COV		Set 1	Set 2	Set 3	Set 4
			0.35%	0.45%	0.55%	0.75%
1.	COV for peak load		7.1 %	14.2 %	7.9 %	8.9 %
2.	COV for peak tensile strength		7.1 %	14.2 %	7.9 %	8.9 %
3.	COV for residual strength at 0.1 deformation		23.5 %	15.4 %	25.4 %	28.7 %
4.	COV of residual tensile strength at	0.003 in./in. [0.3%] circumferential strain	11.0 %	24.8 %	14.5 %	13.5 %
5.		0.01 in./in. [1%] circumferential strain	23.3 %	16.5 %	19.9 %	24.5 %
6.		0.025 in./in. [2.5%] circumferential strain	19.9 %	15.4 %	24.1 %	28.1 %
7.		0.05 in./in. [5%] circumferential strain	24.5 %	-	44.5 %	31.3 %

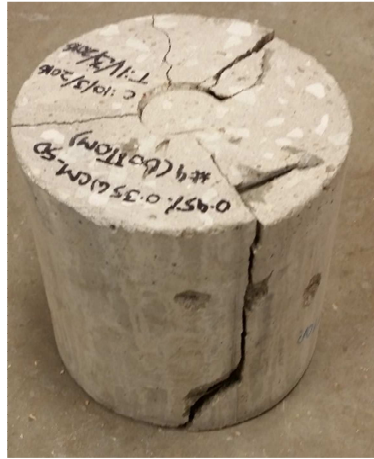


(a)



(b)

Figure 4-3: (a) A bottom sample (Set 4) (b) A top sample (Set 1)



(a)



(b)

Figure 4-4: (a) Crack pattern (Set 2) (b) Crack along the length (Set 4)



Figure 4-5: Bottom and Top specimen (Set 4)

The load-deformation curve for six bottom and six top samples with 0.35% Vf (Set 1) is shown in the Figure 4-6 and Figure 4-7 respectively. For bottom samples, COV at peak load is about 8.3% and COV at 0.1 in deformation is 16.2 % and COV at 0.2 in. about 11.4 %. Similarly, for top samples, COV at peak load is about 5.1 % and COV at 0.1 in

deformation is 20 % and COV at 0.2 in. about 16.6 %. These peak post points of 0.1 in. and 0.15 in. are selected randomly for comparison purpose. The detail calculation and graphs for other sets are presented in Appendix-A.

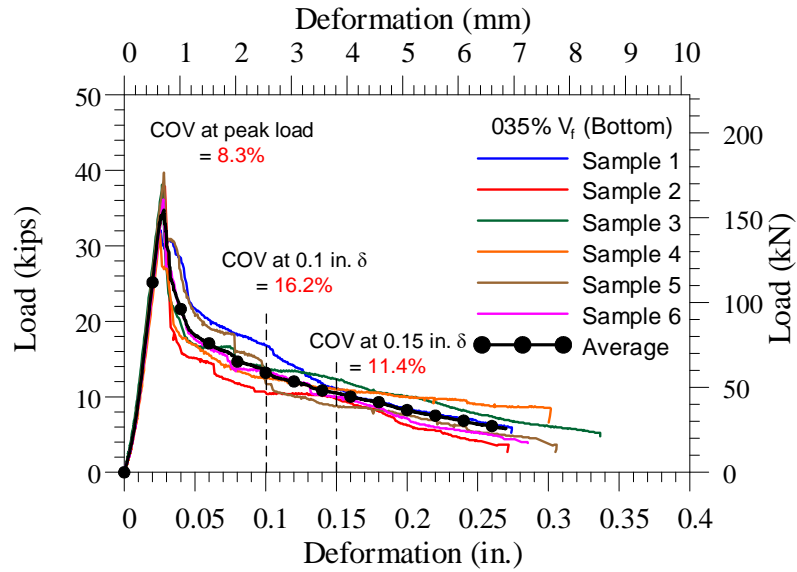


Figure 4-6: Load vs. deformation for bottom samples with 0.35% V_f (Set 1)

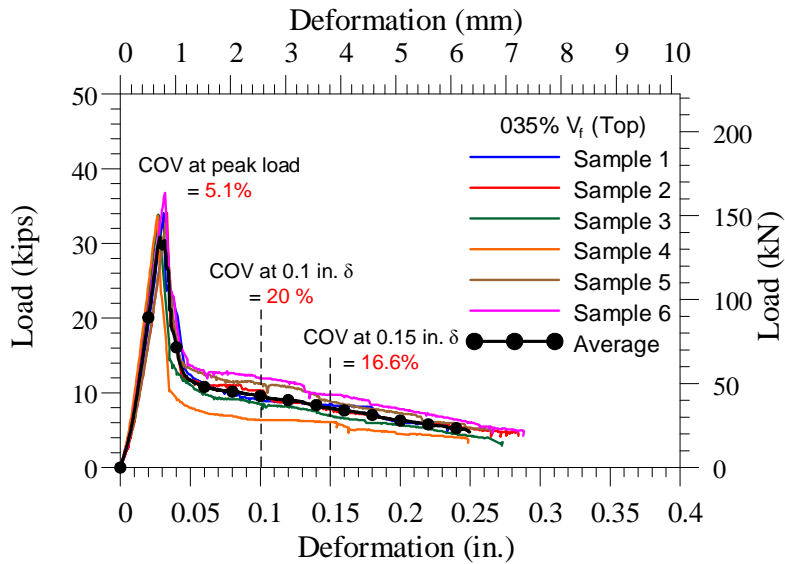
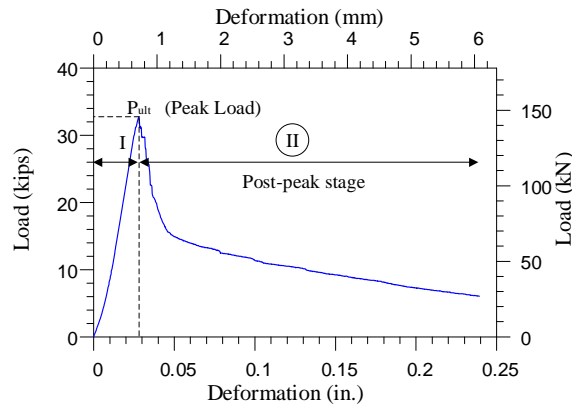


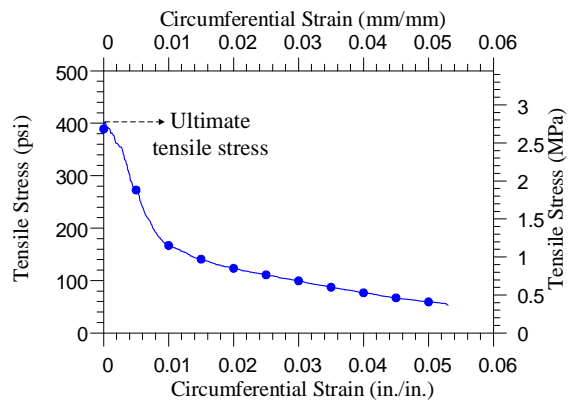
Figure 4-7: Load vs. deformation for top samples with 0.35% V_f (Set 1)

4.2.2 Determination of relation between deformation and circumferential strain

For conventional FRC (with normal compressive strength and a fiber volume fraction approximately less than 1% or 80 kg/m³), the measured circumferential strain along the ascending part of the load and axial deformation (δ) curve is very small and negligible (Figure 4-8 (a) and (b)). However, in the post-peak regime (shown by II in Figure 4-8 (a)) the crack opening or *total crack opening displacement* (TCOD) becomes noticeable and increases at a faster rate.



(a)



(b)

Figure 4-8 (a) Typical load vs deformation for FRC (b) Typical tensile stress vs circumferential strain for FRC

From Figure 4-9, it can be observed that there is an abrupt increase in circumferential elongation at a deformation of 0.03 in. (in some cases 0.04 in.), and maintaining an approximately constant rate up to the end of testing. This could be due to the fact that it requires more energy before initial cracking to form a conical wedge under the punch. Since crack width after peak strength is of interest to the engineering community, only the deformation and circumferential strain after the peak load is considered as shown in Figure 4-10. Figure 4-10 shows that the relationship between deformation and circumferential strain is very close to a linear relationship. Therefore, the slope (α) was determined by means of a linear regression using the data obtained from this experimental program.

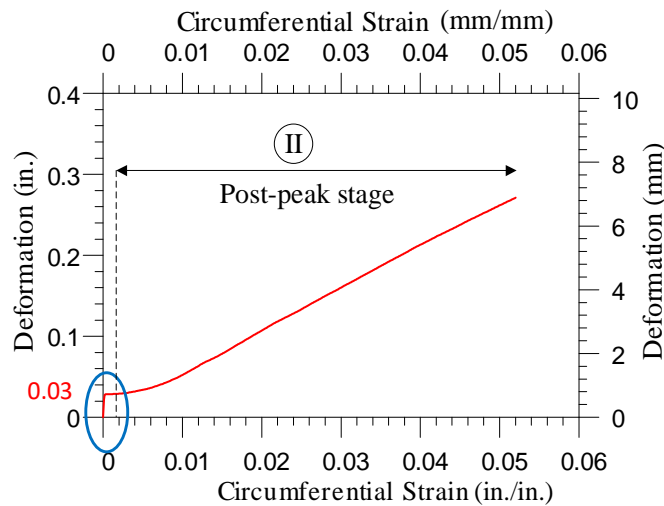


Figure 4-9: Total Deformation vs circumferential strain

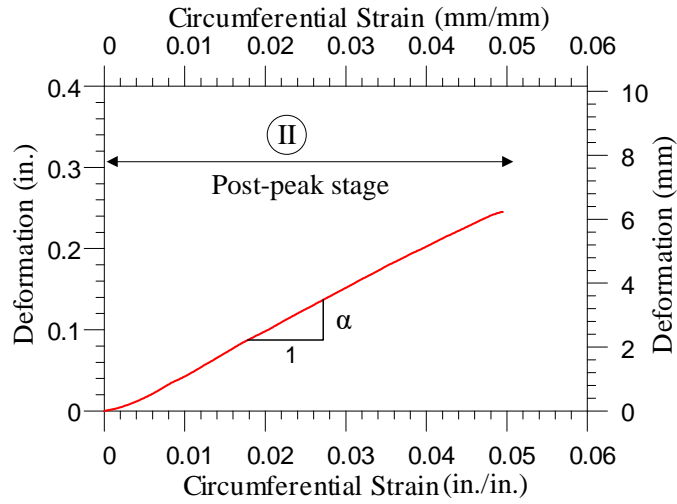


Figure 4-10: Post-peak Deformation vs circumferential strain (after peak only)

Figure 4-11 shows complete δ (vertical deformation) and ϵ (circumferential strain) curves including both pre-peak and after-peak responses, while Figure 4-12 shows the δ and ϵ relation only after the peak load for fiber volume fractions 0.35% (28 kg/m³), 0.45% (36 kg/m³), 0.55% (44kg/m³), and 0.75% (60 kg/m³). A linear regression analysis was performed. The results show good accuracy with R² almost equal to 1, regardless of fiber content and post-cracking behavior. Note while it seems that the fiber dosage has some minor effect on the slope (α), its effect is relatively greater in the residual stresses (Figure 4-2). Therefore, it is decided to keep α as a constant irrespective of the fiber dosage and let the residual stress to reflect the effect of fiber dosage.

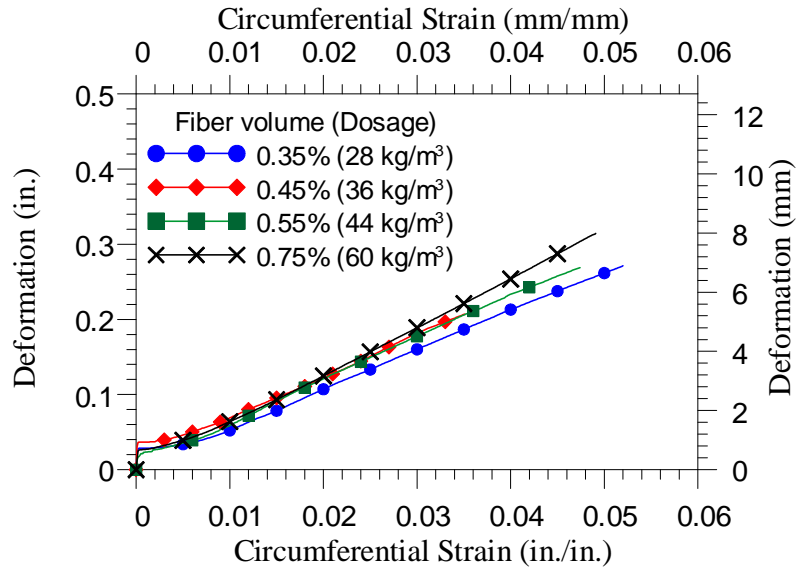


Figure 4-11: δ vs ϵ (before and after peak)

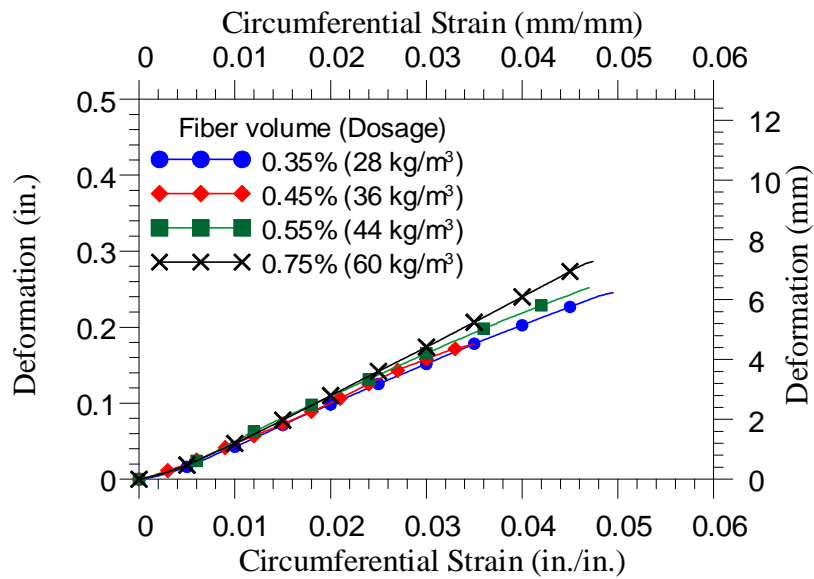


Figure 4-12 δ_P vs ϵ_P (after peak only)

Table 4-4 summarizes the values of α (slope of deformation and circumferential strain curve) from four series of test. α is calculated for 12 specimens in each series. It can be observed that the average α is between 5.1 to 5.9, and can be conservatively taken

as 5.0. α is in general independent of fiber content and displacement rate. Thus, this provides the direct relationship between δ_P and ϵ_P given as:

$$\delta_P = \alpha \epsilon_P \quad \text{where, } \alpha = 5 \quad \text{(Equation 4-1)}$$

$$\delta_P = \delta - \delta_0$$

where δ_0 = deformation at peak load

δ = total vertical deformation from beginning of test

δ_P = post peak deformation

ϵ_P = circumferential strain after peak

Table 4-4: Determination of α

Set	Set 1	Set 2	Set 3	Set 4
V_f	0.35%	0.45%	0.55%	0.75%
Fiber Dosage	28 kg/m ³	36 kg/m ³	44 kg/m ³	60 kg/m ³
Rate (in./min)	0.02	0.02	0.02	0.02
Size (diameter x height)	6 x 6 in.	6 x 6 in.	6 x 6 in.	6 x 6 in.
Sample	α values			
B 1	5.40	5.17	5.83	6.79
B 2	4.66	5.21	7.20	6.43
B 3	6.26	5.50	5.76	7.03
B 4	5.39	4.82	5.83	6.79
B 5	4.64	4.82	4.12	6.35
B 6	5.40	5.36	3.55	6.31
T 1	5.31	5.92	7.64	5.26
T 2	5.33	5.94	7.14	6.42
T 3	4.30	4.58	5.07	4.95
T 4	4.62	4.77	4.55	3.80
T 5	5.36	4.90	5.03	5.40
T 6	4.71	4.55	3.79	4.92
Mean	5.12	5.13	5.5	5.9
Standard deviation	0.5	0.5	1.4	1.0

Note: B and T represent the bottom and top specimens, respectively

The data (Table 4-4) distribution and variability of α for four-fiber dosages are given in Figure 4-13. Mark (X) denotes the mean values and horizontal lines at ends show the minimum and maximum values.

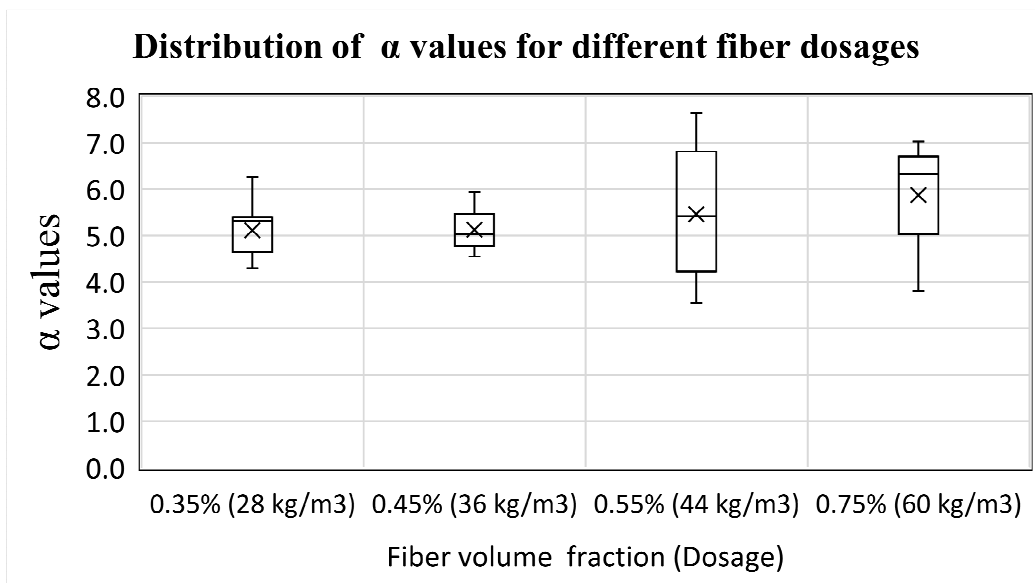


Figure 4-13: Distribution of values for different fiber dosage

4.2.3 Computation of average crack width:

Let D_0 and D_1 be the initial diameter before loading and a diameter under loading of a test specimen. D_1 is measured by a circumferential extensometer. The total crack width along the circumference (TCW) is computed by the increase in the perimeter (P) of the cylinder. TWC at the post-peak stage is represented by:

$$TCW = P_1 - P_0$$

The circumferential strain (ϵ) is the ratio of change in the perimeter of the cylinder to the original perimeter which is given by:

$$\varepsilon = \frac{P_1 - P_0}{P_0}$$

where, P_1 = Final perimeter = πD_1

P_0 = Initial perimeter = πD_0

$$P_1 = P_0(1 + \varepsilon)$$

Since there is no circumferential strain measured before peak for FRC, the initial perimeter (πD_0) is equivalent to the perimeter at the peak and ε_p (circumferential strain at peak) is also the same as ε . The cracks are developed radially from the center to the circumference so average crack width (CW) in a specimen can be determined by dividing the total crack width by the number of cracks (N).

$$CW = \frac{P_1 - P_0}{N} = \frac{P_0 \varepsilon}{N} = \frac{\pi D_0 \times \varepsilon_p}{N}$$

Use Eq. (4-1): $\delta_P = \alpha \varepsilon_p$,

$$CW = \frac{\pi D_0 \times \delta_P}{\alpha N} \quad \text{(Equation 4-2)}$$

The number of cracks is determined by visual inspection after the test. N is in general in the range 2 to 6 (Figure 4-10). The numerical average crack number from Figure 4-10 is 4.2. From this research, it was observed that the most common number of cracks is 4 as about 60% of the specimen has four number of cracks. Only cracks that started radially from the center and propagated at least up to the mid-height of the specimen were considered. The very small minor cracks are considered having less effect on the residual stress.

Table 4-5: Percentage of samples with respective crack number

No of cracks	No. of samples	Percentage (%)
2	2	4.2
3	6	12.5
4	27	56.3
5	9	18.8
6	4	8.3
Total samples	48	

For DPT using 6x12 in. cylinders the average crack width (CW) is determined by substituting $D_0 = 6$ in., $N = 4$, and $\alpha = 5$ in Equation 4-2:

$$CW = \frac{6\pi}{5} \times \frac{\delta_p}{N} = \frac{3.78\delta_p}{N} \quad \text{(Equation 4-3)}$$

4.2.4 Verification from measured maximum crack width

While Equation 4-3 can be used to obtain a reasonable average crack width at certain deformation, estimation of the maximum crack width can be also important. Maximum crack width was measured using crack width comparator and visual inspection and it was measured many times at various displacement. However, the maximum crack width does not have a linear relation with the axial deformation. Table 4-6 and Table 4-7 show the maximum measured crack widths at various deformations for a sample in each batch. The measured maximum crack widths are compared with predicted maximum crack widths (Figure 4-14) along the deformation during and at the end of the tests. However, the number of cracks is counted at the end of the experiment as it is difficult to count crack number while the testing is in progress. The measured maximum crack widths during and at the end of tests were compared with the predicted maximum crack width given by Equation (4-5) for four selected specimens as shown Table 4-6 and Table 4-7.

Table 4-6: Measurement of crack width during experiments for one randomly selected sample from sets of 0.35% and 0.45% V_f

0.35%					0.45%				
δ_P	Measured Crack Width		Predicted Crack width	(a)/(b)	δ_P	Measured Crack Width		Predicted Crack width	(a)/(b)
in.	mm	in. (a)	in. (b)		in.	mm	in. (a)	in. (b)	
0.030	0.25	0.010	0.009	1.09	0.035	0.25	0.010	0.012	0.84
0.036	0.35	0.014	0.012	1.15	0.059	0.8	0.031	0.026	1.23
0.047	0.5	0.020	0.018	1.10	0.089	1.5	0.059	0.047	1.25
0.052	0.6	0.024	0.021	1.13	0.109	2	0.079	0.064	1.24
0.061	0.8	0.031	0.027	1.18	0.168	3.5	0.138	0.123	1.12
0.079	1	0.039	0.039	1.00	0.199	5	0.197	0.158	1.25
0.109	2	0.079	0.064	1.23	0.232	6	0.236	0.199	1.19
0.168	4	0.157	0.123	1.28	0.254	7	0.276	0.228	1.21
0.240	6	0.236	0.209	1.13	0.294	8	0.315	0.284	1.11
0.263	7	0.276	0.240	1.15	0.323	9	0.354	0.327	1.08

Table 4-7: Measurement of crack width during experiments for one selected sample from sets of 0.55% and 0.75% V_f

0.55%					0.75%				
δ_P	Measured Crack Width		Predicted Crack width	(a)/(b)	δ_P	Measured Crack Width		Predicted Crack width	(a)/(b)
in.	mm	in. (a)	in. (b)		in.	mm	in. (a)	in. (b)	
0.034	0.3	0.012	0.011	1.06	0.033	0.25	0.010	0.011	0.91
0.045	0.5	0.020	0.017	1.16	0.041	0.35	0.014	0.015	0.93
0.059	0.625	0.025	0.025	0.98	0.050	0.5	0.020	0.020	0.98
0.071	0.75	0.030	0.034	0.88	0.058	0.6	0.024	0.025	0.96
0.087	1	0.039	0.046	0.86	0.065	0.8	0.031	0.030	1.06
0.101	1.25	0.049	0.057	0.86	0.075	1	0.039	0.036	1.08
0.115	1.5	0.059	0.069	0.85	0.092	1.5	0.059	0.050	1.19
0.132	1.8	0.071	0.085	0.83	0.151	3	0.118	0.104	1.13
0.141	2	0.079	0.094	0.84	0.194	4	0.157	0.152	1.03
0.171	3	0.118	0.126	0.94	0.244	7	0.276	0.215	1.28
0.238	5	0.197	0.207	0.95	0.276	8	0.315	0.258	1.22
0.267	6	0.236	0.246	0.96	0.323	8	0.315	0.327	0.96
0.286	7	0.276	0.272	1.01	0.363	10	0.394	0.389	1.01

Unlike the average crack width, the maximum crack width does not show a linear relation with the deformation, δ . A nonlinear relation between the maximum crack width and δ was developed based on the available data. Table 4-8 and Table 4-9 summarize the data analysis and the relation between deformation and predicated maximum crack width using a non-linear regression (obtained using MATLAB) is in the form of

$\delta_P = \lambda C_{\max}^\beta$ where δ_P = post peak deformation and C_{\max} = predicted maximum crack width.

Table 4-8: Relation between deformation and measured maximum crack width (48 samples)

S.N	Λ				β			
	0.35%	0.45%	0.55%	0.75%	0.35%	0.45%	0.55%	0.75%
B 1	0.5169	0.8423	0.4345	1.1086	0.6459	0.8291	0.5535	0.8488
B 2	0.9242	1.4459	0.6478	0.8142	0.9901	0.7716	0.6119	0.7506
B 3	0.4464	0.5915	0.4859	0.9318	0.6378	0.5459	0.6014	0.7444
B 4	0.5710	0.5192	1.0778	1.0596	0.8652	0.6116	0.7228	0.7411
B 5	0.3250	0.8683	0.8271	0.6190	0.5664	0.6590	0.9637	0.6290
B 6	0.2007	0.6190	0.3702	0.5083	0.3108	0.6290	0.4705	0.4992
T 1	1.1889	0.5147	0.7436	1.5000	0.9792	0.4452	0.8154	1.2094
T 2	0.9398	0.6343	0.2948	0.6998	0.8914	0.7079	0.4031	0.5804
T 3	0.2304	0.4936	0.4467	1.0018	0.2960	0.5363	0.5417	0.7611
T 4	0.7145	0.7823	0.9207	0.4045	0.8297	0.7604	0.8614	0.5787
T 5	0.2416	0.5745	0.5077	0.8246	0.3593	0.5601	0.6818	0.7543
T 6	0.2730	0.6478	0.6982	0.6256	0.3633	0.6119	0.8567	0.7070
Average	0.5477	0.7111	0.6213	0.8415	0.6446	0.6390	0.6736	0.7336

Note: B and T represent the bottom and top specimens, respectively

Table 4-9: Average values of coefficient λ and β

S.N	λ	β
1	0.548	0.645
2	0.711	0.639
3	0.621	0.674
4	0.841	0.734
Average	0.680	0.673

Therefore,

$$\delta_P = 0.68 C_{\max}^{0.67} \quad (\text{Equation 4-4})$$

Also, the above equation can be written as:

$$C_{\max} = 1.78 \delta_P^{1.5} \quad (\text{Equation 4-5})$$

where, δ_P = post peak deformation (in.)

C_{\max} = predicated maximum crack width (in.)

Equation 4-5 represents the approximate median value of the measured maximum crack width. To be more conservative, an upper bound C_{\max} can be estimated by using the following equation.

$$C_{\max} = 1.78 \delta_P^{1.2} \quad (\text{Equation 4-6})$$

The measured maximum crack width for 48 samples of fiber volume fractions 0.35% (28 kg/m³), 0.45% (36 kg/m³), 0.55% (44kg/m³), and 0.75% (60 kg/m³) are shown in Figure 4-14. The data shows that the maximum crack width does not have a direct relationship with the fiber dosage. The predicted maximum crack width Equation 4-5 and Equation 4-6 are also shown. As can be seen, the maximum crack widths have much less variation when the post-peak deformation is less than 0.1 in.

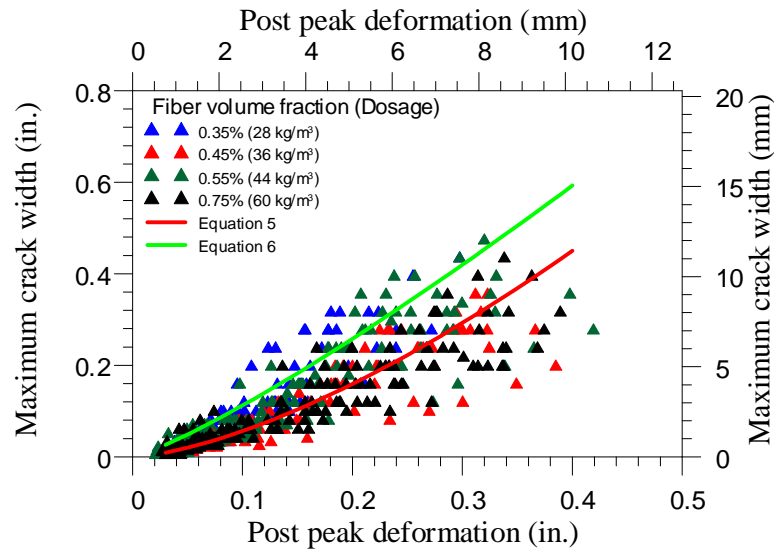


Figure 4-14: Post-peak deformation vs maximum crack width (48 samples)

4.2.5 Effects of displacement rate

Chen (1970) recommended using a stressing rate of 100-200 psi per minute for DPT method. In 1972, Colgrove and Chen reported that increasing the stress rate for DPT gives lower strength for regular concrete specimens and higher strength for lightweight concrete specimens. While using the stress-controlled or load controlled testing procedure, it was difficult to control the shakedown procedure of DPT using a simple machine. On the other hand, soft load-controlled machines may result in the sample being damaged with no effective results. It is most appropriate to do a tensile test in displacement control mode as similar to direct tensile test because the displacement-controlled machines can have a more stable control. It has been found that low strength concrete is much more sensitive to strain/displacement rate than high strength concrete due to fracture and crack propagation rate in the concrete matrix. The strength of the concrete has a major effect on the post-cracking performance of FRC.

The displacement rate used in the study of the influence of fiber volume fraction in DPT was 0.02 in./min (0.5 mm/min) which was also used by various researchers (Mollins et. al. 2007, Pujadas et. al 2012 and Blanco et. al. 2014). It is observed that the displacement rate of 0.02 in./min (0.5 mm/min) for FRC requires about 25 to 30 minutes to complete the test. However, the present 25-30 minutes is considered lengthy for a quality control (QC) test. It is obligatory to alter the displacement rate for testing without affecting the performance and results of FRC. For this purpose, another 8 bottom specimens with displacement rate of 0.012 in./min, 0.02 in./min, 0.04 in./min and 0.05 in./min were tested with 0.55% fiber volume (44kg/m^3). ASTM 1609 permits to use 0.012 in./min for beyond net deflection of $L/900$ for 6 in. x 6in. x 20 in. beam at the highest and 0.02 in./min is the prevailing rate in DPT. In order to determine the optimal displacement rate with good balance between accuracy and time, two more rates of 0.04 in./min and 0.05 in./min was chosen that completes test within 10 to 12 minutes. From Figure 4-15 and Figure 4-16, it can be observed that when 0.05 in./min was used as displacement rate for testing, the peak load increases and the post-cracking curve drop more gradually. While the results from 0.012 in./min, 0.02 in./min and 0.04 in./min were similar in terms of peak load and post-cracking behavior of FRC (Table 4-10). However, difference in strength between 0.02 in./min and 0.04 in./min is minor and the faster test rate of 0.05 in./min cause the apparent increase in strength. Hence, 0.04 in./min was determined to the optimum displacement rate in DPT for comparative assessment of post-cracking behavior for FRC and the testing was also completed within the desired time frame.

Table 4-10 Comparison for various displacement rate with 0.55% V_f

S.N	Displacement rate	Number of samples	V_f	Total time for the test	Average Peak Load	Average peak tensile strength	Average compressive test
Set 5	0.012 in./min	2	0.55% [44 kg/m ³]	48 min	32.1 kips [142.8 kN]	364.7 psi [2.51 MPa]	6.82 ksi [47.1 MPa]
	0.02 in./min	2		27 min	34.1 kips [151.7 kN]	387.5 psi [2.67 MPa]	
	0.04 in./min	2		12.9 min	35.5 kips [157.9 kN]	402.7 psi [2.78 MPa]	
	0.05 in./min	2		11.6 min	39.4 kips [175.3 kN]	446.9 psi [3.1 MPa]	

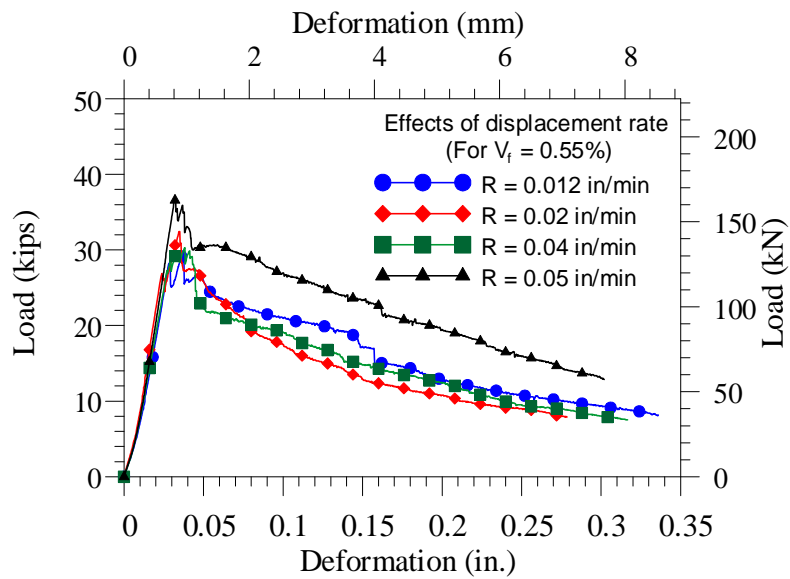


Figure 4-15 Load vs deformation for comparing various displacement rate (0.55% V_f)

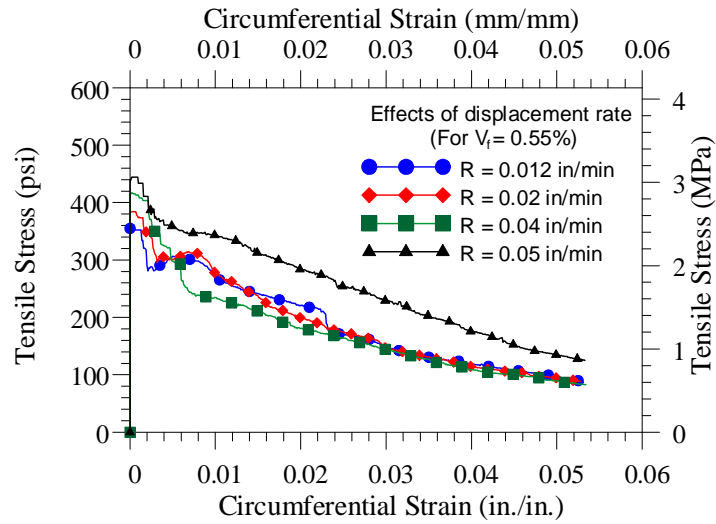


Figure 4-16 Tensile stress vs circumferential strain for comparing various displacement rate (0.55% V_f)

Another set consisting of 12 samples with 0.35% V_f were examined to verify the consistency of post-peak residual strength for displacement rate of 0.02 in./min and 0.04 in./min. Table 4-11 shows the information of each batch for Set 1 and Set 6.

Table 4-11 : Test parameter for FRC with 0.35% fiber volume fraction for rate 0.02 in./min and 0.04 in./min

S.N.	Set 1	Set 6
Specimen size (Diameter x Height)	6 in. x 6 in. [152 mm x 152 mm]	6 in. x 6 in. [152 mm x 152 mm]
Fiber volume fraction (V_f)	0.35%	0.35%
Fiber dosage	28 kg/m ³	28 kg/m ³
Displacement rate	0.02 in./min [0.5 mm/min]	0.04 in./min [1.0 mm/min]
Punch Size (Diameter x Height)	1.5 in. x 1 in. [38 mm x 25.4 mm]	1.5 in. x 1 in. [38 mm x 25.4 mm]
Total number of samples	12	12
Number of bottom samples	6	6
Number of top samples	6	6

Table 4-12 shows important characteristics for the comparative peak and post-peak evaluation of FRC for set 1 and set 6. Both of the set have same volume fraction of fiber about 0.35% and tested with 0.02 in./min and 0.04 in./min respectively.

Table 4-12 Comparison of peak load, peak tensile strength and residual tensile strength with 0.35% fiber volume fraction for rate 0.02 in./min and 0.04 in./min

Parameters		Set 1	Set 6
		0.02 in./min	0.04 in./min
Average compressive strength		5.83 ksi [40.2 MPa]	4.36 ksi [30.1 MPa]
Average peak load		35.6 kips [158.3 kN]	32.6 kips [145 kN]
Average peak tensile strength		403.7 psi [2.8 MPa]	377.6 psi [2.6 MPa]
Average residual strength at 0.1 axial deformation		128.9 psi [0.9 MPa]	135.9 psi [0.94 MPa]
Corresponding tensile stress at	0.003 in./in. [0.3%] circumferential strain	356.5 psi [2.5 MPa]	341.5 psi [2.35 MPa]
	0.01 in./in. [1%] circumferential strain	167.4 psi [1.2 MPa]	166.8 psi [1.2 MPa]
	0.025 in./in. [2.5%] circumferential strain	111.2 psi [0.8 MPa]	114.2 psi [0.8 MPa]
	0.05 in./in. [5%] circumferential strain	60.2 psi [0.41 MPa]	68.5 psi [0.42 MPa]

The coefficient of variation (COV) for peak tensile strength, peak load and residual tensile strength at 0.3% (0.003 in./in.), 1% 0.01 (in./in.), 2.5% (0.025 in./in) and 5% (0.05 in./in.) was used as parameters to asses the post-peak similarity for 0.02 in./min and 0.04 in./min and presented in Table 4-13. It was found that 0.02 in./min and 0.04 in./min were similar in terms of peak load and post cracking behavior in FRC as shown in Figure 4-17 and Figure 4-18.

Table 4-13 Comparison of COV for Set 1 and Set 6.

S.N	COV		Set 1	Set 6
			0.35% 0.02 in./min	0.35% 0.04 in./min
1.	COV for peak load		7.1 %	9.6 %
2.	COV for peak tensile strength		7.1 %	9.6 %
3.	COV for residual strength at 0.1 deformation		23.5 %	28.9 %
4.	COV of residual tensile strength at	0.003 in./in. [0.3%] circumferential strain	11.0 %	21.9 %
5.		0.01 in./in. [1%] circumferential strain	23.3 %	20.7 %
6.		0.025 in./in. [2.5%] circumferential strain	19.9 %	32.1 %
7.		0.05 in./in. [5%] circumferential strain	24.5 %	30.1 %

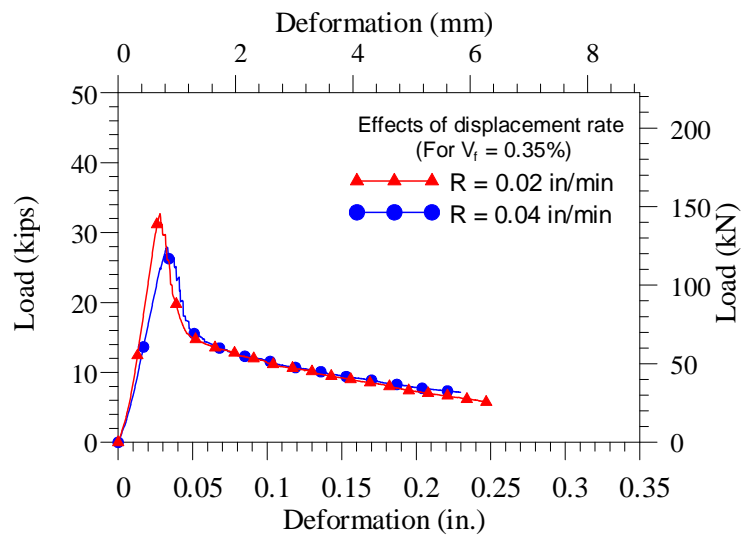


Figure 4-17 Load vs deformation with V_f of 0.35% for 0.02 in/min and 0.04 in/min rates

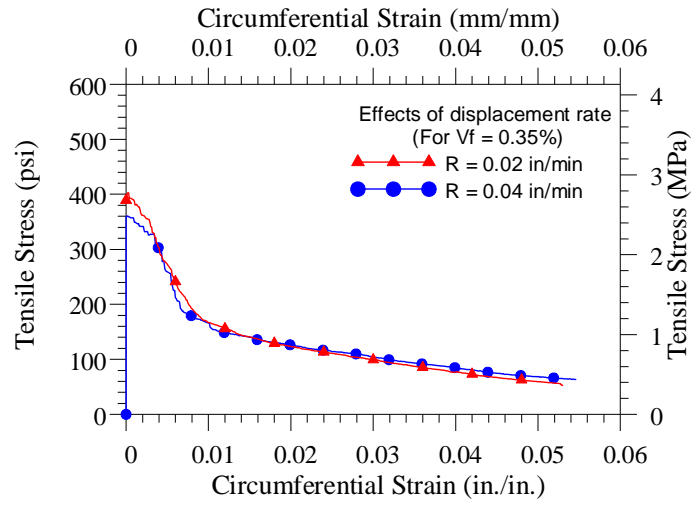


Figure 4-18 Tensile stress vs circumferential strain with V_f of 0.35% for 0.02 in/min and 0.04 in/min rates

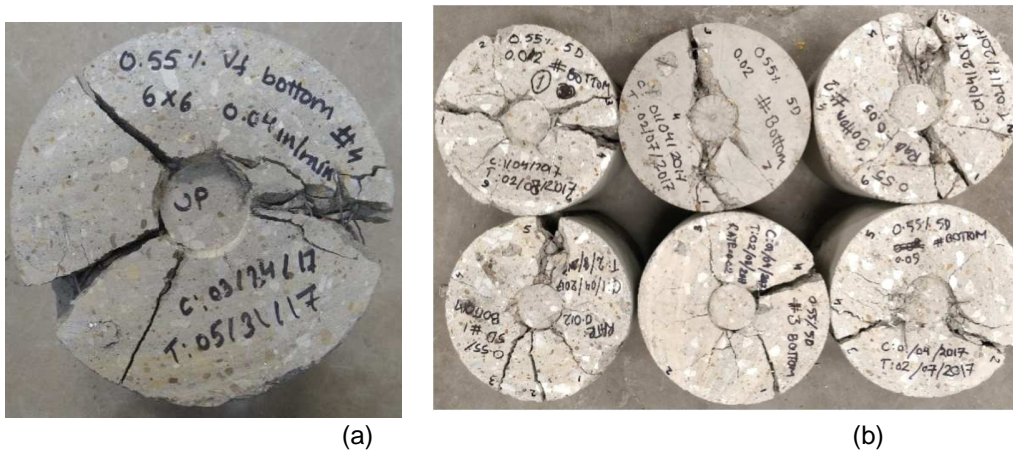


Figure 4-19: (a) Crack pattern (b) Specimen (Set 5)

4.2.6 Effects of specimen sizes

Another three sets of FRC were cast to study the effects of specimen sizes with the same volume fraction of 0.55% and the parameters are in Table 4-15. The test was carried with a displacement rate of 0.04 in/min. Some of the fibers are long and fiber distribution might be an issue as fibers may tend to align in small cylinder. Larger cylinder 8 x 16 in. to inspect fiber length effect with the size of the specimen when long fibers are used. There is no standard formwork available in market and customized formwork were fabricated in CELB using PVC pipes and PVC boards. Larger cylinder size of 8x16 in. were difficult to work as it was heavier.

According to Chen (1970), Equation (2-1) and Equation (2-2) are valid for $b/a \leq 4$ or $H/2a \leq 4$. For any ratio $b/a > 4$ or $H/2a > 4$, the limiting value $b = 4a$ or $H = 8a$ should be used in Equation (2-1) and Equation (2-2) for determination of tensile strength. The punch diameter was increased to 2 inches and punch height remaining the same (1 in.) for testing the specimen size with height 8 in. and diameter 8 in. (Table 4-14). Hence, b/a ratio is also 4 with punch size of 2 in. x 1 in. (diameter x height) for 8x8 specimen and Equation (2-2) is valid for determining tensile strength for 8 x 8 specimen.

Table 4-14 Ratio of b/a for 6 in. and 8 in. specimen

Specimen size (Diameter x Height)	Diameter of specimen 2b	Punch diameter 2a	b/a	Height of specimen h	2b/h
6 x 6	6 in.	1.5 in.	4	6 in.	1
6 x 4	6 in.	1.5 in.	4	4 in.	1.5
8 x 8	8 in.	2 in.	4	8 in.	1

For FRC, in some samples crack may not go all the way through length, it is necessary to investigate that crack length would affect the results or not. Sometimes cracks may start from bottom to top halfway, sometimes from top to bottom halfway. So, some

6x4in. specimen were tested to see the effects of through cracks. It was found that COV was observed to be high for 6 x 4 in. As 8x8 in. gives the similar result to 6x6 in. and 6x4 in. gives higher COV, 6x6 in. specimen size was considered suitable for longer fibers in DPT as well.

Table 4-15 shows the parameter for 6 x 6, 6 x 4 and 8 x 8 specimen with 0.55% volume fraction for comparative assessment of FRC with different specimen sizes. The total number of sample for set 7, set 8 and set 9 are 6, 9 and 12 respectively.

Table 4-15: Test parameter for FRC with different specimen size

S.N	Set 7	Set 8	Set 9
Specimen size (Diameter x Height)	6 in. x 6 in. [152 mm x 152 mm]	6 in. x 4 in. [152 mm x 108 mm]	8 in. x 8 in. [203 mm x 203 mm]
Fiber volume fraction (Vf)	0.55%	0.55%	0.55%
Fiber dosage	44 kg/m ³	44 kg/m ³	44 kg/m ³
Displacement rate	0.04 in/min [1.0 mm/min]	0.04 in/min [1.0 mm/min]	0.04 in/min [1.0 mm/min]
Punch Size (Diameter x Height)	1.5 in. x 1 in. [38 mm x 25.4 mm]	1.5 in. x 1 in. [38 mm x 25.4 mm]	2 in. x 1 in. [25.4 mm x 50.8 mm]
Total number of samples	6	9	12
Number of bottom samples	3	3	6
Number of top samples	3	3	6
Number of middle samples	-	3	-

Table 4-16 shows important characteristics for the comparative peak and post-peak evaluation of FRC with 6 x 6, 6 x 4 and 8 x 8 specimen sizes. It is obvious that peak

load varies with the change in specimen sizes (Figure 4-20 and 4-22). Larger specimen size can resist the greater force as 8 x 8 has the larger peak load. On comparing with 6 x 6 specimen, the peak tensile strength is similar in case of 8 x 8 and the peak tensile strength slightly increased in 6 x 4 increased by computing the tensile strength using Equation (2-2). The coefficient 1.2 also depends on the height of specimen and might need to be calibrated again when 6 x 4 specimen are used. When the ratio of diameter and height of specimen is 1, the post-peak behavior of FRC is similar. It was found that 6 x 6 in. specimen, the peak tensile strength and post cracking behavior is similar in case of 8 x 8 in. Hence, it is advisable to use 6x6 in. for longer fiber as well.

Table 4-16 Comparison of peak load, peak tensile strength and residual tensile strength at 0.3% , 1%, 2.5% and 5% circumferential strain for 6 x 6 , 6 x 4 and 8 x 8 specimen.

Parameters		Set 7 6 x 6	Set 8 6 x 4	Set 9 8 x 8
Average compressive strength		7.05 ksi [48.6 MPa]	7.05 ksi [48.6 MPa]	6.64 ksi [45.8 MPa]
Average peak load		37.5 kips [166.8 kN]	27.9 kips [124.1 kN]	71.4 kips [317.6 kN]
Average peak tensile strength		425 psi [2.93 MPa]	316.3 psi [2.2 MPa]	455.8 psi [3.1 MPa]
Average residual strength at 0.1 deformation		216.9 psi [1.5 MPa]	137.8 psi [0.95 MPa]	272.4 psi [1.9 MPa]
Corresponding tensile stress at	0.003 in./in. [0.3%] circumferential strain	342.1 psi [2.4 MPa]	379.8 psi [2.6 MPa]	376.3 psi [2.6 MPa]
	0.01 in./in. [1%] circumferential strain	234.6 psi [1.6 MPa]	255.3 psi [1.76 MPa]	261.6 psi [1.8 MPa]
	0.025 in./in. [2.5%] circumferential strain	163.7 psi [1.1 MPa]	186.0 psi [1.3 MPa]	148.8 psi [1.03 MPa]
	0.05 in./in. [5%] circumferential strain	89.6 psi [0.62 MPa]	103.7 psi [0.71 MPa]	83.8 psi [0.58 MPa]

Figure 4-20 shows the curve for load vs deformation and Figure 4-21 shows the curve for tensile stress vs circumferential strain for 6 x 6 and 6 x 4 specimens with 0.55% fiber volume.

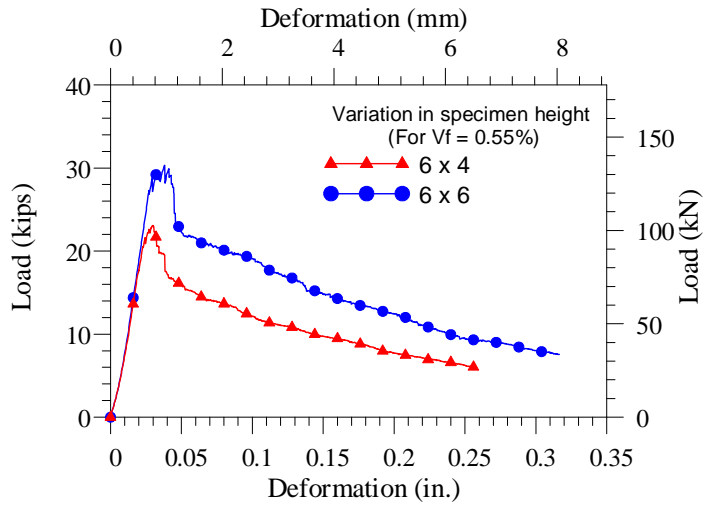


Figure 4-20 Load vs deformation for comparing specimen height (0.55% V_f)

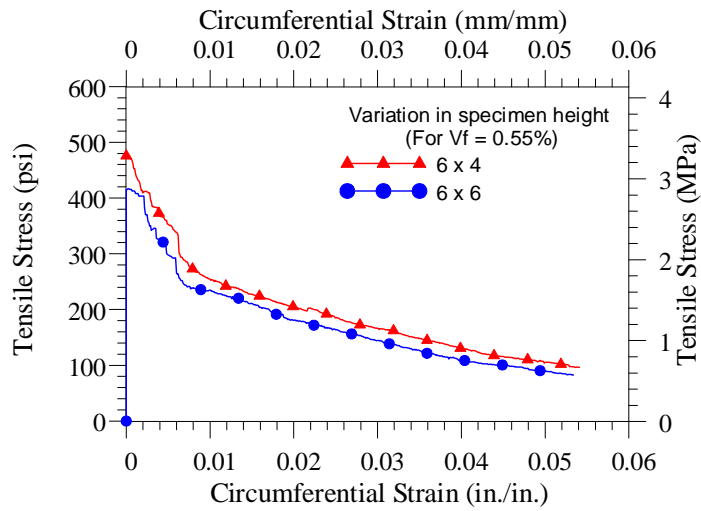


Figure 4-21 Tensile stress vs circumferential strain for comparing specimen height (0.55% V_f)

Figure 4-22 shows the curve for load vs deformation and Figure 4-23 shows the curve for tensile stress vs circumferential strain for 6 x 6 and 6 x 4 specimens with 0.55% fiber volume.

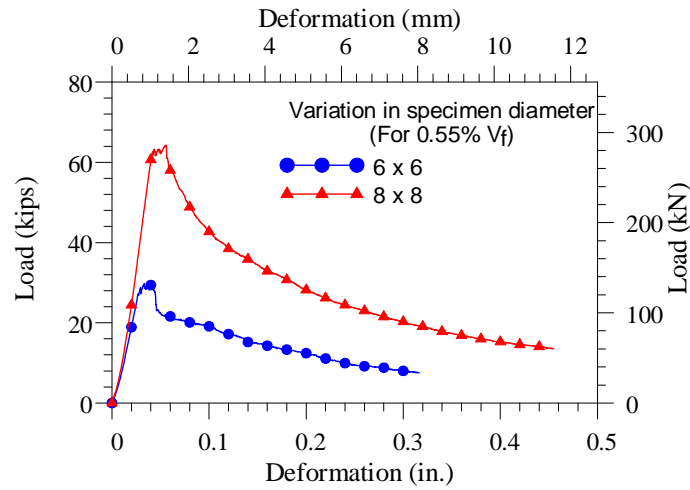


Figure 4-22 Load vs deformation for comparing specimen diameter (0.55% V_f)

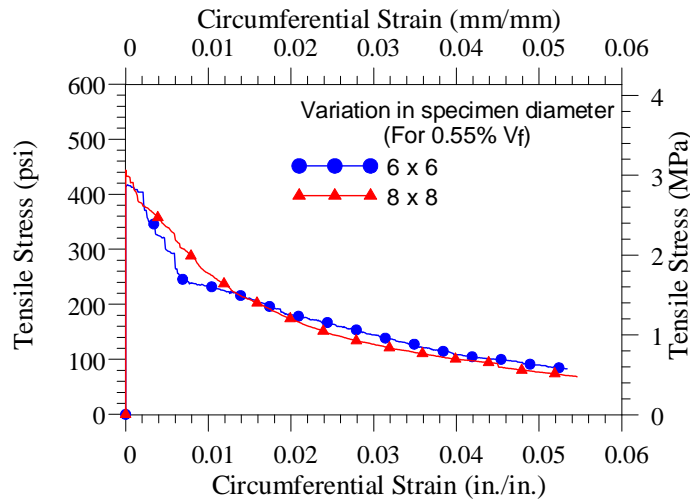


Figure 4-23 Tensile stress vs circumferential strain for comparing specimen diameter (0.55% V_f)

Table 4-17 shows important characteristics for the comparative peak and post-peak evaluation of FRC for 6x6 in., 6x4in. and 8x8 specimen. COV for 6x4 in. are higher in comparison to 6x6 in. and 8x8 in. specimen.

Table 4-17: Comparison of COV for Set 7, 8 and 9

S.N	COV	Set 7	Set 8	Set 9	
		6 x 6	6 x 4	8 x 8	
1.	COV for peak load	8.9 %	11.0 %	7.7 %	
2.	COV for peak tensile strength	8.9 %	11.0 %	7.7 %	
3.	COV for residual strength at 0.1 deformation	21.2 %	25.3 %	19.7 %	
4.	COV of residual tensile strength at	0.003 in./in. [0.3%] circumferential strain	11.4 %	15.0 %	14.9 %
5.		0.01 in./in. [1%] circumferential strain	21.3 %	19.7 %	15.1 %
6.		0.025 in./in. [2.5%] circumferential strain	14.2 %	20.0 %	21.4 %
7.		0.05 in./in. [5%] circumferential strain	20.6 %	22.0 %	30.1 %

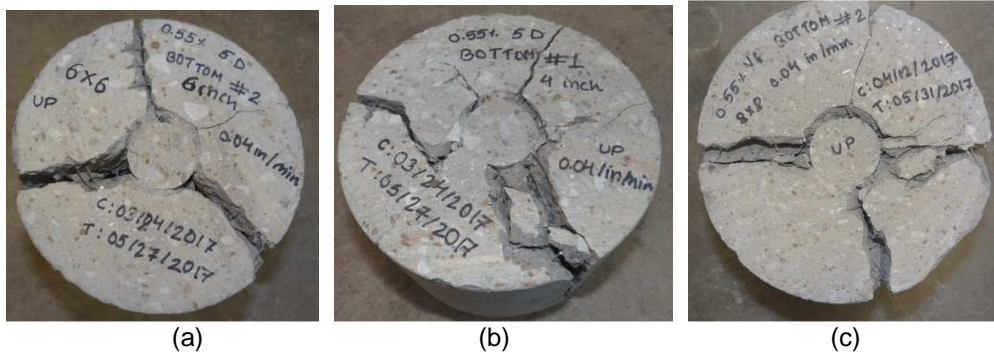


Figure 4-24 Plan view (a) 6 x 6 in. bottom (b) 6 x 4 in. bottom (c) 8 x 8 in. bottom

Table 4-18 Comparison between double punch test (DPT) and direct tensile test (DTT)

Set	Volume fraction (V_f)	Dosage	Peak tensile stress		DTT/DPT
			Double punch test (DPT)	Direct tensile test (DDT)	
Set 6	0.35%	28 kg/m ³	377.6 psi [2.6 MPa]	319.7 psi [2.2 MPa]	0.86
Set 4	0.75%	60 kg/m ³	344.4 psi [2.4 MPa]	387.31 psi [2.67 MPa]	1.12

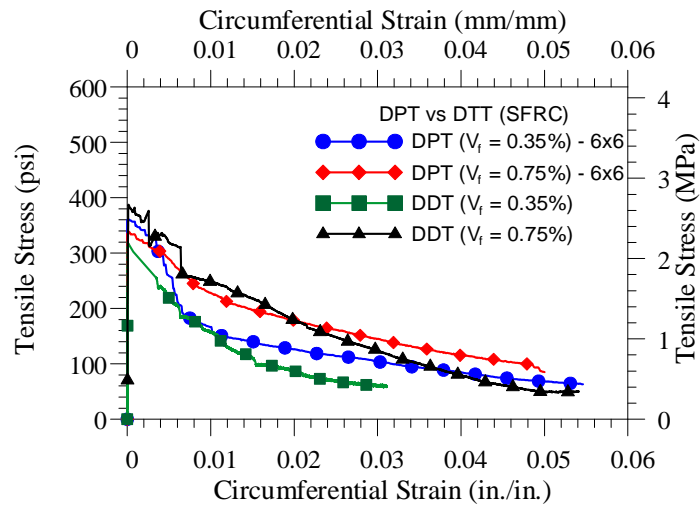


Figure 4-27 Comparison between double punch test and direct tensile test for FRC

4.3 Double Punch Test with UHP-FRC (Phase 2)

In this phase, the double punch test method was used to determine the equivalent tensile strength and compared the results with the direct tensile test for UHP-FRC. The comparison was carried on the following criteria:

1. To examine the influence of fiber type with steel and PE fiber for UHP-FRC.
2. To explore the effect of displacement rate for the experiment.
3. To investigate the effect of specimen sizes in DPT.
4. To compare the results obtained from DPT with the direct tensile test.

4.3.1 *Effects of displacement rates and influence of fiber type*

The displacement rates of 0.02 in./min and 0.04 in./min as used in Phase 1 were used in Phase 2. In this study of influence of fiber type in UHP-FRC, the rate of 0.02 in/min (0.5 mm/min) which was also used by various researchers for DPT (Mollins et. al. 2007, Pujadas et. al 2012 and Blanco et. al. 2014) requires about 30 to 32 minutes to complete the test for UHP-FRC. This required testing time is longer than that of SFRC. The optimum displacement rate with 0.04 in./min for SFRC was also used in UHP-FRC and the total test time was about 15 minutes. However, the average time required for steel fiber 15 minutes and was higher than with PE fiber for UHP-FRC about 12 minutes as shown in Table 4-19. Moreover, on comparing UHP-FRC with 3% steel fiber and 0.75% PE fiber, the UHP-FRC with steel fibers has higher compressive and tensile strength and is more ductile as shown in Figure 4-31 and Figure 4-32. The test parameter and COV of peak load, peak tensile strength and residual tensile strength at 0.3%, 1%, 2.5% and 5% circumferential strain are shown in Table 4-20 and Table 4-21.

Table 4-19 Comparison of testing time for UHP-FRC

S.N	Displacement rate	Number of samples	Total time for the test	Average peak tensile strength
3% Steel	0.02 in./min	4	31.5 min	1131.8 psi [7.8 MPa]
	0.04 in./min	6	15 min	971.6 psi [6.69 MPa]
0.75% PE	0.04 in./min	12	10.7 min	741.7 psi [5.11 MPa]

Table 4-20: Test parameter for UHP-FRC with different fiber type

S.N	Set 10	Set 11	Set 12	Set 13
Specimen size (Diameter x Height)	6 in. x 6 in. [152 mm x 152 mm]	6 in. x 6 in. [152 mm x 152 mm]	6 in. x 6 in. [152 mm x 152 mm]	6 in. x 6 in. [152 mm x 152 mm]
Fiber volume fraction (Vf)	3% Steel	3% Steel	3% Steel	0.75% PE
Displacement rate	0.02 in/min [0.5 mm/min]	0.02 in/min [0.5 mm/min]	0.04 in/min [1.0 mm/min]	0.04 in/min [1.0 mm/min]
Punch Size (Diameter x Height)	1.5 in. x 1 in. [38 mm x 25.4 mm]	1.5 in. x 1 in. [38 mm x 25.4 mm]	1.5 in. x 1 in. [38 mm x 25.4 mm]	1.5 in. x 1 in. [38 mm x 25.4 mm]
Total number of samples	8	4	6	12
Number of bottom samples	4	4	3	6
Number of top samples	4	-	3	6

Table 4-21 shows important characteristics for the comparative peak and post-peak evaluation of UHP-FRC with 3% steel and 0.75% PE fibers. The average peak load and average peak tensile strength were found higher for UHP-FRC with steel fiber than with PE fibers.

Table 4-21: Comparison of peak load, peak tensile strength and residual tensile strength at 0.3%, 1%, 2.5% and 5% circumferential strain for set 10, set 11, set 12 and set 13.

Parameters		Set 10	Set 11	Set 12	Set 13
		0.02 in/min 3% Steel	0.02 in/min 3% Steel	0.04 in/min 3% Steel	0.04 in/min 0.75% PE
Average compressive strength		20.8 ksi [143.42 MPa]	18.5 ksi [127.6 MPa]	18.5 ksi [127.6 MPa]	17.5 ksi [30.1 MPa]
Average peak load		112.1 kips [498.65 kN]	99.7 kips [443.45 kN]	85.6 kips [380.8 kN]	65.4 kips [290.91 kN]
Average peak tensile strength		1272.0 psi [8.77 MPa]	1131.8 psi [7.8 MPa]	971.6 psi [6.69 MPa]	741.7 psi [5.11 MPa]
Average residual strength at 0.1 deformation		1165.4 psi [8.04 MPa]	804.4 psi [5.55 MPa]	403.6 psi [2.78 MPa]	218.1 psi [1.51 MPa]
Corresponding tensile stress at	0.003 in./in. [0.3%] circumferential strain	1185.8 psi [8.18 MPa]	1100.0 psi [7.58 MPa]	958.5 psi [6.61 MPa]	731.5 psi [5.04 MPa]
	0.01 in./in. [1%] circumferential strain	1083.2 psi [7.47 MPa]	769.1 psi [5.3 MPa]	525.2 psi [3.62 MPa]	411.1 psi [2.83 MPa]
	0.025 in./in. [2.5%] circumferential strain	483.0 psi [3.33 MPa]	300.5 psi [2.07 MPa]	245 psi [1.69 MPa]	151.13 psi [1.04 MPa]
	0.05 in./in. [5%] circumferential strain	195.8 psi [1.35 MPa]	105.0 psi [0.72 MPa]	100.6 psi [0.7 MPa]	64.5 psi [0.44 MPa]

Table 4-22 Comparison of COV for set 10, set 11, set 12 and set 13.

S.N	COV	Set 10	Set 11	Set 12	Set 13
		0.02 in/min 3% Steel	0.02 in/min 3% Steel	0.04 in/min 3% Steel	0.04 in/min 0.75% PE
1.	COV for peak load	10.4 %	13.8 %	12.1 %	14.6 %
2.	COV for peak tensile strength	10.4 %	13.8 %	12.1 %	14.6 %
3.	COV for residual strength at 0.1 axial deformation	21.3 %	49.9 %	24.4 %	38 %

4.	COV of residual tensile strength at	0.003 in./in. [0.3%] circumferential strain	7.9 %	12.5 %	12.8 %	13.9 %
5.		0.01 in./in. [1%] circumferential strain	22.8 %	49.9 %	15.9 %	32.9 %
6.		0.025 in./in. [2.5%] circumferential strain	30.7 %	33.2 %	30.1 %	35.1 %
7.		0.05 in./in. [5%] circumferential strain	49.5 %	29.7 %	60.8 %	47.2 %



(a)



(b)

Figure 4-28: Plan view (a) 6x6 in. with steel fiber (b) 6x6 in. with PE fiber



(a)



(b)

Figure 4-29: Side view (a) 6x6 in. with steel fiber (b) 6x6 in. with PE fiber



(a)



(b)

Figure 4-30: Crack pattern (a) UHP-FRC with steel fibers (b) UHP-FRC with PE fibers

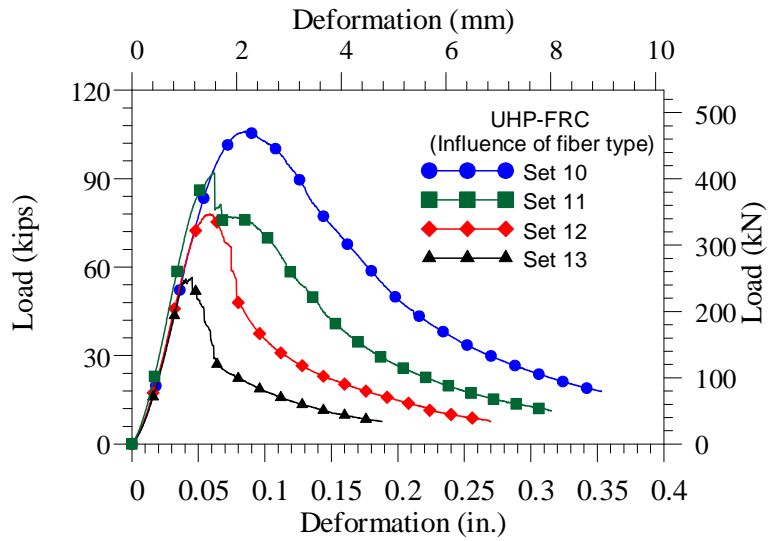


Figure 4-31 Load vs deformation for UHP-FRC with 3% Steel and 0.75% PE fiber and 6x6 specimen

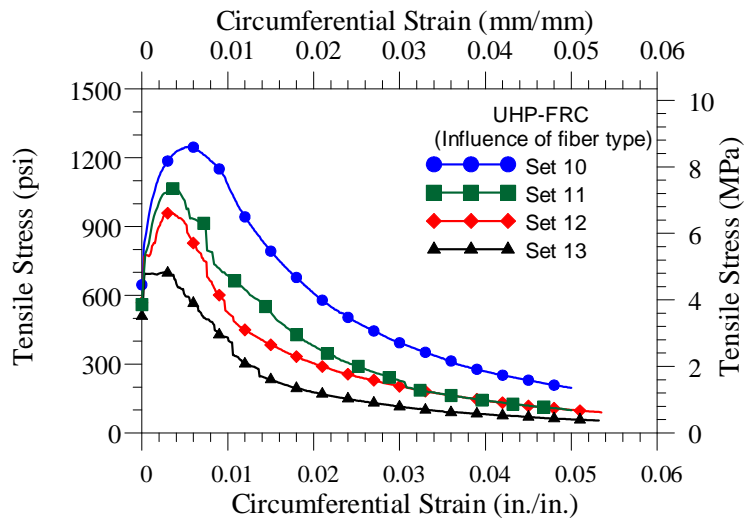


Figure 4-32 Tensile stress vs circumferential strain for UHP-FRC with 3% Steel and 0.75% PE fiber and 6x6 specimen



Figure 4-33 Tested specimen (UHP-FRC)

4.3.2 Effects of specimen height

Another test variable was the height of the specimen as 6 inches and 4 inches for UHP-FRC with 3% steel and 0.75% PE fiber. The test was carried with a displacement rate of 0.04 in/min. It was found that the COV was higher for 6x4 specimen than 6x6 specimen for both the type of fibers as shown in Table 4-24. From Figure 4-34 and Figure 4-35, the peak tensile strength slightly increased in 6 x 4 increased by computing the tensile strength using Equation (2-2) and the load resisted by 6x6 specimen is higher than that of 6x4 specimen. The coefficient 1.2 also depends on the height of specimen and may need to be when 6 x 4 specimen are used.

Table 4-23 Test parameter for UHP-FRC with different specimen size and fiber type

S.N	Set 12	Set 14	Set 13	Set 15
Specimen size (Diameter x Height)	6 in. x 6 in. [152 mm x 152 mm]	6 in. x 4 in. [152 mm x 108 mm]	6 in. x 6 in. [152 mm x 152 mm]	6 in. x 4 in. [152 mm x 108 mm]
Fiber volume fraction (Vf)	3% Steel	3% Steel	0.75% PE	0.75% PE
Displacement rate	0.04 in/min [1.0 mm/min]	0.04 in/min [1.0 mm/min]	0.04 in/min [1.0 mm/min]	0.04 in/min [1.0 mm/min]
Punch Size (Diameter x Height)	1.5 in. x 1 in. [38 mm x 25.4 mm]	1.5 in. x 1 in. [38 mm x 25.4 mm]	1.5 in. x 1 in. [38 mm x 25.4 mm]	1.5 in. x 1 in. [38 mm x 25.4 mm]
Total number of samples	6	9	12	9
Number of bottom samples	3	3	6	3
Number of top samples	3	3	6	3

Table 4-24 shows the parameter for 6 x 6 and 6 x 4 specimen with 3% steel fiber and 0.75% PE fiber for comparative assessment of UHP-FRC with different specimen sizes. The total number of sample for set 7, set 8 and set 9 respectively.

Table 4-24: Comparison of peak load, peak tensile strength and residual tensile strength at 0.3% , 1%, 2.5% and 5% circumferential strain for UHP-FRC with 6 x 6 and 6 x 4 specimen.

Parameters	Set 12	Set 14	Set 13	Set 15
	6 x 6 3% Steel	6 x 4 3% Steel	6 x 6 0.75% PE	6 x 4 0.75% PE
Average compressive strength	18.5 ksi [127.6 MPa]	18.5 ksi [127.6 MPa]	17.5 ksi [30.1 MPa]	17.5 ksi [30.1 MPa]
Average peak load	85.6 kips [380.8 kN]	77.5 kips [344.74 kN]	65.4 kips [290.91 kN]	49.1 kips [218.4 kN]

Average peak tensile strength		971.6 psi [6.69 MPa]	1336.2 psi [9.21 MPa]	741.7 psi [5.11 MPa]	847.8 psi [5.85 MPa]
Average residual strength at 0.1 deformation		403.6 psi [2.78 MPa]	512.0 psi [3.53 MPa]	218.1 psi [1.51 MPa]	173.2 psi [1.19 MPa]
Corresponding tensile stress at	0.003 in./in. [0.3%] circumferential strain	958.5 psi [6.61 MPa]	1305 psi [9.0 MPa]	731.5 psi [5.04 MPa]	406.8 psi [2.8 MPa]
	0.01 in./in. [1%] circumferential strain	525.2 psi [3.62 MPa]	892.9 psi [6.16 MPa]	411.1 psi [2.83 MPa]	796.7 psi [5.49 MPa]
	0.025 in./in. [2.5%] circumferential strain	245 psi [1.69 MPa]	343.3 psi [2.37 MPa]	151.13 psi [1.04 MPa]	139.8 psi [0.96 MPa]
	0.05 in./in. [5%] circumferential strain	100.6 psi [0.7 MPa]	121.6 psi [0.84 MPa]	64.5 psi [0.44 MPa]	49.5 psi [0.34 MPa]

Table 4-25 Comparison of COV for set 11, set 12, set 13 and set 14.

S.N	COV	Set 12	Set 14	Set 13	Set 15	
		6 x 6 3% Steel	6 x 4 3% Steel	6 x 6 0.75% PE	6 x 4 0.75% PE	
1.	COV for peak load	12.1 %	13.1 %	14.6 %	14.9 %	
2.	COV for peak tensile strength	12.1 %	13.1 %	14.6 %	14.6 %	
3.	COV for residual strength at 0.1 deformation	24.4 %	39.5 %	38 %	36.9 %	
4.	COV of residual tensile strength at	0.003 in./in. [0.3%] circumferential strain	12.8 %	13.6 %	13.9 %	16.4 %
5.		0.01 in./in. [1%] circumferential strain	15.9 %	31.1 %	32.9 %	41.6 %
6.		0.025 in./in. [2.5%] circumferential strain	30.1 %	35.0 %	35.1 %	26.7 %
7.		0.05 in./in. [5%] circumferential strain	40.8 %	69.9 %	47.2 %	32.1 %

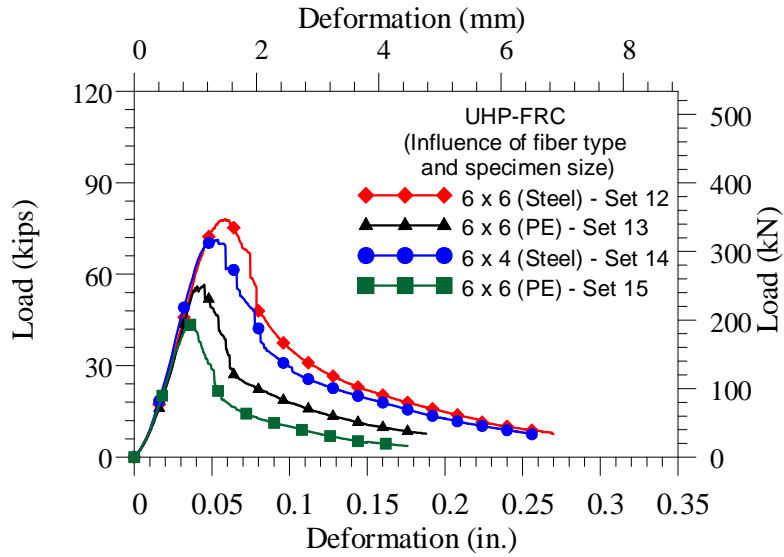


Figure 4-34: Load vs deformation for UHP-FRC with 3% Steel and 0.75% PE fiber for 6x6 and 6x4 specimen

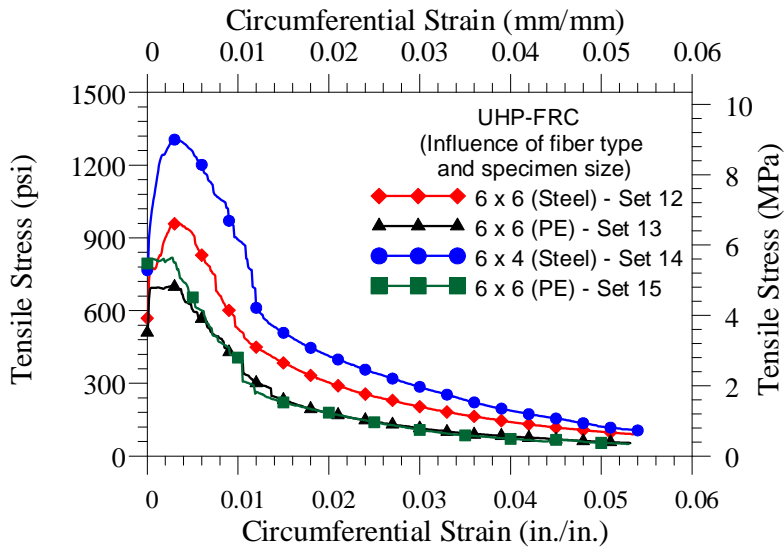


Figure 4-35: Tensile stress vs circumferential strain for UHP-FRC with 3% Steel and 0.75% PE fiber for 6x6 and 6x4 specimen



(a) (b)
 Figure 4-36: Plan view (a) 6 x 4 in. (UHP-FRC with steel fibers)
 (b) 6 x 4 in. (UHP-FRC with PE fibers)



Figure 4-37: Side view (a) 6 x 4 in. (UHP-FRC with steel fibers)
 (b) 6 x 4 in. (UHP-FRC with PE fibers)

4.3.3 Determination of relation between deformation and circumferential strain

UHP-FRC shows the crack opening or *total crack opening displacement* (TCOD) even in the ascending part of the load and deformation curve in the slower rate and the first cracking starts even before the peak load (or peak tensile strength). The total crack opening displacement (TCOD) becomes more noticeable and increases at a faster rate after the peak load as shown in Figure 4-38 and Figure 4-39.

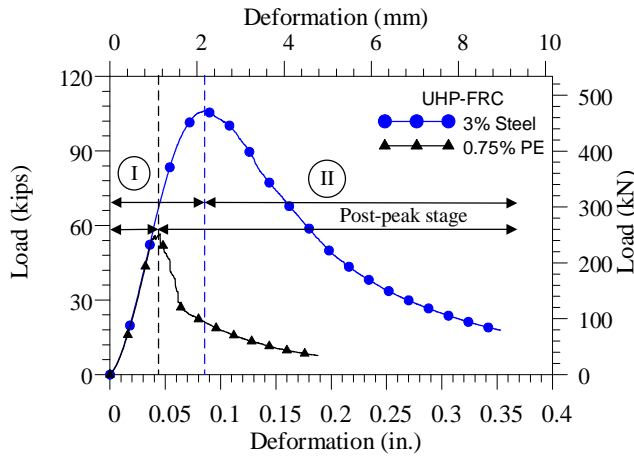


Figure 4-38 Typical load vs deformation for UHP-FRC (b) Typical tensile stress vs circumferential strain for FRC

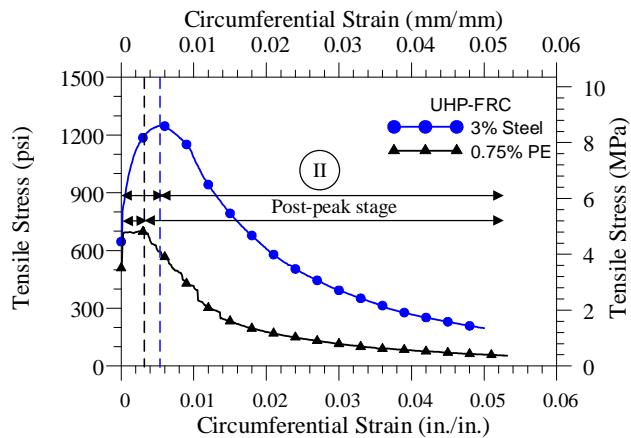


Figure 4-39 Typical tensile stress vs circumferential strain for UHP-FRC

From Figure 4-40, it can be observed that there is an abrupt increase in circumferential elongation at an axial deformation of 0.04 in. and maintaining an approximately constant rate up to the end of testing. This could be due to the fact that it requires more energy before initial cracking to form a conical wedge under the punch. Since crack width after peak strength is of interest to the engineering community, only the deformation and circumferential strain after the peak load is considered as shown in Figure

4-41. Figure 4-41 shows that the relationship between deformation and circumferential strain is very close to a linear relationship. Therefore, the slope (α) was determined by means of a linear regression using the data obtained from this experimental program.

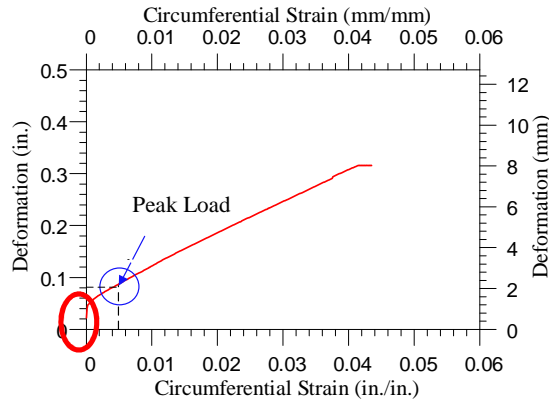


Figure 4-40: Total Deformation vs circumferential strain (UHP-FRC)

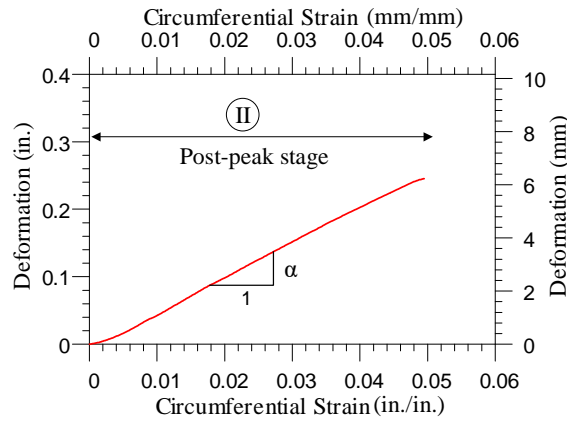


Figure 4-41 Post-peak Deformation vs circumferential strain for UHP-FRC (after peak only)

Table 4-26 summarizes the values of α (slope of deformation and circumferential strain curve) for UHP-FRC. α is calculated for 6x6 specimens for UHP-FRC with steel and PE fiber. The results from 6x6 specimen and displacement rate of 0.04 in./min are used to determine the relation between post peak deformation and circumferential strain. .Figure

4-42 shows the post-peak deformation vs circumferential strain for UHP-FRC with steel and PE fiber (after peak only).

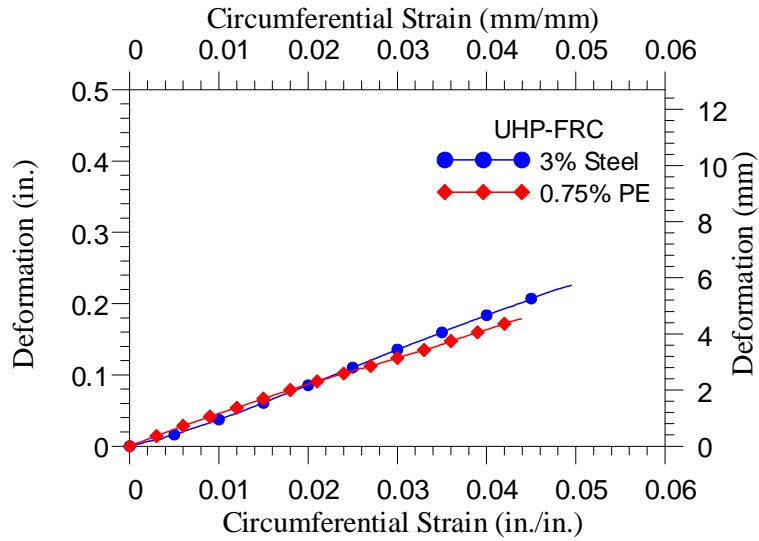


Figure 4-42: Post-peak Deformation vs circumferential strain for UHP-FRC with steel and PE fiber (after peak only)

It can be observed that the average α is between 4.1 to 4.2 for displacement rate of 0.04 in./min for UHP-FRC with steel and PE fibers, and can be conservatively taken as 4.0. Thus, this provides the direct relationship between δ_P and ϵ_P given as:

$$\delta_P = \alpha \epsilon_P \quad \text{where, } \alpha = 4 \quad \text{(Equation 4-7)}$$

$$\delta_P = \delta - \delta_0$$

where δ_0 = deformation at peak load

δ = total vertical deformation from the beginning of the test

δ_P = post peak deformation

ϵ_P = circumferential strain after peak

Table 4-26: Determination of α for UHP-FRC

Set	Set 12	Set 13
V_f	3% steel	0.75% PE
Fiber Dosage	238 kg/m ³	60 kg/m ³
Rate (in./min)	0.04	0.04
Size (diameter x height)	6 x 6 in.	6 x 6 in.
Sample	α values	
B 1	4.8667	4.3649
B 2	4.6694	4.1657
B 3	3.8498	3.8115
B 4		3.74
T 1	4.5913	4.7982
T 2	3.8498	4.0072
T 3	2.8635	5.6384
T 4		4.1657
T 5		3.9632
T 6		3.6574
Mean	4.1	4.2
Standard deviation	0.7	0.6

Note: B and T represent the bottom and top specimens, respectively

The data (Table 4-26) distribution and variability of α for UHP-FRC with steel and PE fibers are given in Figure 4-43. Mark (X) denotes the mean values and horizontal lines at ends show the minimum and maximum values.

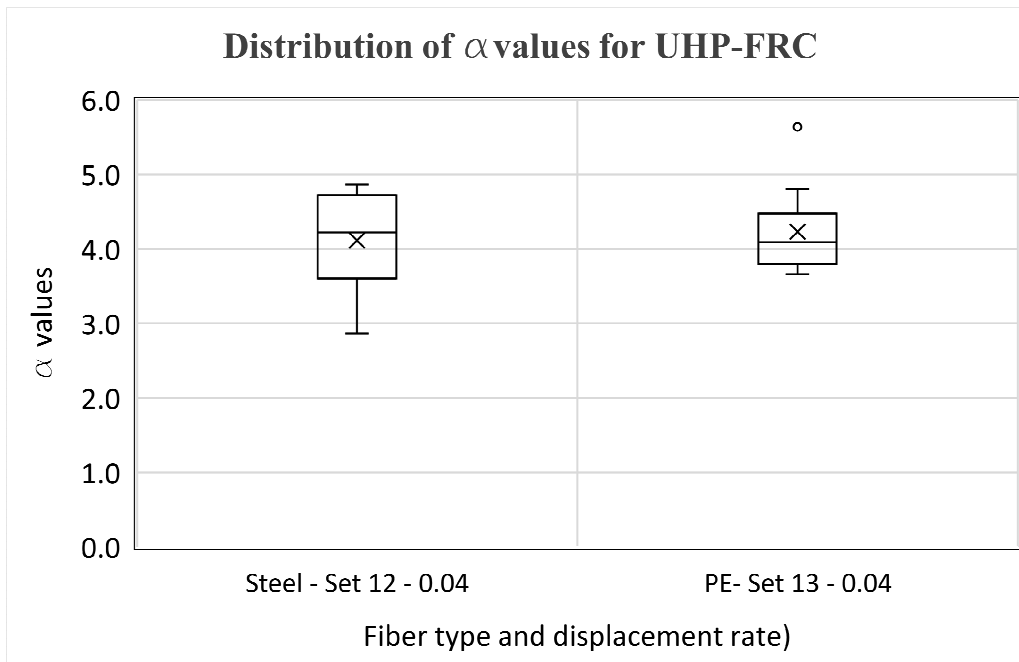


Figure 4-43: Determination of α values for UHP-FRC

4.3.4 Computation of average crack width

Let D_0 and D_1 be the initial diameter before loading and a diameter under loading of a test specimen. D_1 is measured by a circumferential extensometer. The total crack width along the circumference (TCW) is computed by the increase in the perimeter (P) of the cylinder. TWC at the post-peak stage is represented by:

$$TCW = P_1 - P_0$$

The circumferential strain (ϵ) is the ratio of change in the perimeter of the cylinder to the original perimeter which is given by:

$$\epsilon = \frac{P_1 - P_0}{P_0}$$

where, $P_1 = \text{Final perimeter} = \pi D_1$

$P_0 = \text{Initial perimeter} = \pi D_0$

$$P_1 = P_0(1 + \varepsilon)$$

Since there is no circumferential strain measured before peak for FRC, the initial perimeter (πD_0) is equivalent to the perimeter at the peak and ε_p (circumferential strain at peak) is also the same as ε . The cracks are developed radially from the center to the circumference so average crack width (CW) in a specimen can be determined by dividing the total crack width by the number of cracks (N).

$$CW = \frac{P_1 - P_0}{N} = \frac{P_0 \varepsilon}{N} = \frac{\pi D_0 \times \varepsilon_p}{N}$$

Use Eq. (4-1): $\delta_p = \alpha \varepsilon_p$,

$$CW = \frac{\pi D_0 \times \delta_p}{\alpha N} \quad \text{(Equation 4-8)}$$

The number of cracks is determined by visual inspection after the test. N is 2 for UHP-FRC with steel fiber (6x6) and in the range of 4 to 9 for UHP-FRC with PE fiber (6x6). From this research, it was observed that the most common number of cracks is 2 for UHP-FRC with steel fiber and 5 for UHP-FRC with PE fiber as about 35% of the specimen has five number of cracks. Only cracks that started radially from the center and propagated at least up to the mid-height of the specimen were considered. The very small minor cracks are considered having less effect on the residual stress.

Table 4-27: Percentage of samples with respective crack number
(UHP-FRC with steel and PE fiber)

Fiber type	No of cracks	No. of samples	Percentage (%)
UHP-FRC (Steel)	2	12	100
UHP-FRC (PE)	4	2	16.7
	5	4	33.3
	6	2	16.7
	7	1	8.3
	8	2	16.7
	9	1	8.3
	Total samples	12	

For DPT using 6x12 in. cylinders the average crack width (CW) is determined by substituting $D_0 = 6$ in., $N = 2$ (for steel fiber) and 5 (for PE fiber) and $\alpha = 4$ in

$$CW = \frac{\pi D_0 \times \delta_p}{\alpha N} \quad \text{(Equation 4-2)}$$

UHP-FRC with steel and PE fibers:

$$CW = \frac{6\pi}{4} \times \frac{\delta_p}{N} = \frac{4.72\delta_p}{N} \quad \text{(Equation 4-9)}$$

4.3.5 Verification from measured maximum crack width

While Equation 4-9 can be used to obtain a reasonable average crack width at certain deformation, estimation of the maximum crack width can be also important. However, the maximum crack with does not have a linear relation with the axial deformation. Table 4-28 shows the maximum measured crack widths at various deformations for a sample in each batch. However, the number of cracks is counted at the end of the experiment as it is difficult to count crack number while the testing is in progress. The measured maximum crack widths during and at the end of tests were compared with

the predicted maximum crack width given by Equation 4-12 for a selected specimen as shown Table 4-28.

Table 4-28: Measurement of crack width during experiments for one selected sample from sets of UHP-FRC with steel and PE fibers.

UHP-FRC (steel)					UHP-FRC (PE)				
δ_p	Measured Crack Width		Predicted Crack width	(a)/(b)	δ_p	Measured Crack Width		Predicted Crack width	(a)/(b)
	in.	mm	in. (a)			in. (b)	in.	mm	
0.062	0.5	0.020	0.024	0.81	0.054	0.25	0.010	0.009	1.14
0.082	0.8	0.031	0.036	0.88	0.073	0.35	0.014	0.017	0.82
0.095	1	0.039	0.045	0.88	0.082	0.5	0.020	0.022	0.90
0.137	1.5	0.059	0.074	0.80	0.102	0.8	0.031	0.036	0.88
0.161	2	0.079	0.093	0.85	0.110	1	0.039	0.042	0.94
0.190	2.5	0.098	0.117	0.84	0.153	2.5	0.098	0.087	1.13
0.230	4.5	0.177	0.153	1.16	0.172	3	0.118	0.112	1.05
0.242	5	0.197	0.165	1.20	0.195	4	0.157	0.149	1.05
0.297	6	0.236	0.219	1.08	0.216	5	0.197	0.186	1.06
					0.232	6	0.236	0.219	1.08

Unlike the average crack width, the maximum crack width does not show a linear relation with the deformation, δ . A nonlinear relation between the maximum crack width and δ was developed based on the available data. Table 4-29 summarizes the data analysis and the relation between deformation and predicted maximum crack width using a non-linear regression (obtained using MATLAB) is in the form of

$$\delta_p = \lambda C_{\max}^\beta$$

where δ_p = post peak deformation, in.

C_{\max} = predicted maximum crack width, in.

Table 4-29: Relation between deformation and measured maximum crack width

S.N	λ		β	
	Set 12	Set 13	Set 12	Set 13
	Steel 0.04 in./min	PE 6x6	Steel 0.04 in./min	PE 6x6 0.04 in./min
B 1	0.5100	0.3110	0.4210	0.3151
B 2	0.3860	0.3440	0.3756	0.3789
B 3	0.5331	0.5025	0.4752	0.4565
B 4		0.6388		0.6268
T 1	2.2237	0.3305	1.3708	0.3138
T 2	0.5578	0.5503	0.6008	0.4955
T 3	1.2363	0.4849	1.0247	0.7103
T 4		0.3924		0.4227
T 5		0.3976		0.3833
T 6		0.5984		0.4480
Average	0.9078	0.4550	0.7114	0.4551

Note: B and T represent the bottom and top specimens, respectively

Equation 4-11 represents the approximate median value of the measured maximum crack width. The two equations are predicted to determine the crack width for UHP-FRC with steel and PE fibers.

Table 4-30: Average values of coefficient λ and β for the 6x6 specimen and rate 0.04 in./min.

S.N	λ	β	Equation 4-10	Equation 4-11
UHP-FRC steel	0.9078	0.7114	$\delta_P = 0.91 C_{max}^{0.71}$	$C_{max} = 1.14 \delta_P^{1.41}$
UHP-FRC PE	0.4550	0.4551	$\delta_P = 0.46 C_{max}^{0.45}$	$C_{max} = 5.61 \delta_P^{2.22}$

where δ_P = post peak deformation (in.)

C_{max} = predicated maximum crack width (in.)

4.3.6 Comparison with Direct Tensile Test

The results from double punch test were compared with the direct tensile test for UHP-FRC in Figure 4-44. The peak tensile strength results and post-peak behavior from double punch test and direct tensile test are as shown in Figure 4-27.

Table 4-31 Comparison between double punch test (DPT) and direct tensile test (DTT) for UHP-FRC

Set	Volume fraction (V_f)	Peak tensile stress		DTT/DPT
		Double punch test (DPT)	Direct tensile test (DDT)	
Set 10 & 12	3% Steel	1272.0 psi [8.77 MPa]	920.58 psi [6.35 MPa]	0.73
Set 12	3% Steel	971.6 psi [6.69 MPa]	1102.08 psi [7.60 MPa]	0.89
Set 13	0.75% PE	741.7 psi [5.11 MPa]	641.56 psi [4.43 MPa]	1.15

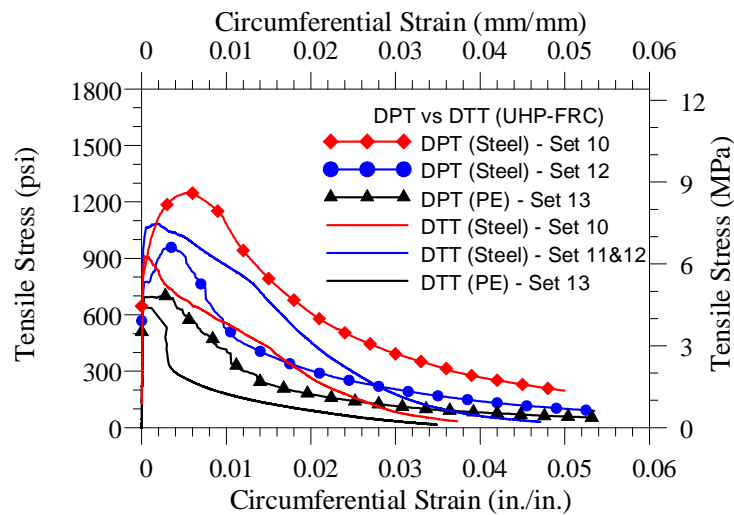


Figure 4-44: Comparison between DPT and DTT for UHP-FRC

4.4 Comparison between Double Punch Test (DPT) and Direct Tensile Test (DTT) for FRC and UHP-FRC

The results from double punch test (DPT) and direct tensile test were compared for FRC with 0.35% and 0.75% volume fraction and also for UHP-FRC with steel and PE fibers.

From

Figure 4-45, it shows that DPT and DTT gives the similar result in terms of peak tensile strength and the difference in peak tensile strength was found be within 15% (Table 2-1).

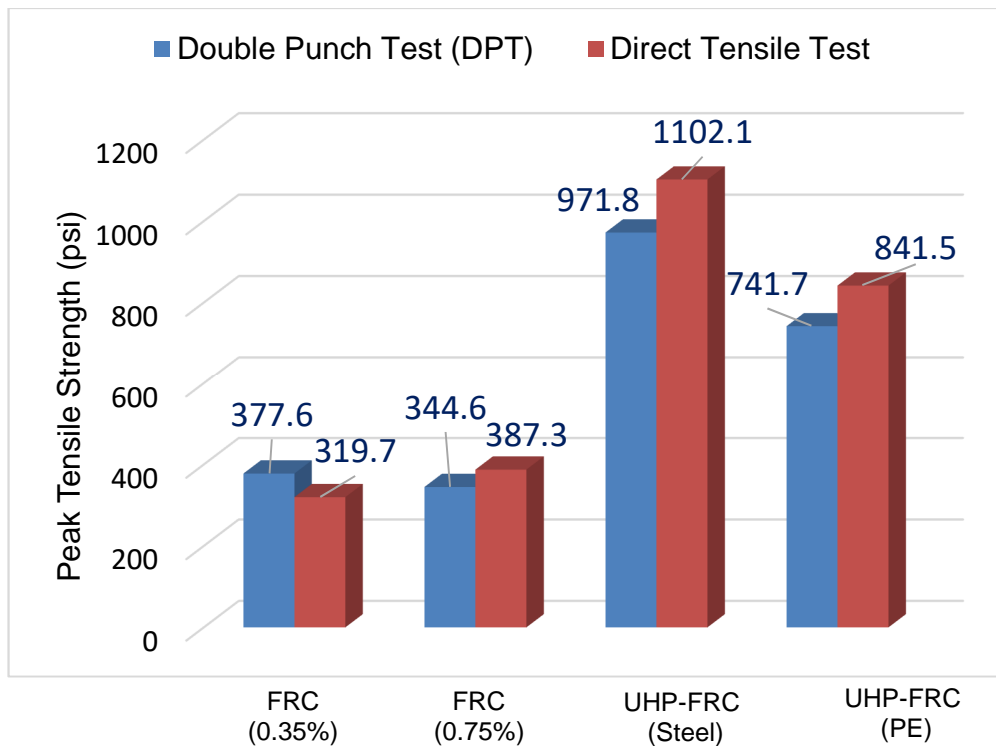


Figure 4-45: Comparison between peak tensile strength obtained from DPT and DTT

Table 4-32: Difference in peak tensile strength from DPT and DTT

Concrete Type	Set	DPT	DTT	Difference in Peak Tensile Strength
FRC (0.35%)	1	377.6 psi	319.7 psi	14 %
FRC (0.75%)	4	344.6 psi	387.3 psi	12 %
UHP-FRC (Steel)		971.8 psi	1102.1 psi	11 %
UHP-FRC (PE)		741.7 psi	841.5 psi	15 %

From Figure 4-46, it can be seen that UHP-FRC has higher peak tensile strength than FRC. UHP-FRC shows strain hardening but FRC does not. UHP-FRC with steel fibers is more ductile than UHP-FRC with PE fibers.

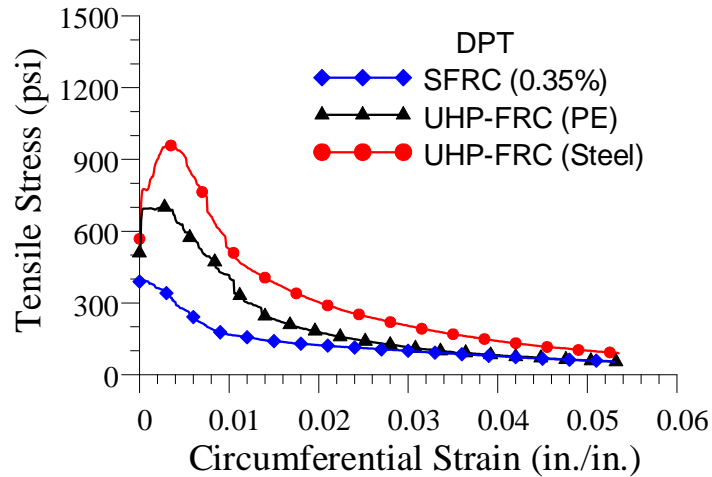


Figure 4-46: Tensile stress vs. circumferential strain from DPT for FRC and UHP-FRC

4.5 Comparison between formula in DPT

Several analytical expressions for determining tensile strength from double punch test are available in the literature and are tabulated in Table 4-33. The calculations for tensile stress were carried and compared using six formulas listed in Table 4-33. From Figure 4-48 and Figure 4-49 shows that the curve using Equation 2-1 is similar to the curve obtained from Equation 2-5. Also, the curve obtained using Equation 2-3 and Equation 2-6 is similar to Equation 2-2. This can be observed for both FRC and UHP-FRC with 6 x 6 in. and 8 x 8 in. specimen.

Table 4-33 Expression for tensile strength using DPT

Equation	Expression	Hypothesis/approach	Author
Equation 2-1	$f_t = \frac{P}{\pi(1.2bh - a^2)}$	Limit analysis of perfect elasto-plastic material	Chen (1970)
Equation 2-2	$f_t = \frac{0.75 \times P}{\pi(1.2bh - a^2)}$	Finite element analysis considering concrete as a linear elastic, plastic strain-hardening and fracture material	Chen and Yuan (1988)
Equation 2-3	$f_t = \frac{0.4P}{d^2} \cdot \sqrt{1 + \frac{d}{\lambda d_a}}$	Non-linear fracture mechanics	Marti (1989)
Equation 2-4	$f_t = \frac{P}{\pi(bh - a^2 \cot \alpha)}$	Modified coulomb like failure criterion for concrete	Bortolotti (1988)
Equation 2-5	$f_t = \frac{4P_f}{9\pi aH}$	Strut and tie model	Mollins et. al. (2007)
Equation 2-6	$f_t = \frac{F_p}{2\pi A} \times \frac{\cos \beta - \mu_k \sin \beta}{\sin \beta + \mu_k \cos \beta}$	Analytical formulation based on simplified multilinear	Blanco et. al. (2014)

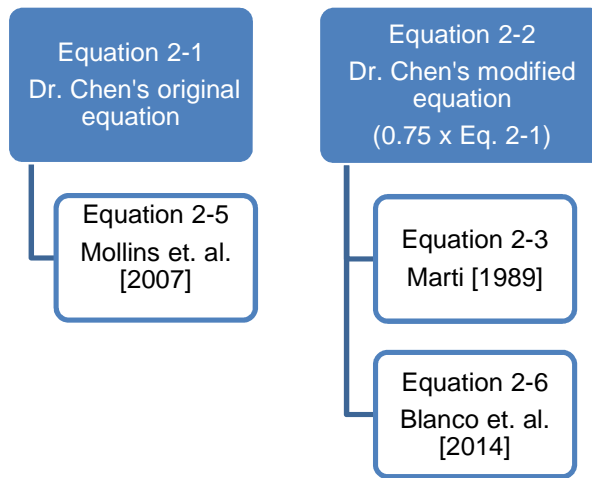


Figure 4-47: Comparison between available expression in the literature

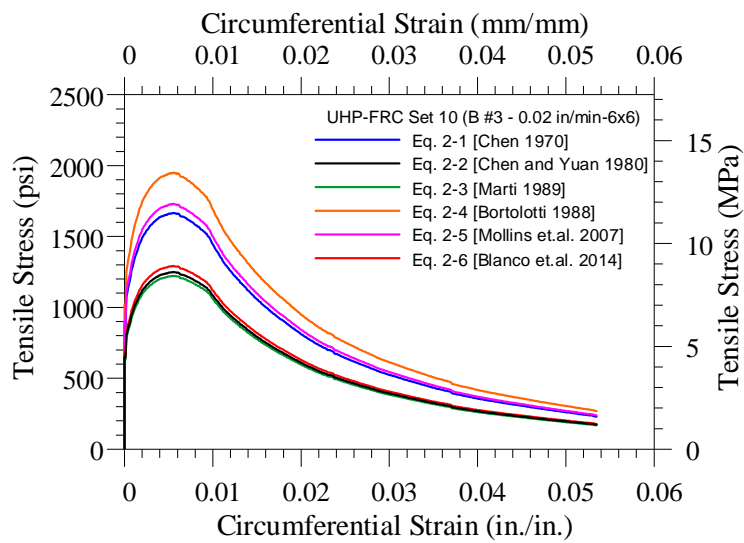


Figure 4-48: Tensile stress vs. circumferential strain (UHP-FRC with steel fibers) with different stress formulas

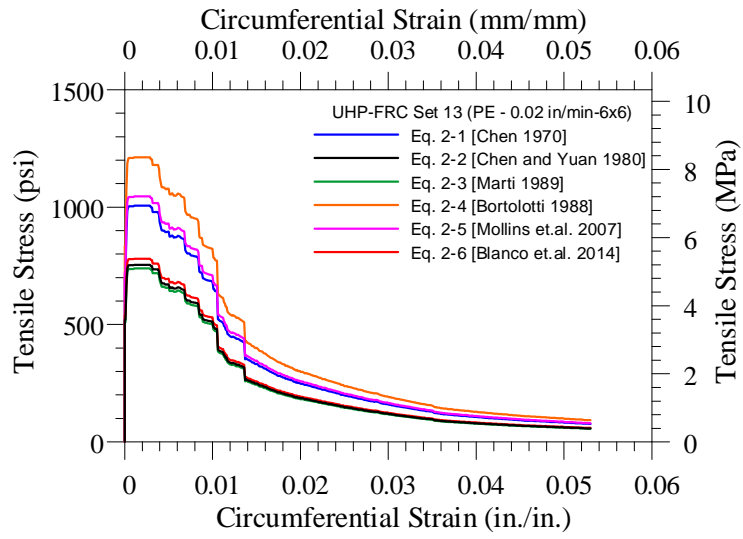


Figure 4-49: Tensile stress vs. circumferential strain (UHP-FRC with PE fibers) with different stress formulas

Chapter 5

Summary and conclusion

The Double Punch Test is an alternative test method for evaluating the performance of FRC and UHP-FRC. The DPT test can be carried by cutting the 6x12 cylinder into two halves. The test setup consists of two LVDTs, a load cell and two punches through which the compressive force can be applied using a simple compression testing machine. The experimental investigation was carried out in two phases. Phase 1 covers the results from 95 samples for steel fiber reinforced concrete and Phase 2 covers the results obtained from 48 samples with ultra-high performance fiber reinforced concrete (UHP-FRC). Fiber volume fraction of 0.35%, 0.45%, 0.55% and 0.75% steel fiber was used in the first phase and comparison based on peak load, peak tensile strength and residual tensile strength at 0.3%, 1%, 2.5% and 5% circumferential strain was carried out. The effects of displacement rates and specimen sizes were also investigated and compared with the direct tensile test in the first phase. Phase 2 was carried out to assess the suitability of DPT method for UHP-FRC material in determining tensile strength and behavior in post cracking phase. The comparison based on peak load, peak tensile strength and residual tensile strength at 0.3%, 1%, 2.5% and 5% circumferential strain was also carried out for phase 2. The effects of displacement rates and specimen height were also studied similar to phase 1.

The statistical analysis verifies the validity of the DPT for comparison purposes. The Double Punch Test can also be used to characterize other aspects of the mechanical performance of SFRC, such as resistance to cracking and residual strength. The simplified testing arrangement, straightforward procedure and reliable result of the DPT makes this method attractive for testing FRC and UHP-FRC. The following conclusions are based on

the results of the DPT for SFRC and UHP-FRC and statistical analysis described in this thesis.

1. Double punch test is simple, easy, reliable and effective test method that is suitable for both SFRC and UHP-FRC.
2. DPT can be used to compare the post-cracking ductility and performance of mixtures containing different fiber types (manufacturer and geometry) as well as different fiber volume fractions (fiber dosage).
3. The test results obtained from DPT represent an averaged mechanical behavior as the failure mechanism occurs along multiple planes; the typical crack pattern is concentrated along three or four radial planes for FRC and two to nine for UHP-FRC.
4. DPT is able to evaluate and compare the quality of mixture from the nature of the cracks (number and crack width) for FRC and UHP-FRC.
5. The displacement rate of 0.04 in./min is recommended for a standard systematic test procedure of DPT. This is the optimum rate for good balance between accuracy, efficiency and time for the test.
6. A correlation between deformation and the circumferential strain was found to be linear for FRC and UHP-FRC. Formulas were derived to estimate the average crack width and maximum crack width at the specified post-peak vertical deformation of DPT samples. This allows DPT to only use LVDTs without using circumferential extensometer and other instrumentation.

For FRC:

$$\text{Average crack width: } CW = \frac{3.78\delta_p}{N}$$

Maximum crack width $C_{\max} = 1.78\delta_p^{1.5}$ (from test data);

Maximum crack width $C_{\max} = 1.78\delta_p^{1.2}$ (upper bound value from test data)

For UHP-FRC with steel fiber:

$$\text{Average crack width: } CW = \frac{4.72\delta_p}{N}$$

Maximum crack width $C_{\max} = 1.14\delta_p^{1.41}$ (median value from test data)

For UHP-FRC with PE fiber:

$$\text{Average crack width: } CW = \frac{4.72\delta_p}{N}$$

Maximum crack width $C_{\max} = 5.61\delta_p^{2.2}$ (median value from test data)

7. The specimen size of 6x6 in. has more consistent results than 6x4 in. and results obtained from 8x8 in. the specimen is almost similar to 6x6 in. The 6x4 in. specimen exhibited a throughout crack in the specimen is lighter than 6x6. However, the coefficient of variation for 6x4 specimen was higher than 6x6.

Recommendation for DPT:

1. If bottom portions have a greater fiber density for a given fiber volume fraction due to segregation during casting, the top and bottom specimens should not be combined directly. It is recommended that the COV in the peak load in the bottom and the top portion should be less than 20% in order to consider both top and bottom samples for average computation.
2. A dimensional guide for the centering plate and steel punches as presented in Figure 3-25 is recommended for use to avoid eccentric loading. The centroid of each steel punch should align with the centroid of the cylinder surface within ± 0.1 in. [± 2.5 mm].

3. Specimen surfaces shall be smoothed so that the steel punches make uniform (flat) contact with the top and bottom faces of the specimen. Smooth contact surfaces can be obtained by grinding the ends of the cylinder.
4. Shakedown procedure is recommended to seat punches and avoid possible unevenness of the surfaces of the specimen. In the shakedown procedure, the load is applied up to 2 kips and then unloaded down to 0.5 kips, and again reloaded to failure.
5. It is recommended to subtract the initial deformation offset from each deformation reading during the reloading phase. The resulting deformations are termed "corrected deformations." Using the recorded loads and the corrected deformations, the maximum load, and residual load/strength are calculated.

Appendix A

Detail calculation and graphs for Phase 1

Table A-1 Calculation of Coefficient of Variation for set 1 (0.35% V_i)

Set 1	At Peak Load		At 0.1 in deformation		Corresponding residual tensile strength at			
	Peak Load	Peak Tensile Strength	Corresponding load at 0.1 in. deformation	Equivalent Tensile Strength	0.003 circumferential strain	0.01 circumferential strain	0.025 circumferential strain	0.05 circumferential strain
	kips	psi	kips	psi	psi	psi	psi	psi
B 1	34.09	386.8	16.4	186.1	338.5	241.8	145.1	73.2
B 2	38.2	433.8	10.8	123.0	424.1	172.7	117.4	48.4
B 3	39.0	442.1	13.8	156.1	386.8	187.9	129.9	64.9
B 4	31.9	361.9	12.5	142.3	308.1	183.7	127.1	98.1
B 5	39.7	450.4	11.9	135.4	368.9	218.3	102.2	53.9
B 6	36.2	410.3	13.4	152.0	310.8	196.2	136.8	58.0
T 1	34.3	389.6	9.0	102.2	308.1	142.3	95.3	-
T 2	34.9	396.5	10.3	117.4	366.1	124.3	85.7	53.9
T 3	34.3	389.6	8.4	95.3	388.2	136.8	92.6	47.0
T 4	33.8	384.0	6.3	71.8	316.4	113.3	71.8	47.0
T 5	32.9	373.0	11.3	128.5	368.9	147.8	120.2	59.4
T 6	37.6	426.9	12.1	136.8	393.7	143.7	110.5	58.0
Average	35.6	403.7	11.4	128.9	356.5	167.4	111.2	60.2
Standard Deviation	2.5	28.5	2.7	30.3	39.3	39.3	22.2	14.9
COV (%)	7.1	7.1	23.5	23.5	11.0	23.5	19.9	24.7

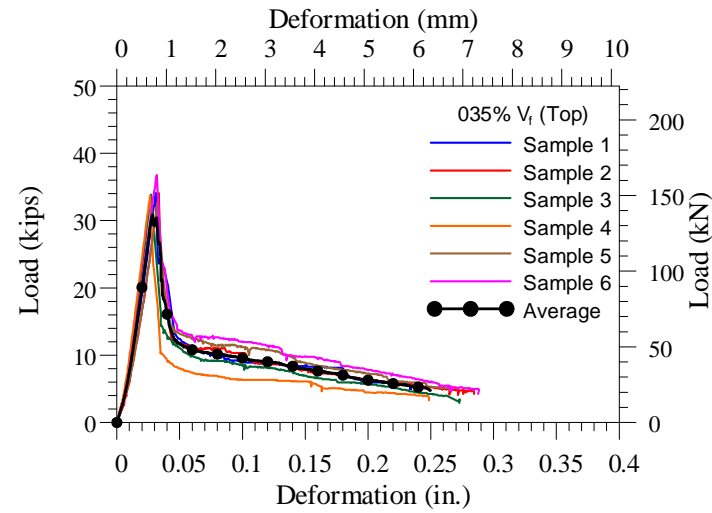
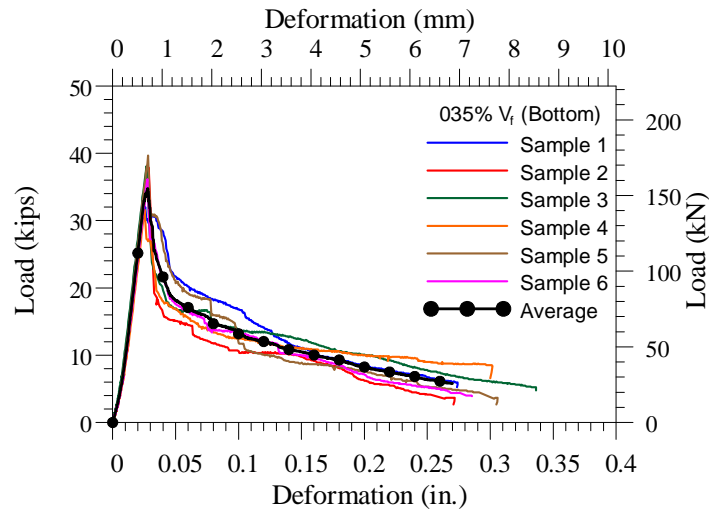


Figure A-1: Load vs. Deformation - Set 1 (With 0.35% Bottom and Top Cylinders)

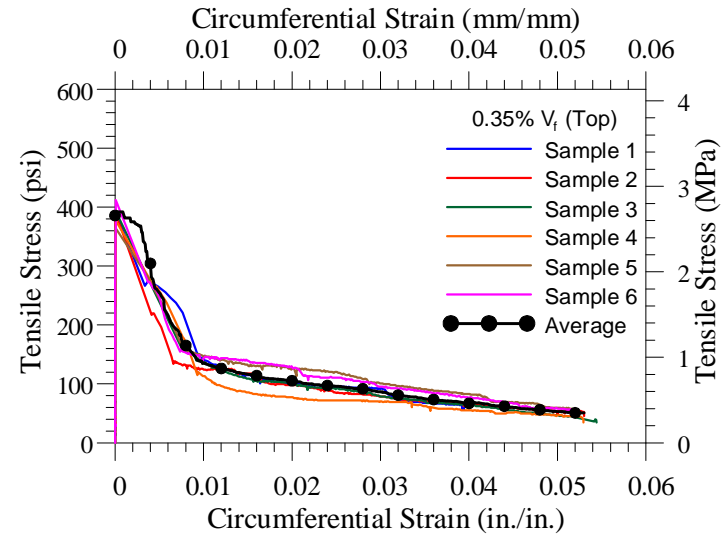
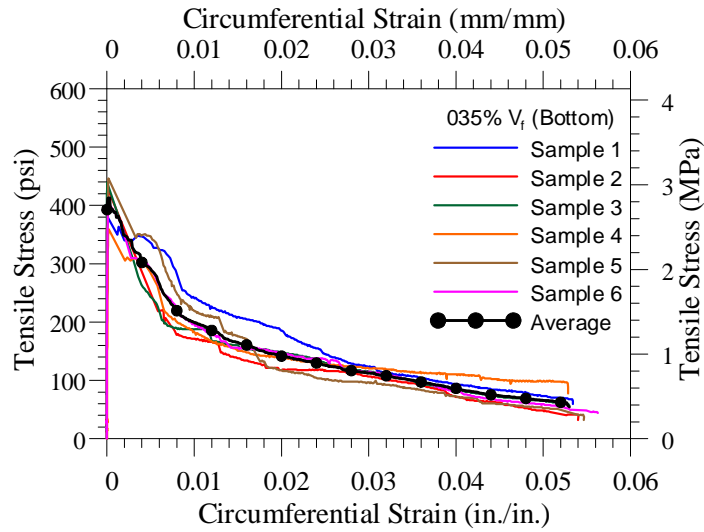


Figure A-2: Tensile Stress vs. Circumferential Strain - Set 1 (With 0.35% Bottom and Top Cylinders)

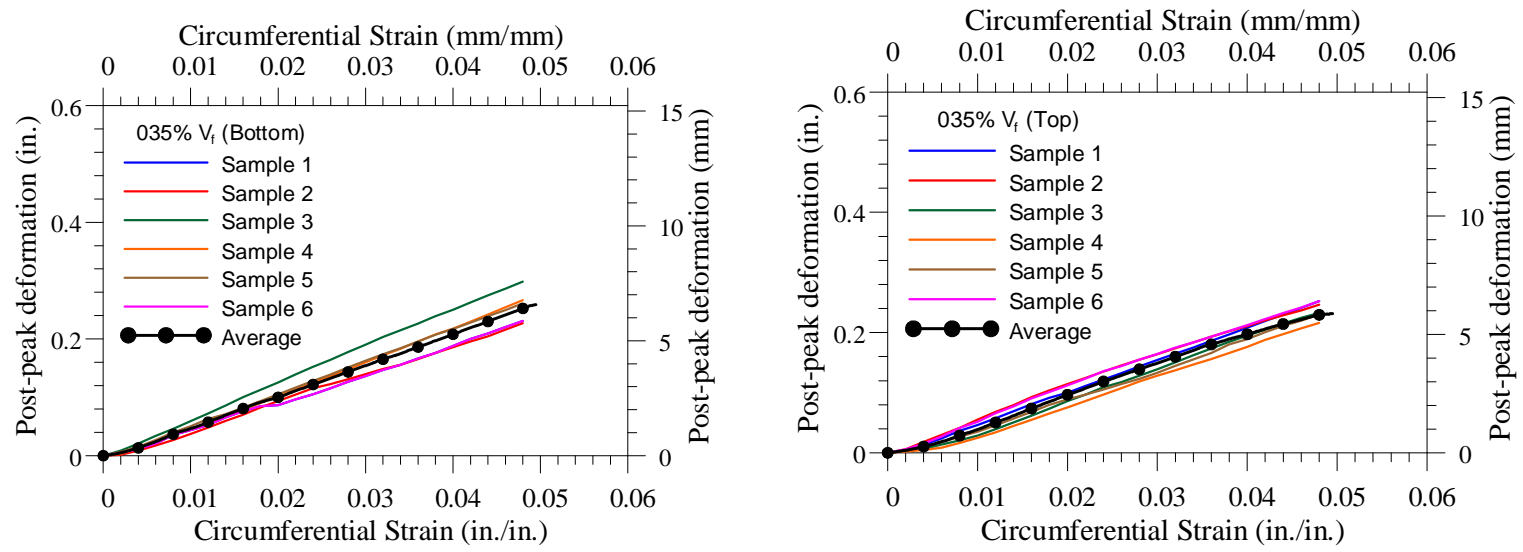


Figure A-3: Post-peak deformation vs. Circumferential Strain – Set 1 (With 0.35% Bottom and Top Cylinders)

Table A-2 Calculation of Coefficient of Variation for set 2 (0.45% V_i)

Set 2	At Peak Load		At 0.1 in deformation		Corresponding residual tensile strength at		
	Peak Load	Peak Tensile Strength	Corresponding load at 0.1 in. deformation	Equivalent Tensile Strength	0.003 circumferential strain	0.01 circumferential strain	0.025 circumferential strain
	kips	psi	kips	psi	psi	psi	psi
B 1	42.9	486.6	17.8	201.6	439.2	234.4	157.3
B 2	37.6	426.2	19.8	224.5	377.6	248.6	184.9
B 3	33.8	383.4	15.9	180.5	277.1	220.0	133.2
B 4	42.0	477.0	19.2	218.0	199.3	212.0	137.7
B 5	42.4	481.6	20.2	228.7	407.9	293.3	176.7
B 6	40.0	454.0	17.2	195.6	447.7	218.0	150.4
T 1	40.5	459.1	15.9	180.7	273.7	194.6	127.5
T 2	40.1	454.6	17.2	194.9	441.4	207.8	122.3
T 3	33.8	383.0	13.0	147.1	328.4	193.6	123.0
T 4	31.7	359.7	15.9	180.7	237.1	179.5	117.8
T 5	30.1	342.0	11.8	134.0	298.5	147.9	118.1
T 6	27.7	314.4	15.0	169.8	253.0	232.9	141.2
Average	36.9	418.5	16.6	188.0	331.7	215.2	140.9
Standard Deviation	5.2	59.5	2.6	29.0	87.9	36.5	22.5
COV (%)	14.2	14.2	15.4	15.4	26.5	17.0	15.9

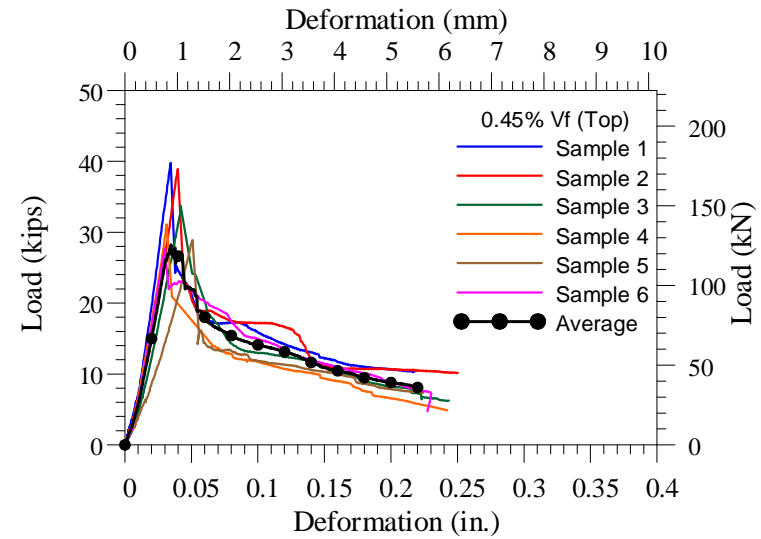
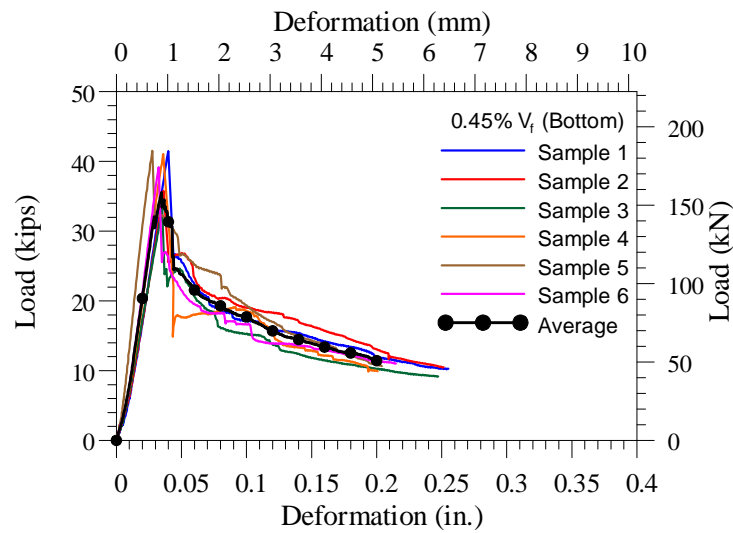


Figure A-4: Load vs. Deformation – Set 2 (With 0.45% Bottom and Top Cylinders)

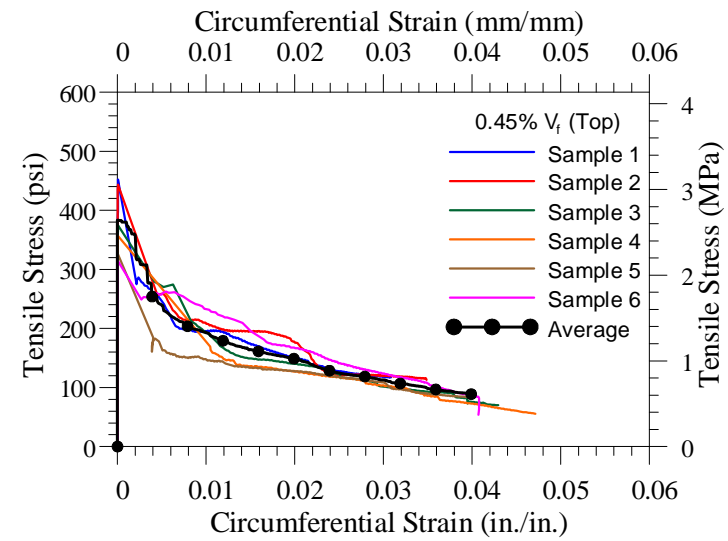
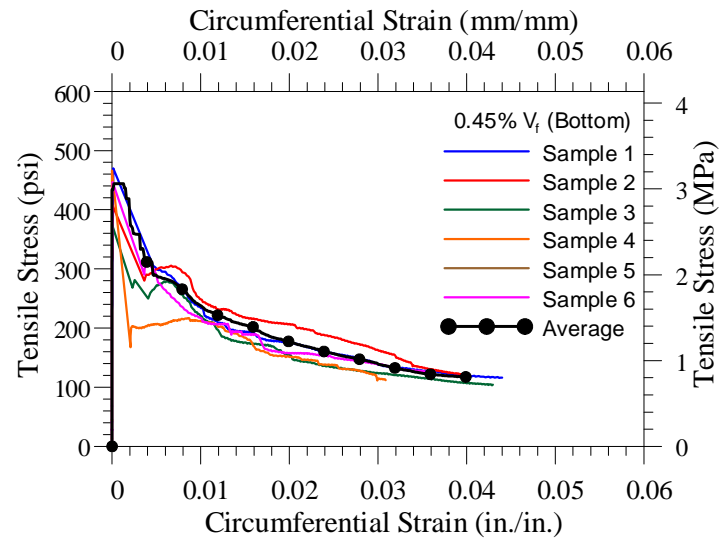


Figure A-5: Tensile Stress vs. Circumferential Strain – Set 2 (With 0.45% Bottom and Top Cylinders)

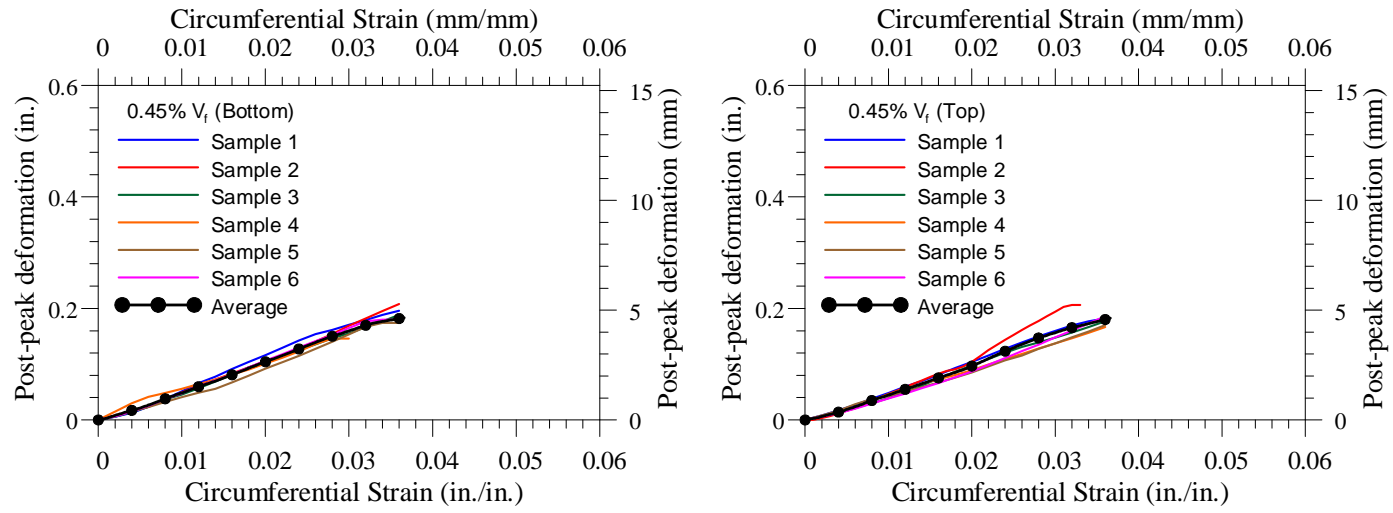


Figure A-6: Post-peak deformation vs. Circumferential Strain – Set 2 (With 0.45% Bottom and Top Cylinders)

Table A-3 Calculation of Coefficient of Variation for set 3 (0.55% V_i)

Set 3	At Peak Load		At 0.1 in deformation		Corresponding residual tensile strength at			
	Peak Load	Peak Tensile Strength	Corresponding load at 0.1 in. deformation	Equivalent Tensile Strength	0.003 circumferential strain	0.01 circumferential strain	0.025 circumferential strain	0.05 circumferential strain
	kips	psi	kips	psi	psi	psi	psi	psi
B 1	32.6	370.1	15.7	178.2	329.3	203.6	143.4	80.5
B 2	30.6	346.9	15.5	175.5	303.5	198.4	130.0	74.6
B 3	33.8	383.8	15.1	171.0	295.3	230.4	168.8	98.7
B 4	36.3	412.3	23.4	265.7	399.4	281.9	223.0	141.7
B 5	32.6	370.3	21.7	246.6	360.2	274.2	189.4	116.6
B 6	33.4	379.3	11.6	131.2	283.1	181.7	127.8	91.0
T 1	28.7	325.4	10.9	124.0	266.2	196.1	118.1	63.9
T 2	30.5	346.5	11.4	129.3	258.0	192.9	111.9	20.9
T 3	28.4	322.6	16.4	186.4	268.0	220.7	125.5	63.6
T 4	28.4	322.4	15.0	170.5	316.9	190.4	127.0	66.1
T 5	33.9	385.0	13.5	152.9	276.4	166.8	112.1	45.5
T 6	32.6	369.9	13.1	148.4	280.9	202.8	122.5	39.0
Average	31.8	361.2	15.3	173.3	303.1	211.7	141.6	75.2
Standard Deviation	2.5	28.5	3.9	44.0	42.3	35.1	34.5	33.6
COV (%)	7.9	7.9	25.4	25.4	14.0	16.6	24.4	44.8

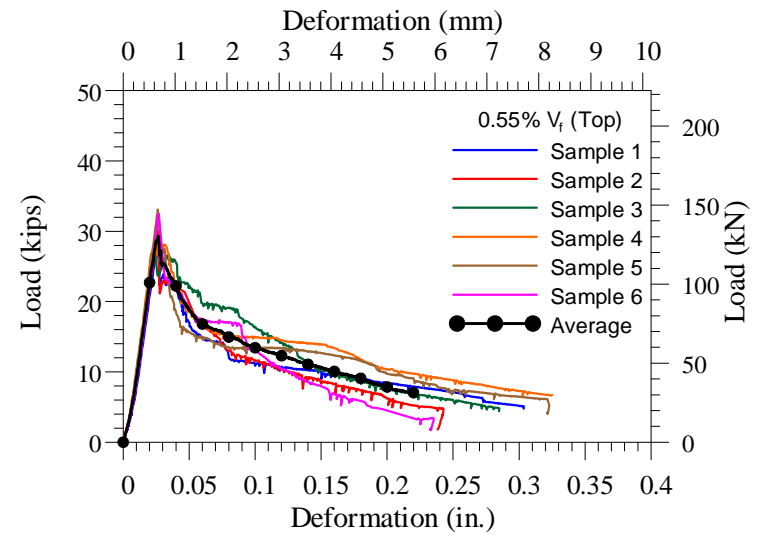
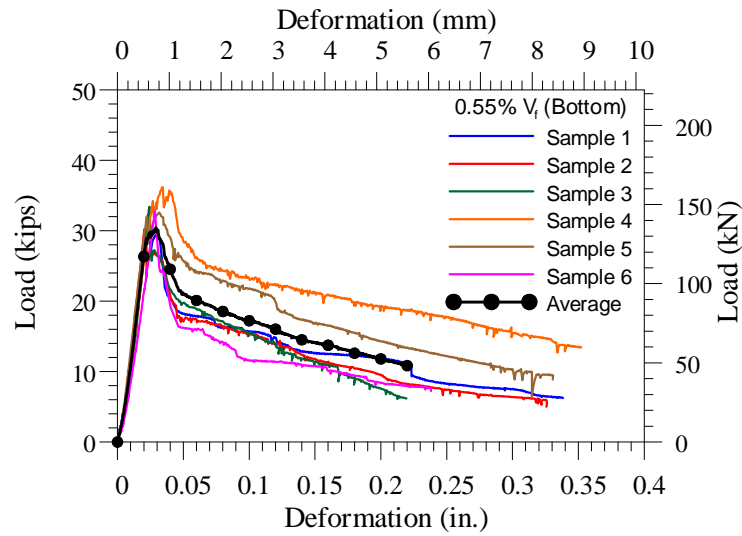


Figure A-7: Load vs. Deformation – Set 3 (With 0.55% Bottom and Top Cylinders)

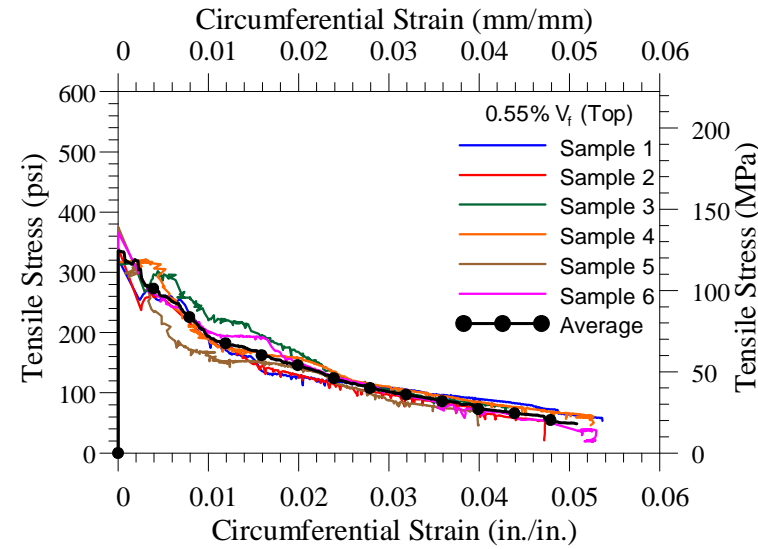
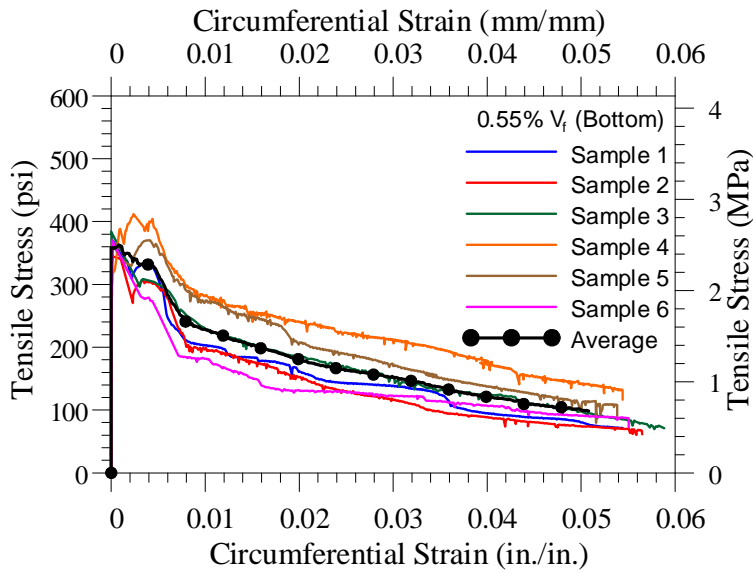


Figure A-8: Tensile Stress vs. Circumferential Strain – Set 3 (With 0.55% Bottom and Top Cylinders)

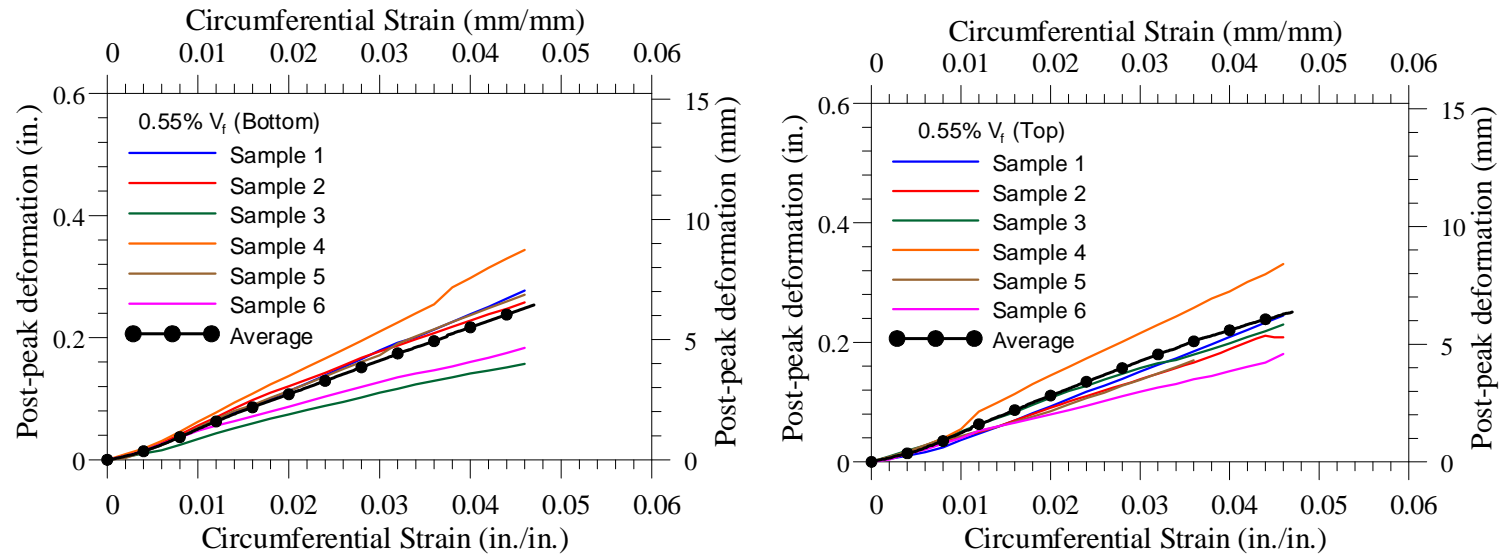


Figure A-9: Post-peak deformation vs. Circumferential Strain – Set 3 (With 0.55% Bottom and Top Cylinders)

Table A-4 Calculation of Coefficient of Variation for set 4 (0.75% Vf)

Set 4	At Peak Load		At 0.1 in deformation		Corresponding residual tensile strength at			
	Peak Load	Peak Tensile Strength	Corresponding load at 0.1 in. deformation	Equivalent Tensile Strength	0.01 circumferential strain	0.003 circumferential strain	0.025 circumferential strain	0.05 circumferential strain
	kips	psi	kips	psi	psi	psi	psi	psi
B 1	31.65	359.2	19.6	222.4	244.5	355.0	186.5	120.2
B 2	33.1	375.8	20.0	226.6	259.7	327.4	182.4	85.7
B 3	33.7	382.7	24.0	272.2	301.2	370.2	227.9	147.8
B 4	34.3	389.6	18.0	204.5	230.7	356.4	161.6	67.7
B 5	29.3	332.9	15.9	181.0	192.0	315.0	167.2	109.1
B 6	31.8	360.6	25.2	286.0	319.1	315.0	245.9	89.8
T 1	31.2	353.7	9.9	111.9	136.8	262.5	102.2	64.9
T 2	30.2	342.6	12.4	140.9	183.7	259.7	118.8	87.0
T 3	27.9	316.4	15.3	174.1	219.7	298.4	143.7	91.2
T 4	26.4	299.8	10.5	118.8	183.7	250.0	98.1	48.4
T 5	26.8	303.9	17.9	203.1	241.8	263.9	164.4	91.2
T 6	27.9	316.4	14.2	161.6	226.6	297.0	142.3	59.4
Average	30.4	344.4	16.9	191.9	228.3	305.9	161.7	88.5
Standard Deviation	2.7	30.7	4.9	55.1	51.1	41.3	45.4	27.7
COV (%)	8.9	8.9	28.7	28.7	22.4	13.5	28.1	31.3

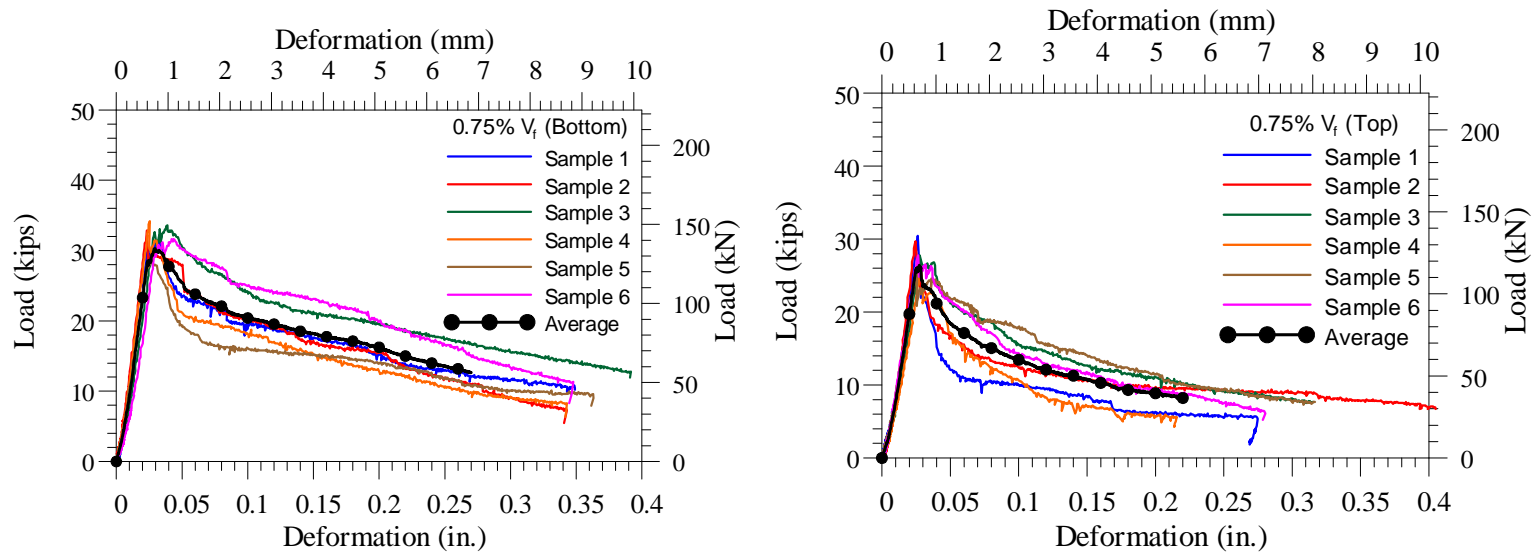


Figure A-10: Load vs. Deformation – Set 4 (With 0.75% Bottom and Top Cylinders)

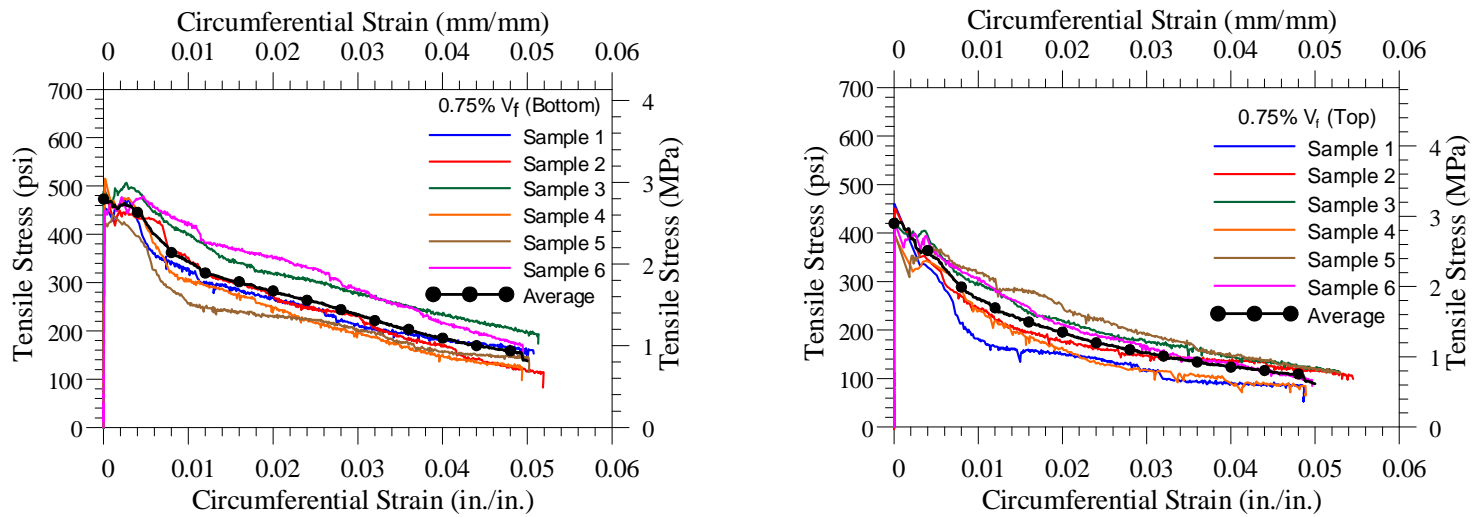


Figure A-11: Tensile Stress vs. Circumferential Strain – Set 4 (With 0.75% Bottom and Top Cylinders)

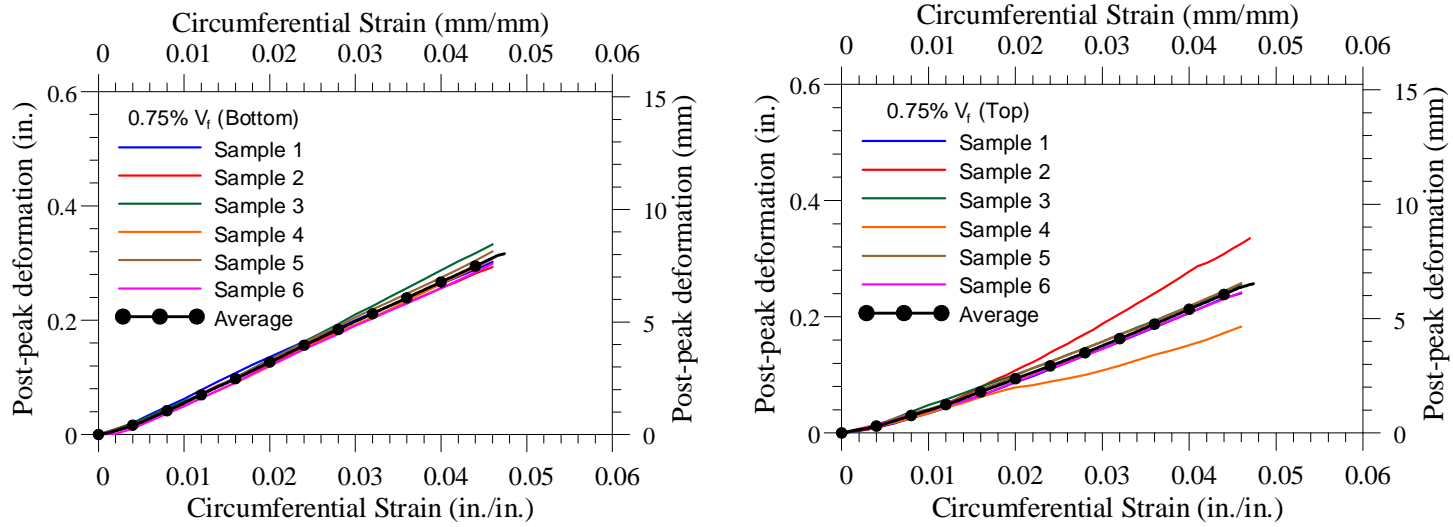


Figure A-12: Post-peak deformation vs. Circumferential Strain – Set 4 (With 0.75% Bottom and Top Cylinders)

Table A-5 Calculation of Coefficient of Variation for set 6 (0.35% V_f and 0.04 in./min displacement rate)

Set 5	At Peak Load		At 0.1 in deformation		Corresponding residual tensile strength at			
	Peak Load	Peak Tensile Strength	Corresponding load at 0.1 in. deformation	Equivalent Tensile Strength	0.01 circumferential strain	0.003 circumferential strain	0.025 circumferential strain	0.05 circumferential strain
	kips	psi	kips	psi	psi	psi	psi	psi
B 1	34.57	400.7	11.8	136.8	519.4	186.0	171.3	106.8
B 2	31.90	369.6	5.97	69.1	335.7	193.4	69.1	42.8
B 3	37.13	430.3	13.15	152.4	406.2	161.6	105.0	70.5
B 4	29.70	344.2	8.64	100.2	254.2	124.3	76.0	53.9
B 5	36.16	419.0	12.54	145.3	397.9	160.3	92.6	47.0
B 6	32.63	378.1	10.71	124.2	360.6	143.7	106.4	69.1
T 1	33.72	390.8	12.66	146.7	291.5	176.8	117.4	56.6
T 2	29.58	342.8	7.55	87.5	326.0	95.3	78.7	58.0
T 3	36.52	423.2	15.22	176.4	348.1	196.2	158.9	93.9
T 4	32.36	375.0	9.98	115.7	327.5	150.6	96.7	59.4
T 5	28.97	335.8	17.90	207.4	273.5	215.5	175.4	98.1
T 6	27.76	321.7	14.61	169.3	257.0	197.6	123.0	66.3
Average	32.6	377.6	11.7	135.9	341.5	166.8	114.2	68.5
Standard Deviation	3.1	36.4	3.4	39.3	74.9	34.6	36.6	20.6
COV (%)	9.6	9.6	28.9	28.9	21.9	20.7	32.1	30.1

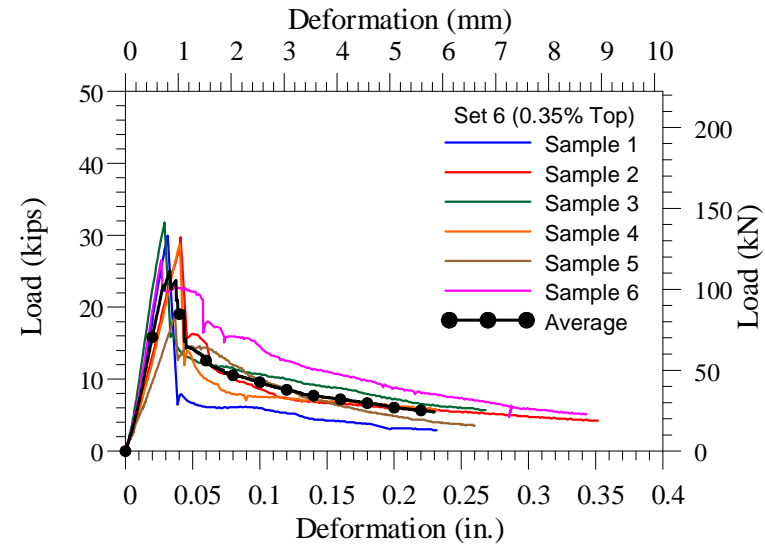
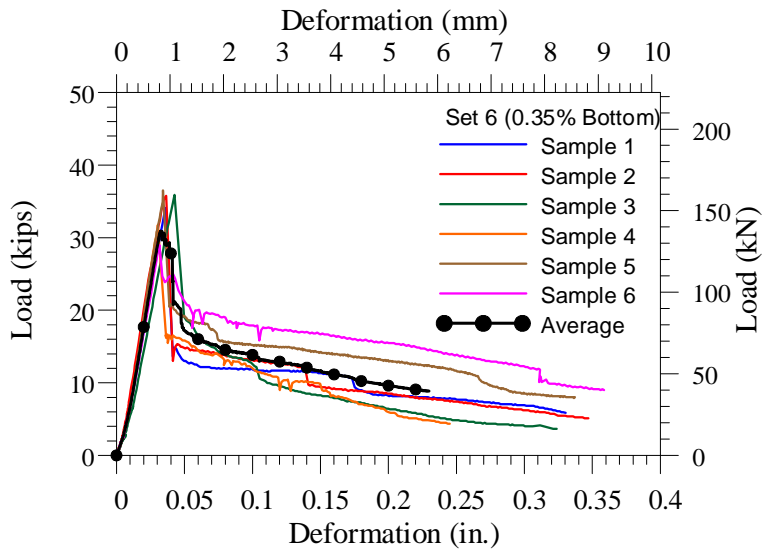


Figure A-13: Load vs. Deformation – Set 6 (With 0.35% Bottom and Top Cylinders)

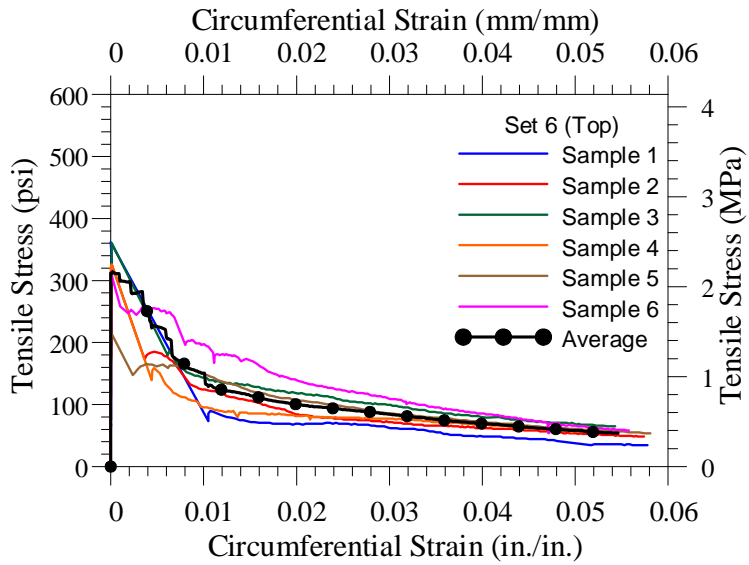
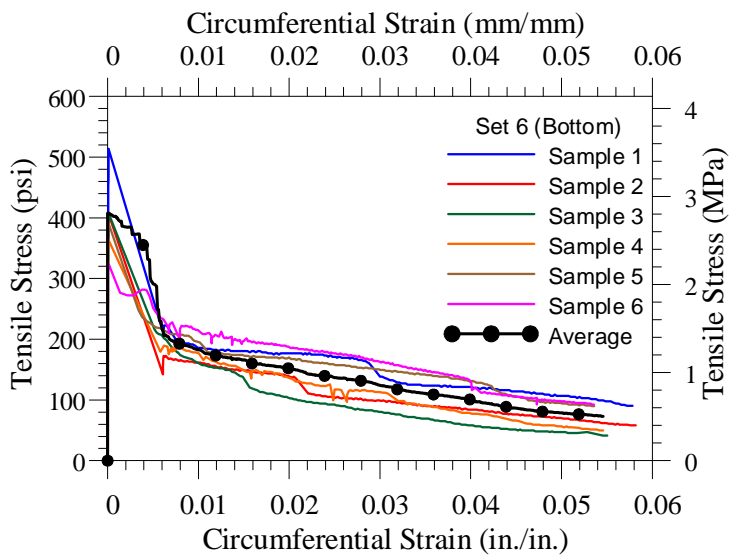


Figure A-14: Tensile Stress vs. Circumferential Strain – Set 6 (With 0.35% Bottom and Top Cylinders)

Table A-6 Calculation of Coefficient of Variation for set 7 (0.55% V_f , 0.04 in./min displacement rate and 6x6 in. size)

Set 7	At Peak Load		At 0.1 in deformation		Corresponding residual tensile strength at			
	Peak Load	Peak Tensile Strength	Corresponding load at 0.1 in. deformation	Equivalent Tensile Strength	0.01 circumferential strain	0.003 circumferential strain	0.025 circumferential strain	0.05 circumferential strain
	kips	psi	kips	psi	psi	psi	psi	psi
B 1	36.40	413.1	13.76	156.1	374.4	157.5	129.9	95.3
B 2	42.85	486.3	24.47	277.7	352.3	291.5	189.3	98.1
B 3	34.57	392.3	20.94	237.6	355.0	255.6	168.5	98.1
T 1	34.45	391.0	17.53	198.9	287.3	223.8	165.8	64.9
T 2	40.05	454.5	15.95	181.0	382.7	203.1	143.7	69.1
T 3	36.40	413.1	22.03	250.0	301.2	276.3	185.1	111.9
Average	37.5	425.0	19.1	216.9	342.1	234.6	163.7	89.6
Standard Deviation	3.3	37.8	4.0	45.9	39.1	49.9	23.2	18.5
COV (%)	8.9	8.9	21.2	21.2	11.4	21.3	14.2	20.6

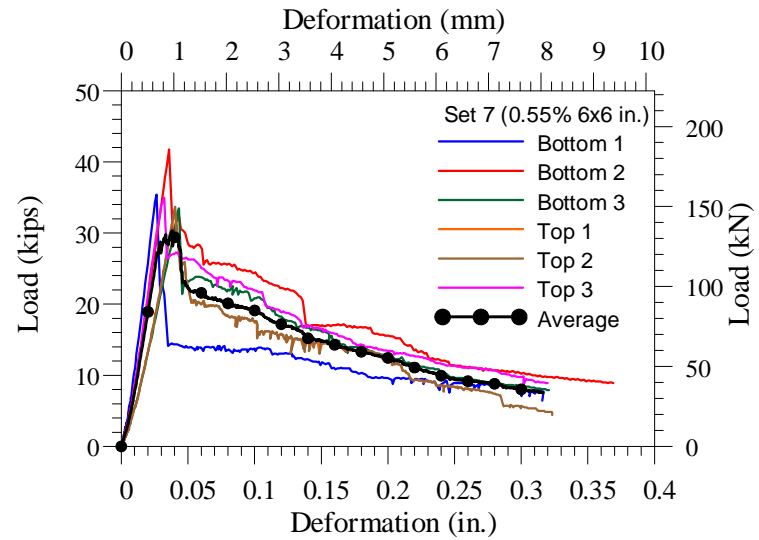


Figure A-15: Load vs. Deformation – Set 7 (With 0.55% Bottom and Top Cylinders and 6x6 in.)

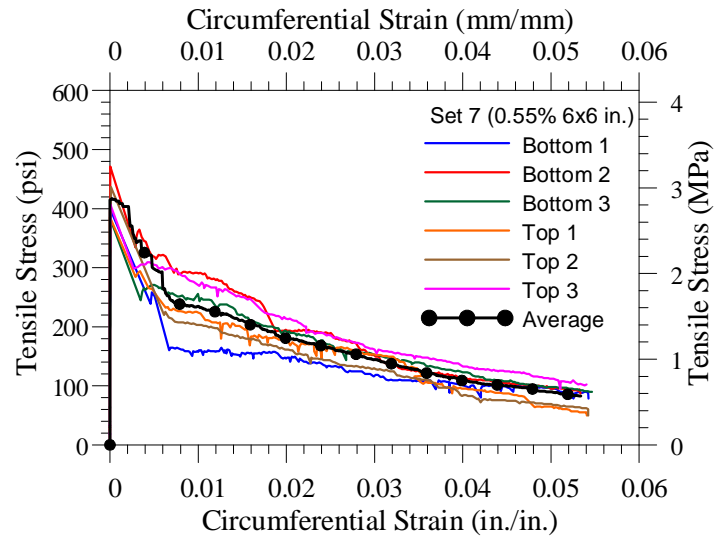


Figure A-16: Tensile Stress vs. Circumferential Strain – Set 7 (With 0.55% Bottom and Top Cylinders and 6x6 in.)

Table A-7 Calculation of Coefficient of Variation for set 8 (0.55% V_f , 0.04 in./min displacement rate and 6x4 in. size)

Set 8	At Peak Load		At 0.1 in deformation		Corresponding residual tensile strength at			
	Peak Load	Peak Tensile Strength	Corresponding load at 0.1 in. deformation	Equivalent Tensile Strength	0.01 circumferential strain	0.003 circumferential strain	0.025 circumferential strain	0.05 circumferential strain
	kips	psi	kips	psi	psi	psi	psi	psi
B 1	28.97	328.8	14.37	163.0	434.8	315.0	205.8	109.2
B 2	23.13	262.5	14.00	158.9	348.6	310.8	195.3	98.7
B 3	29.83	338.5	13.76	156.1	382.3	258.3	199.5	119.7
M 1	30.30	343.8	5.83	66.2	489.1	197.2	113.2	62.8
M 2	28.73	326.0	14.49	164.4	407.5	300.3	214.2	100.8
M 3	32.26	366.1	10.10	114.7	372.8	199.5	193.2	86.8
T 1	26.90	305.3	15.34	174.1	346.5	291.9	235.2	147.0
T 2	23.37	265.2	11.32	128.5	304.5	212.1	172.2	102.9
T 3	27.39	310.8	10.10	114.7	331.8	212.1	144.9	105.0
Average	27.9	316.3	12.1	137.8	379.8	255.3	186.0	103.7
Standard Deviation	3.1	34.7	3.1	34.9	56.8	50.3	37.3	22.8
COV (%)	11.0	11.0	25.3	25.3	15.0	19.7	20.0	22.0

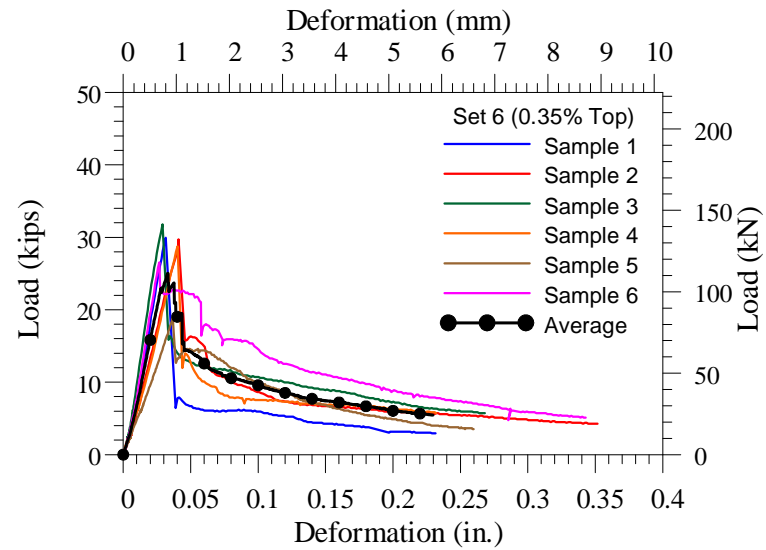


Figure A-17: Load vs. Deformation – Set 8 (With 0.55% Bottom and Top Cylinders and 6x4 in.)

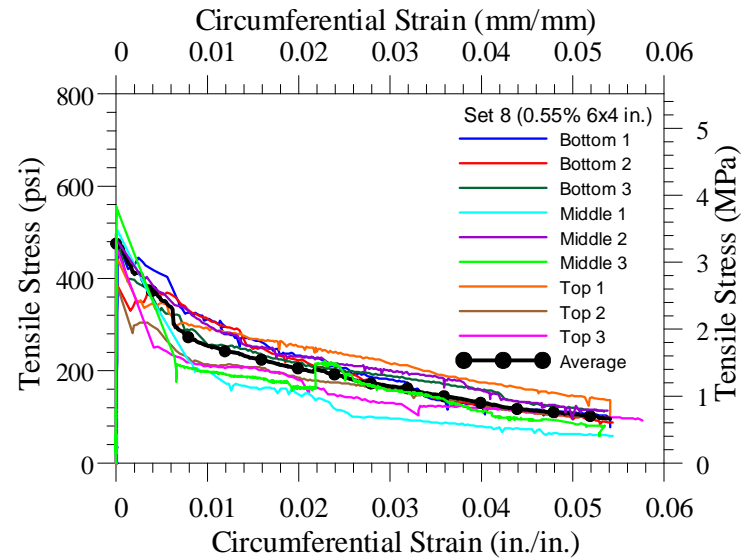


Figure A-18: Tensile Stress vs. Circumferential Strain – Set 8 (With 0.55% Bottom and Top Cylinders and 6x4 in.)

Table A-8 Calculation of Coefficient of Variation for set 9 (0.55% V_f , 0.04 in./min displacement rate and 8x8 in. size)

Set 9	At Peak Load		At 0.1 in deformation		Corresponding residual tensile strength at			
	Peak Load	Peak Tensile Strength	Corresponding load at 0.1 in. deformation	Equivalent Tensile Strength	0.01 circumferential strain	0.003 circumferential strain	0.025 circumferential strain	0.05 circumferential strain
	kips	psi	kips	psi	psi	psi	psi	psi
B 1	60.63	387.0	48.3	308.5	384.7	262.7	152.3	87.0
B 2	66.47	424.3	39.81	254.1	313.2	242.4	148.4	88.6
B 3	69.27	442.2	32.75	209.0	330.3	212.1	114.2	58.3
B 4	78.52	501.2	58.80	375.3	348.9	272.0	174.8	83.9
B 5	71.58	456.9	44.31	282.9	425.8	327.2	199.7	143.0
B 6	77.30	493.4	34.94	223.0	279.7	197.4	111.9	73.0
T 1	63.67	406.4	43.58	278.2	364.1	267.3	178.2	98.3
T 2	74.02	472.5	50.16	320.2	366.0	304.6	152.3	83.1
T 3	73.77	470.9	46.99	300.0	383.1	259.5	116.6	53.6
T 4	71.58	456.9	29.83	190.4	406.4	215.3	115.8	59.1
T 5	73.89	471.7	47.48	303.1	428.9	297.6	192.7	110.3
T 6	76.21	486.5	35.18	224.6	484.9	281.3	128.2	67.6
Average	71.4	455.8	42.7	272.4	376.3	261.6	148.8	83.8
Standard Deviation	5.5	35.1	8.4	53.8	56.0	39.4	31.9	25.2
COV (%)	7.7	7.7	19.7	19.7	14.9	15.1	21.4	30.1

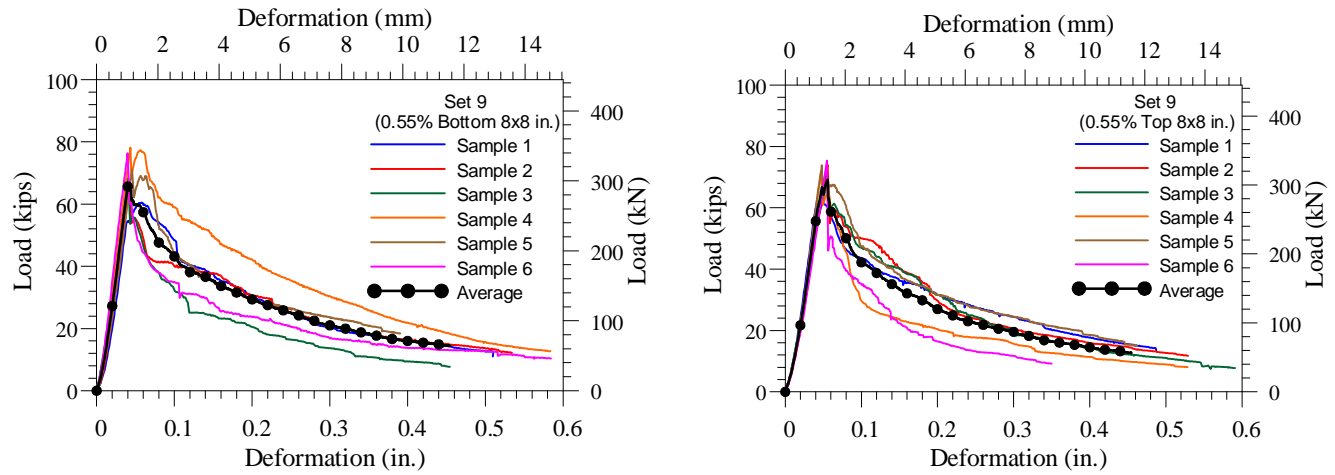


Figure A-19: Load vs. Deformation- Set 9 (With 0.55% Bottom and Top Cylinders and 8x8 in.)

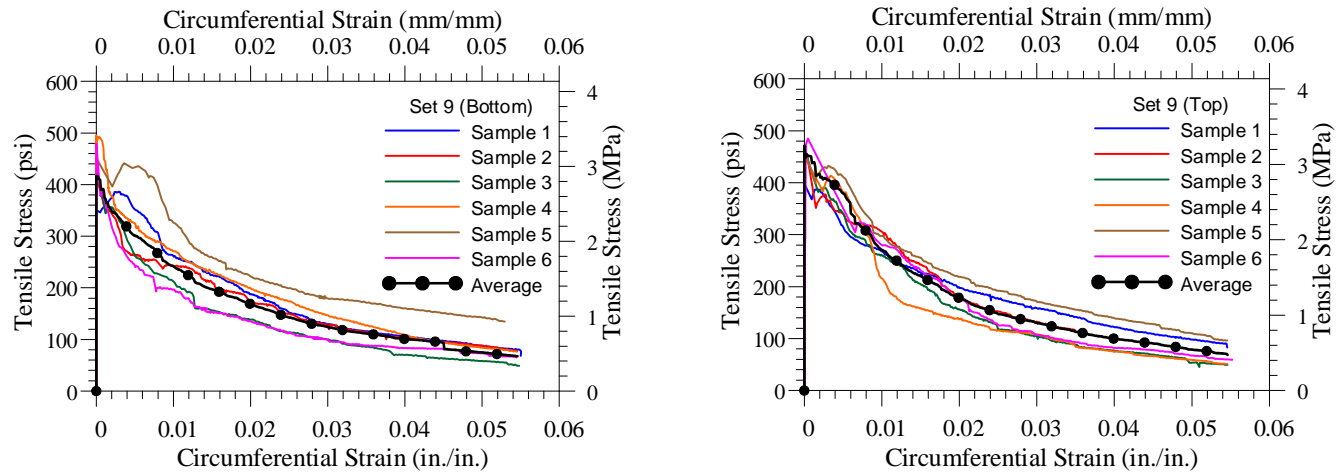


Figure A-20: Tensile Stress vs. Circumferential Strain – Set 9 (With 0.55% Bottom and Top Cylinders and 8x8 in.)

Appendix B

Detail calculation and graphs for Phase 2

Table B-1 Calculation of Coefficient of Variation for set 10 (UHP-FRC with 3% steel fiber and 6 x 6 in. size)

Set 10	At Peak Load		At 0.1 in deformation		Corresponding residual tensile stress at			
	Peak Load	Peak Tensile Strength	Corresponding load at 0.1 in. deformation	Equivalent Tensile Strength	0.003 circumferential strain	0.01 circumferential strain	0.025 circumferential strain	0.05 circumferential strain
	kips	psi	kips	psi	psi	psi	psi	psi
B 1	122.2	1387.0	121.4	1377.3	1298.6	1215.7	480.8	127.1
B 2	122.8	1393.9	121.1	1374.6	1254.4	1295.8	704.6	373.0
B 3	113.5	1287.5	104.7	1188.1	1237.8	1018.1	327.4	123.0
B 4	108.0	1225.4	97.0	1101.0	1125.9	1183.9	678.3	308.1
T 1	115.9	1315.2	113.7	1290.3	1167.3	1130.0	367.5	110.5
T 2	123.8	1405.0	123.0	1395.3	1275.1	1366.3	529.1	194.8
T 3	94.2	1069.3	70.5	799.9	1054.1	645.1	321.9	129.9
T 4	96.3	1092.7	70.2	797.1	1073.4	810.9	454.5	200.3
Average	112.1	1272.0	102.7	1165.4	1185.8	1083.2	483.0	195.8
Standard Deviation	11.7	132.7	21.9	248.1	94.1	246.5	148.2	96.9
COV (%)	10.4	10.4	21.3	21.3	7.9	22.8	30.7	49.5

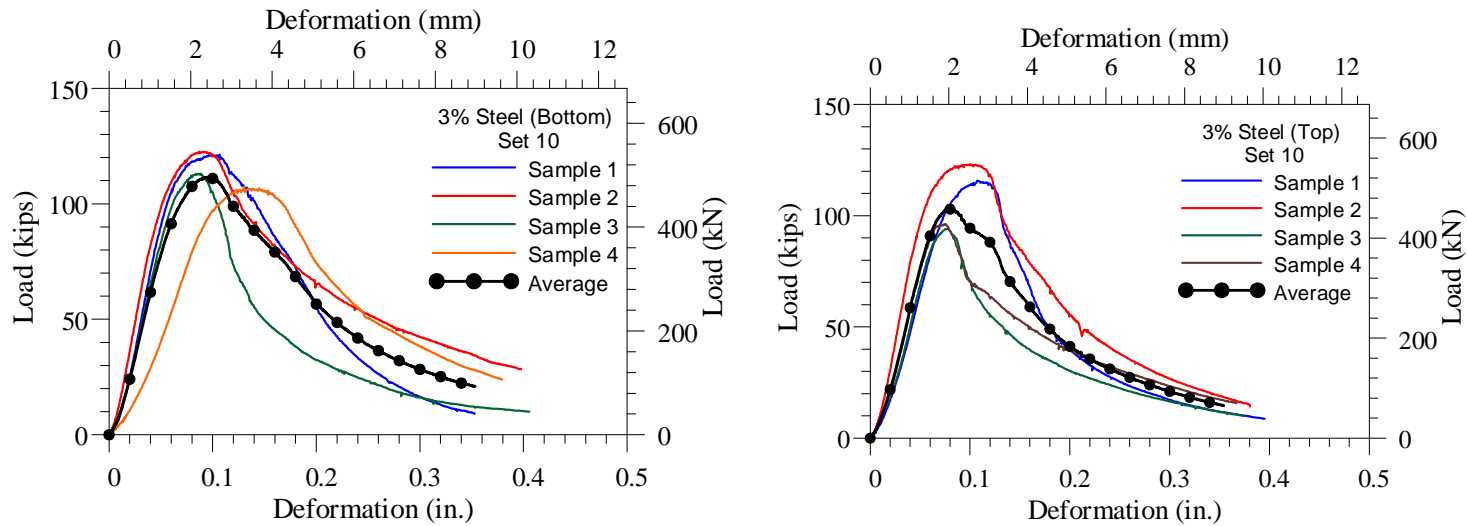


Figure B-1: Load vs. Deformation – Set 10 (With 3% Steel fibers Bottom and Top Cylinders)

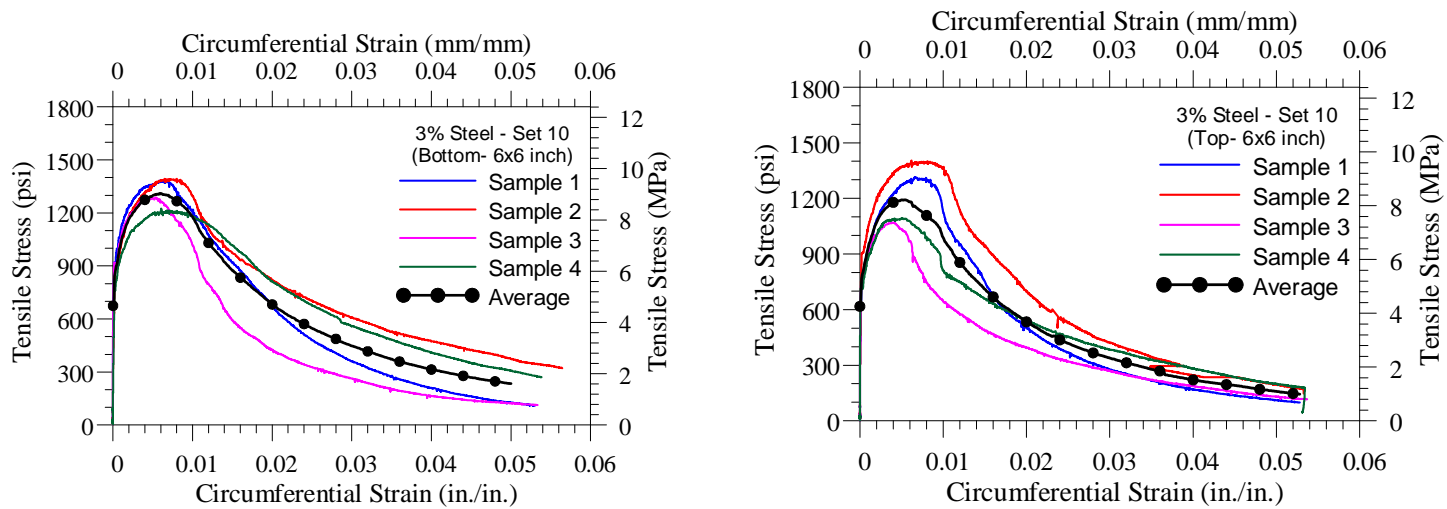


Figure B-2: Tensile Stress vs. Circumferential Strain – Set 10 (With 3% steel fibers Bottom and Top Cylinders)

Table B-2 Calculation of Coefficient of Variation for set 11 (UHP-FRC with 3% steel fiber and 6 x 6 in. size)

Set 11	At Peak Load		At 0.1 in deformation		Corresponding residual tensile stress at			
	Peak Load	Peak Tensile Strength	Corresponding load at 0.1 in. deformation	Equivalent Tensile Strength	0.003 circumferential strain	0.01 circumferential strain	0.025 circumferential strain	0.05 circumferential strain
	kips	psi	kips	psi	psi	psi	psi	psi
B 1	113.5	1287.5	104.7	1188.1	1018.1	1237.8	327.4	123.0
B 2	107.6	1221.2	104.3	1183.9	1148.0	1167.3	399.2	110.5
B 3	82.4	935.3	22.5	255.6	313.6	918.7	161.6	59.4
B 4	95.4	1083.1	52.0	589.9	596.8	1076.2	313.6	127.1
Average	99.7	1131.8	70.9	804.4	769.1	1100.0	300.5	105.0
Standard Deviation	13.8	156.3	40.7	461.3	384.2	137.8	99.9	31.2
COV (%)	13.8	13.8	57.4	57.4	49.9	12.5	33.2	29.7

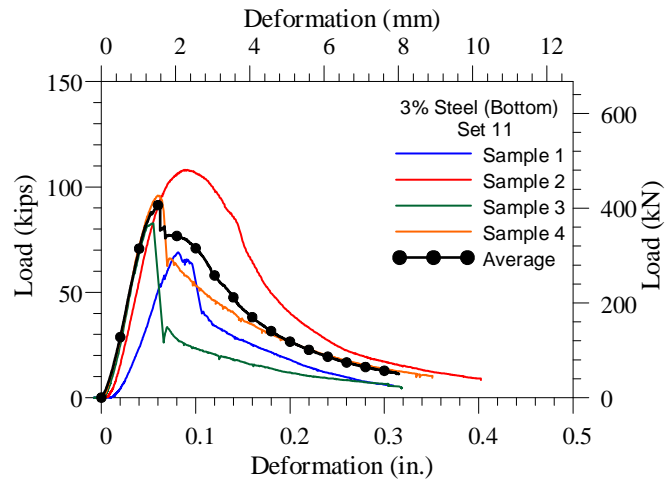


Figure B-3: Load vs. Deformation – Set 11 (With 3% Steel fibers Bottom and Top Cylinders)

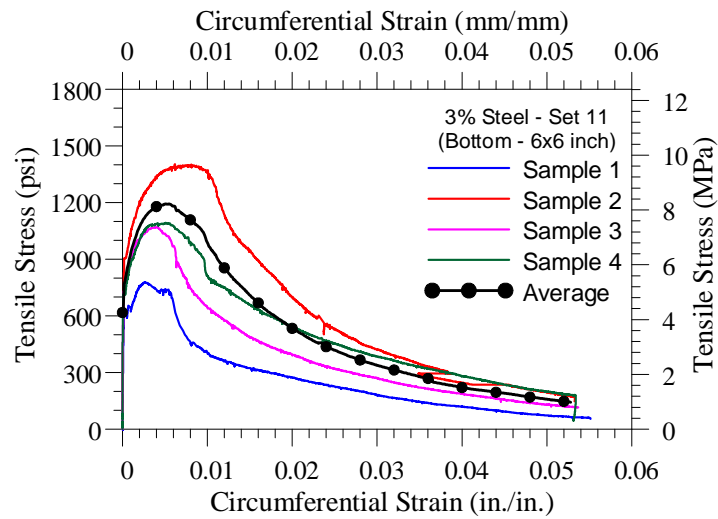


Figure B-4: Tensile Stress vs. Circumferential Strain – Set 11 (With 3% steel fibers Bottom and Top Cylinders)

Table B-3 Calculation of Coefficient of Variation for set 12 (UHP-FRC with 3% steel fiber, 0.04 in./min and 6 x 6 in. size)

Set 12	At Peak Load		At 0.1 in deformation		Corresponding residual tensile stress at			
	Peak Load	Peak Tensile Strength	Corresponding load at 0.1 in. deformation	Equivalent Tensile Strength	0.003 circumferential strain	0.01 circumferential strain	0.025 circumferential strain	0.05 circumferential strain
	kips	psi	kips	psi	psi	psi	psi	psi
B 1	98.12	1113.5	41.76	473.8	1113.5	453.1	215.5	74.6
B 2	92.76	1052.7	44.80	508.4	1036.1	617.5	355.0	203.1
B 3	90.69	1029.2	25.93	294.3	1023.7	571.9	158.9	29.0
T 1	69.88	793.0	24.59	279.1	780.5	396.5	181.0	59.4
T 2	78.28	888.3	41.88	475.2	866.2	570.5	269.4	114.7
T 3	84.00	953.2	34.45	391.0	931.1	541.5	290.1	123.0
Average	85.6	971.6	35.6	403.6	958.5	525.2	245.0	100.6
Standard Deviation	10.4	117.6	8.7	98.7	122.7	83.4	73.7	61.2
COV (%)	12.1	12.1	24.4	24.4	12.8	15.9	30.1	60.8

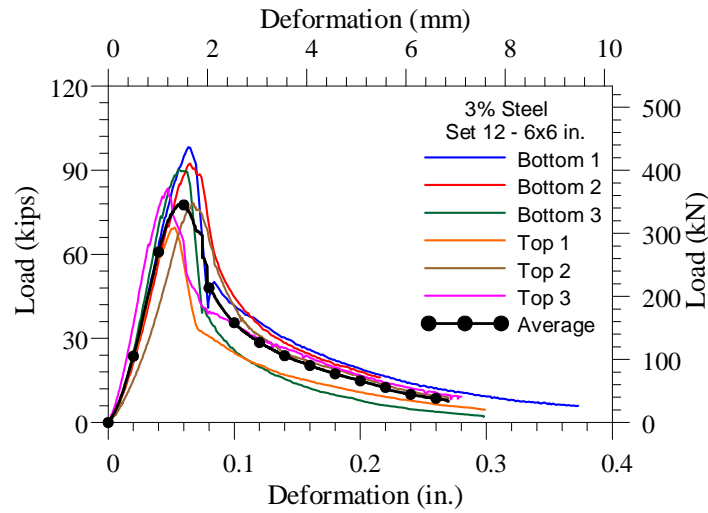


Figure B-5: Load vs. Deformation – Set 12 (With 3% Steel fibers Bottom and Top Cylinders)

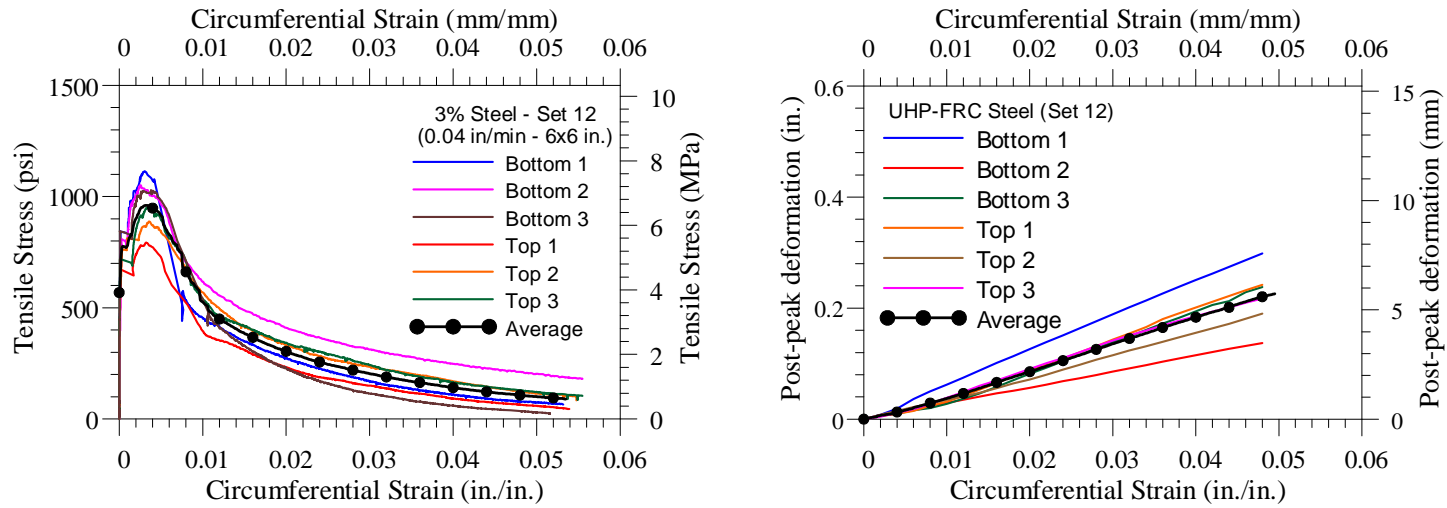


Figure B-6: Tensile Stress vs. Circumferential Strain and Post-peak deformation vs. Circumferential Strain
– Set 12 (With 3% steel fibers Bottom and Top Cylinders)

Table B-4 Calculation of Coefficient of Variation for set 13 ((UHP-FRC with 0.75% PE fiber, 0.04 in./min and 6 x 6 in. size)

Set 13	At Peak Load		At 0.1 in deformation		Corresponding residual tensile strength at			
	Peak Load	Peak Tensile Strength	Corresponding load at 0.1 in. deformation	Equivalent Tensile Strength	0.01 circumferential strain	0.003 circumferential strain	0.025 circumferential strain	0.05 circumferential strain
	kips	psi	kips	psi	psi	psi	psi	psi
B 1	79.01	896.6	18.26	207.2	896.6	668.6	165.8	64.9
B 2	76.57	868.9	17.53	198.9	841.3	632.7	163.0	59.4
B 3	72.80	826.1	18.99	215.5	790.2	385.4	165.8	84.3
B 4	70.36	798.5	13.39	152.0	781.9	248.7	89.8	24.9
T 1	58.80	667.3	24.23	274.9	667.3	373.0	136.8	
T 2	59.89	679.7	28.85	327.4	679.7	379.9	204.5	78.7
T 3	54.42	617.5	4.87	55.3	617.5	406.2	53.9	26.2
T 4	63.79	723.9	16.43	186.5	701.8	299.8	134.0	48.4
T 5	67.69	768.1	19.96	226.6	768.1	328.8	157.5	70.5
T 6	50.28	570.5	29.70	337.1	570.5	388.2	241.8	123.0
Average	65.4	741.7	19.2	218.1	731.5	411.1	151.3	64.5
Standard Deviation	9.5	108.3	7.3	82.9	101.8	135.2	53.1	30.3
COV (%)	14.6	14.6	38.0	38.0	13.9	32.9	35.1	47.1

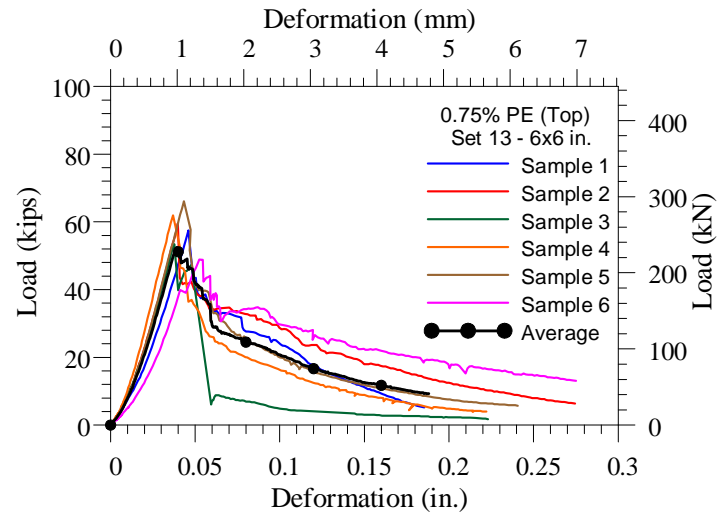
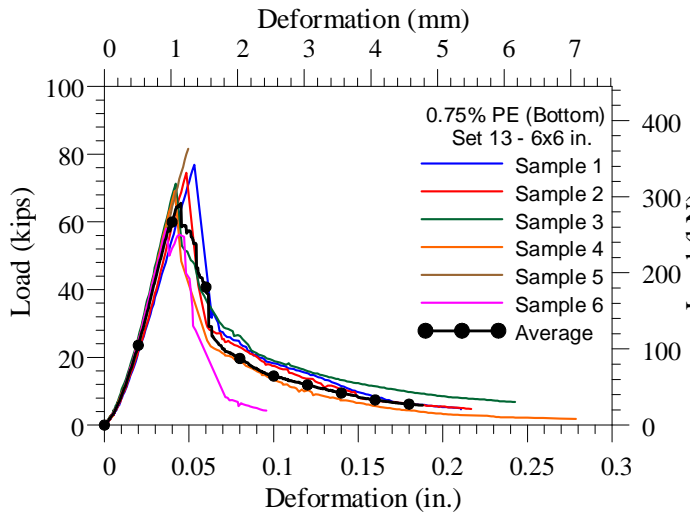


Figure B-7: Load vs. Deformation – Set 13 (With 0.75% PE fibers Bottom and Top Cylinders)

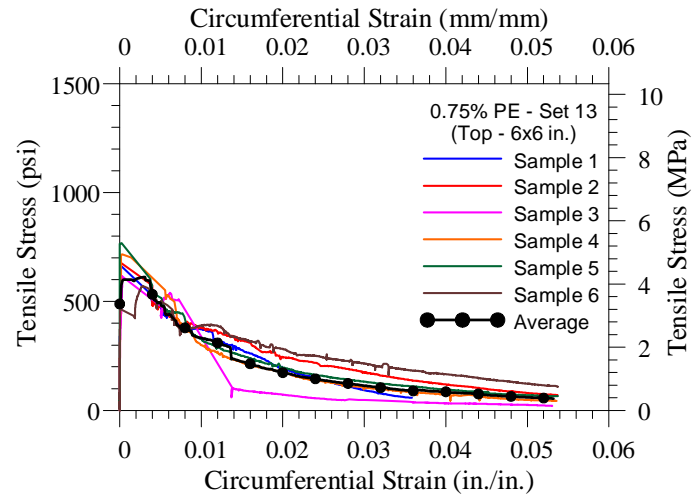
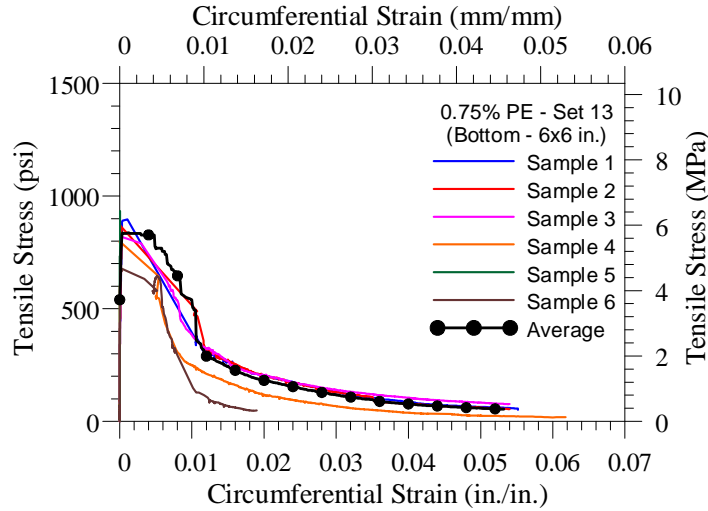


Figure B-8: Tensile Stress vs. Circumferential Strain – Set 13 (With 0.75% PE fibers Bottom and Top Cylinders)

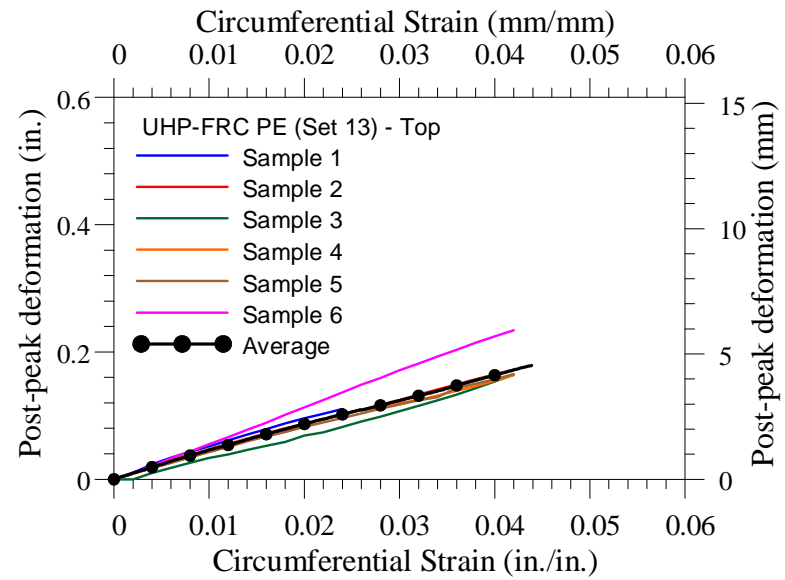
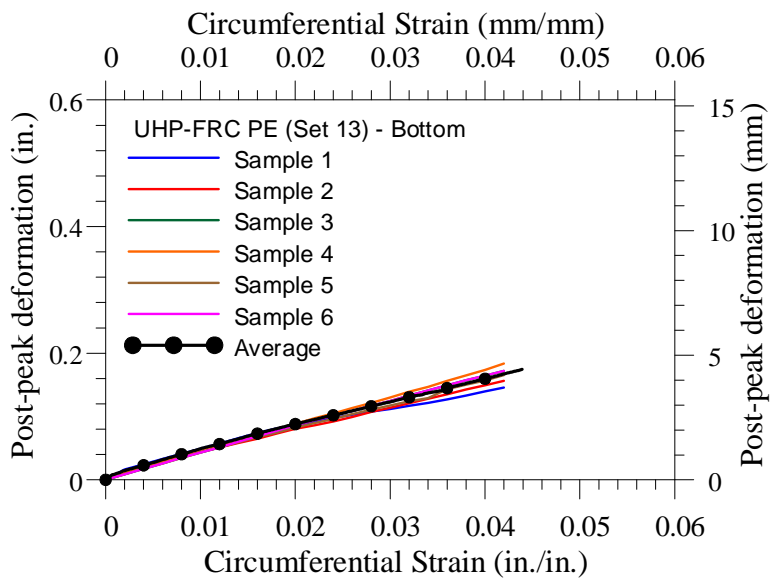


Figure B-9: Post-peak deformation vs. Circumferential Strain – Set 13 (With 0.75% PE fiber and 6x6 in.)

Table B-5 Calculation of Coefficient of Variation for set 14 (UHP-FRC with 3% steel fiber and 6 x 4 in. size)

Set 14	At Peak Load		At 0.1 in deformation		Corresponding residual tensile stress at			
	Peak Load	Peak Tensile Strength	Corresponding load at 0.1 in. deformation	Equivalent Tensile Strength	0.003 circumferential strain	0.01 circumferential strain	0.025 circumferential strain	0.05 circumferential strain
	kips	psi	kips	psi	psi	psi	psi	psi
B 1	71.09	1226.6	18.87	325.5	1153.1	449.5	218.4	35.7
B 2	91.06	1571.0	48.45	835.9	1554.2	928.3	363.3	134.4
B 3	86.07	1484.9	34.57	596.5	1482.8	884.2	426.4	123.9
M 1	62.45	1077.4	14.12	243.6	1064.8	796.0	176.4	39.9
M 2	88.63	1529.0	27.63	476.8	1474.4	1243.4	361.2	123.9
M 3	74.26	1281.2	23.98	413.8	1277.0	754.0	298.2	102.9
T 1	65.13	1123.7	29.58	510.4	1090.0	632.2	409.6	201.6
T 2	77.43	1335.8	46.63	804.4	1304.3	1033.3	571.3	294.0
T 3	80.96	1396.7	23.25	401.2	1344.2	1314.8	264.6	37.8
Average	77.5	1336.2	29.7	512.0	1305.0	892.9	343.3	121.6
Standard Deviation	10.1	175.1	11.7	202.3	177.4	277.3	120.2	85.0
COV (%)	13.1	13.1	39.5	39.5	13.6	31.1	35.0	69.9

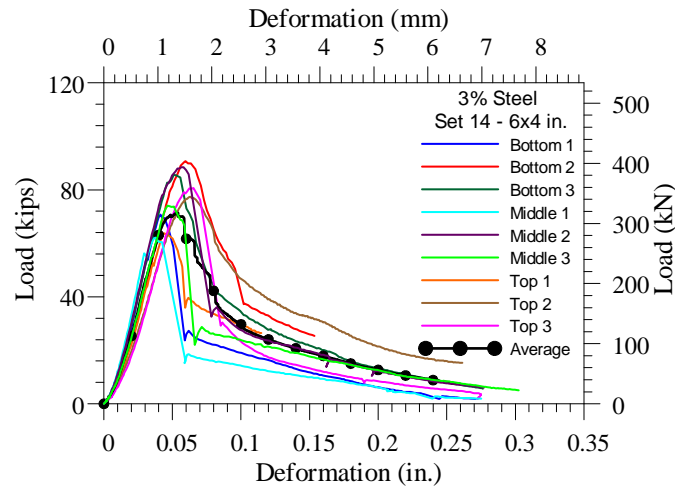


Figure B-10: Load vs. Deformation – Set 14 (With 3% Steel fibers 6x4 in. Bottom, Middle and Top Cylinders)

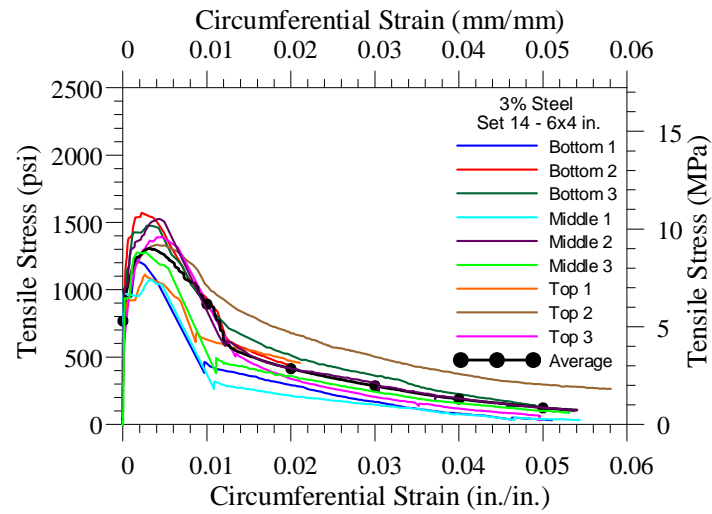


Figure B-11: Tensile Stress vs. Circumferential Strain – Set 14 (With 3% steel fibers 6 x4 in. Bottom, Middle and Top Cylinders)

Table B-6: Calculation of Coefficient of Variation for set 15 (UHP-FRC with 0.75% PE fiber and 6 x 4 in. size)

Set 15	At Peak Load		At 0.1 in deformation		Corresponding residual tensile stress at			
	Peak Load	Peak Tensile Strength	Corresponding load at 0.1 in. deformation	Equivalent Tensile Strength	0.003 circumferential strain	0.01 circumferential strain	0.025 circumferential strain	0.05 circumferential strain
	kips	psi	kips	psi	psi	psi	psi	psi
B 2	48.09	829.6	11.08	191.1	810.7	319.2	134.4	60.9
B 3	50.03	863.2	14.49	249.9	817.0	399.1	193.2	42.0
B 4	51.62	890.5	5.36	92.4	884.2	747.7	96.6	56.7
M 2	55.15	951.4	10.96	189.0	951.4	315.0	142.8	46.2
M 3	53.32	919.9	4.87	84.0	911.5	640.6	84.0	31.5
M 4	55.51	957.7	8.28	142.8	688.9	277.2	123.9	52.5
T 2	50.40	869.5	8.40	144.9	835.9	273.0	138.6	31.5
T 3	46.87	808.6	11.20	193.2	749.8	344.4	151.2	42.0
T 4	31.29	539.8	15.70	270.9	520.9	344.4	193.2	81.9
Average	49.1	847.8	10.0	173.2	796.7	406.8	139.8	49.5
Standard Deviation	7.3	126.1	3.7	63.9	130.8	169.4	37.3	15.9
COV (%)	14.9	14.9	36.9	36.9	16.4	41.6	26.7	32.1

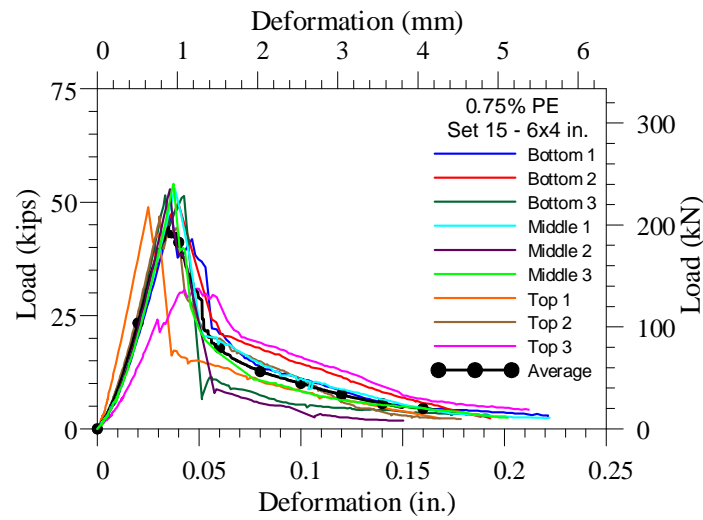


Figure B-12: Load vs. Deformation – Set 15 (With 0.75% PE fibers 6x4 in. Bottom, Middle and Top Cylinders)

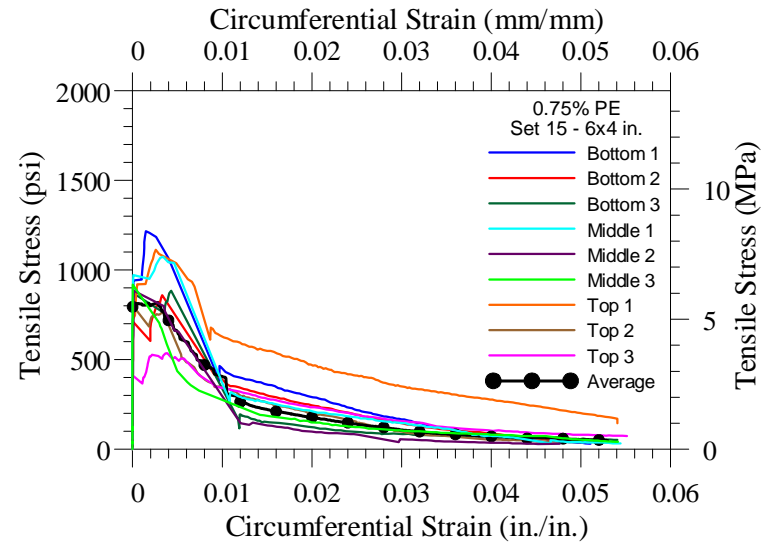


Figure B-13: Tensile Stress vs. Circumferential Strain – Set 15 (With 0.75% PE fibers 6x4 in. Bottom, Middle and Top Cylinders)

Appendix C

ASTM Draft Ballot for Standardization of Double Punch Test



C.X ASTM DRAFT BALLOT FOR STANDARDIZATION OF DOUBLE-PUNCH TEST

**Standard Test Method for
Evaluating the Tensile Performance of Fiber-Reinforced Concrete (Using
Cylindrical Specimens with Double-Punch Loading)¹**

This standard is issued under the fixed designation X XXXX; the number immediately following the designation indicates the year of original adoption or, in the case of revision, the year of last revision. A number in parentheses indicates the year of last reapproval. A superscript epsilon (ε) indicates an editorial change since the last revision or reapproval.

1. Scope

1.1 This test method covers the determination of the ultimate tensile strength and post-crack capacity up to a specified deformation or circumferential tensile strain. In this test a concrete cylinder is placed vertically between the loading platens of a test machine and compressed by two steel punches located concentrically on the top and bottom surfaces of the cylinder. The applied compression results in uniformly distributed, indirect tension along radial planes of the cylindrical specimen. The performance of specimens tested by this method is quantified in terms of the initial stiffness, peak load, and residual strength at a specified deformation or circumferential tensile strain, and crack widths.

1.2 This test method can be applied to plain concrete, fiber-reinforced concrete (FRC), high-performance fiber-reinforced concrete (HP-FRC), or ultra-high performance fiber-reinforced concrete (UHP-FRC) cylindrical specimens, such as molded cylinders and drilled cores.

1.3 The values stated in either SI units or inch-pound units are to be regarded separately as standard. The values stated in each system may not be exact equivalents; therefore, each system

¹ This test method is under the jurisdiction of ASTM Committee and is the direct responsibility of Subcommittee. Current edition approved XXX. XX, XXXX. Published XX XXXX. DOI:10.1520/XXXXX-XX

23 *shall be used independently of the other. Combining values from the two systems may result in*
 24 *non-conformance with the standard.*

25 1.4 *This standard does not purport to address all of the safety concerns, if any, associated*
 26 *with its use. It is the responsibility of the user of this standard to establish appropriate safety and*
 27 *health practices and determine the applicability of regulatory limitations prior to use.*

28 **2. Referenced Documents**

29 2.1 *ASTM Standards:*

- 30 **C31/C31M Practice for Making and Curing Concrete Test Specimens in the Field**
- 31 **C39/C39M Test Method for Compressive Strength of Cylindrical Concrete Specimens**
- 32 **C42/C42M Test Method for Obtaining and Testing Drilled Cores and Sawed Beams of Concrete**
- 33 **C172 Practice for Sampling Freshly Mixed Concrete**
- 34 **C192/C192M Practice for Making and Curing Concrete Test Specimens in the Laboratory**
- 35 **C496/C496M Test Method for Splitting Tensile Strength of Cylindrical Concrete Specimens**
- 36 **C823 Practice for Examination and Sampling of Hardened Concrete in Constructions**
- 37 **C1609/C1609M Test Method for Flexural Performance of Fiber-Reinforced Concrete (Using**
 38 **Beam with Third-Point Loading)**
- 39 **C1399/C1399M Test Method for Obtaining Average Residual-Strength of Fiber-Reinforced**
 40 **Concrete**

41 **3. Terminology**

42 3.1 *Definitions:*

43 3.1.1 circumferential strain after peak ϵ_p , the circumferential strain obtained at specified
 44 deformation after peak.

45 3.1.2 deformation at peak load, δ_0 , the net deformation value on the load-deformation curve
 46 at peak load.

47 3.1.3 peak load, P_p , the maximum load on the load-deformation curve.

48 3.1.4 total vertical deformation, δ , the corrected vertical deformations in reloading phase and
 49 post peak phase.

50 3.1.5 $\delta_{0+0.1}$ – vertical deformation measured by linear variable differential transformers
51 (LVDTs) at a deformation of 0.1 in. (2.5 mm) from the deformation of the peak load.

52 3.1.6 $P_{P+0.1}$ – residual load at $\delta_{0+0.1}$.

53 3.1.7 number of cracks, N , consider the cracks that starts radially from the center and
54 propagated at least up to the mid-height of the specimen.

55 **4. Summary of Test Method**

56 4.1 This test method consists of loading molded cylinders or drilled cores, at a rate that is
57 within a prescribed range, through cylindrical steel punches at each end, until a prescribed
58 deformation is reached. Test results are the initial stiffness of the specimen, its maximum strength,
59 and its residual strength at $\delta_{0+0.1}$, average crack widths and maximum crack widths.

60 **5. Significance and Use**

61 5.1 The test provides the entire load-deformation curve, before and after cracking, for a
62 concrete or fiber-reinforced concrete cylinder specimen loaded axially through cylindrical steel
63 punches at each end. Key parameters (initial stiffness, peak load, and $P_{P+0.1}$) are obtained from the
64 load versus deformation curve, and are useful for evaluating the elastic and plastic behavior of
65 FRC with different fiber types and dosage rates. The test is appropriate for comparing the behavior
66 of different classes of fiber-reinforced concrete.

67 5.2 $P_{P+0.1}$ (the residual load at $\delta_{0+0.1}$) shall be used for comparison between the residual strengths
68 at 0.1 in. for different FRC. This key parameter in load-deformation gives the relative toughness
69 (energy absorption ability) beyond cracking. It should be noted that, however, if a mixture has
70 significant lower ascending slope (which means lower modulus of elasticity), using the 0.1 in.
71 deformation might lead to unconservative results and unfair comparison with a FRC having stiffer
72 ascending branch. In such a case the second point can be taken at the point 0.05 in. beyond the

73 deformation at the peak strength. This criterion could also be applied to FRC mixtures with ultra-
74 high performance when the 0.1 in. deformation is still within its ascending branch of the load
75 versus deformation curve.

76 5.3 This test estimates the average crack width and maximum crack width at the specified post-
77 peak vertical deformation from LVDTs only without using circumferential extensometer. This test
78 allows the qualitative and comparative assessment of the influence of fiber dosage and quality of
79 mixture from the nature of the cracks (number and crack width).

80 5.4 The test results obtained from DPT represent an averaged mechanical behavior as the
81 failure mechanism occurs along multiple planes; the typical crack pattern is concentrated along
82 three or four radial planes for FRC and two to nine for UHP-FRC.

83 5.5 The motivation for using the “Double-Punch Test (DPT)” set up is based on the within-
84 batch, intra-laboratory repeatability and consistency of the failure mode that arises through the use
85 of steel punches.²⁻¹²

86 **6. Apparatus**

87 6.1 *Testing Machine* – The testing machine shall meet the requirements of Sections 5.1 through
88 5.4 of Specification C 39.

89 6.2 *Steel Punches* – The steel punches shall be cylindrical in shape, with a diameter of 1.5 in.
90 (38.1 mm) \pm 0.1 in. (\pm 2.5 mm) and a height of 1.0 in. (25.4 mm) \pm 0.1 in. (\pm 2.5 mm)². The punches
91 shall be machined from tool steel with a yield strength between 75 ksi [517 MPa] and 90 ksi [620
92 MPa].

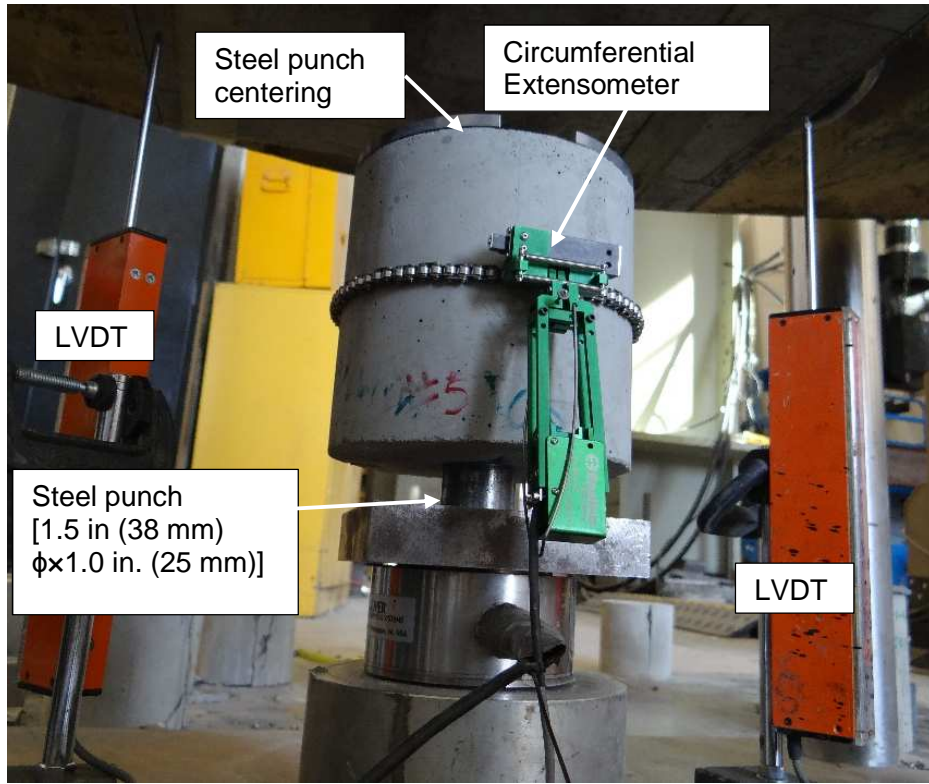
93 6.3 *Instrumentation for Measuring Deformations* – Measure the deformation of the loading
94 head using a dial indicator, or a pair of linear potentiometers, or a pair of linear variable differential
95 transformers with a range of at least 1 in. (25 mm) and a precision of at least 1% of that range. A

96 circumferential extensometer can be placed at the mid-height of the specimen simultaneously to
 97 measure the total crack opening displacement that gives equivalent tensile strains or Equation (3)
 98 can be used to determine equivalent tensile strains at specific post-peak deformation.

- 99
- 100 ² Chen, W. F., “Double Punch Test for Tensile Strength of Concrete”, ACI Journal, December 1970, pp. 993-995.
- 101 ³ Chen, W. F., and Yuan R. L., “Tensile strength of concrete: Double-Punch Test”, Journal of Structural Division,
 102 Proceeding of American Society of Engineers, Vol. 106, No ST8, August, 1980.
- 103 ⁴ Karki, B. K., “Flexural Behavior of Steel Fiber Reinforced Prestressed Concrete Beams and Double-Punch Test for
 104 Fiber Reinforced Concrete”, PhD dissertation, Department of Civil Engineering, University of Texas at Arlington,
 105 2011.
- 106 ⁵ Chao, S.-H., Karki, N. B., Cho, J.-S., and Waweru, R. N. (2011) “Use of double punch test to evaluate the mechanical
 107 performance of fiber reinforced concrete,” High Performance Fiber Reinforced Cement Composites (HPFRCC 6),
 108 International Workshop, Ann Arbor MI., June 20-22, 2011.
- 109 ⁶ Woods, A.P. “Double-Punch Test for Evaluating the Performance of Steel Fiber-Reinforced Concrete.” MS Thesis,
 110 Department of Civil Engineering, University of Texas at Austin, 2012.
- 111 ⁷ Woods, A. P., Klingner, R., Jirsa, J., Chao, S.-H, Karki, N., and Bayrak, O. “Evaluating Concrete With High-
 112 Performance Steel Fibers Using Double-Punch Testing,” International Conference on Construction Materials and
 113 Structures, Johannesburg, South Africa 24-26 November 2014.
- 114 ⁸ Molins, C., Aguado, A. and Marí, A.R. Quality control test for SFRC to be used in precast segments, Tunnelling and
 115 Underground Space Technology, 2006, 21:423-424.
- 116 ⁹ Molins, C., Aguado, A. and Saludes, S. Double Punch Test to control the energy dissipation in tension of FRC
 117 (Barcelona test), Materials and Structures, 2009, 42(4):415-425.
- 118 ¹⁰ Pujadas, P., Blanco, A., Cavalaro, S., de la Fuente, A. and Aguado, A. New analytical model to generalize the
 119 Barcelona test using axial displacement, Journal of Civil Engineering and Management, 2013, 19(2):259-271.
- 120 ¹¹ Blanco, A., Pujadas, P., Cavalaro, S., de la Fuente, A. and Aguado, A. Constitutive model for fibre reinforced
 121 concrete based on the Barcelona test, Cement and Concrete Composites, 2014, 53: 327-340.
- 122 ¹² Aire C., Carmona, S., Aguado A., and Molins C., “Double-Punch Test of Fiber-Reinforced Concrete: Effect of
 123 Specimen Origin and Size,” ACI Materials Journal, V. 112, No. 2, March-April 2015: 199-208.

124
 125
 126

127

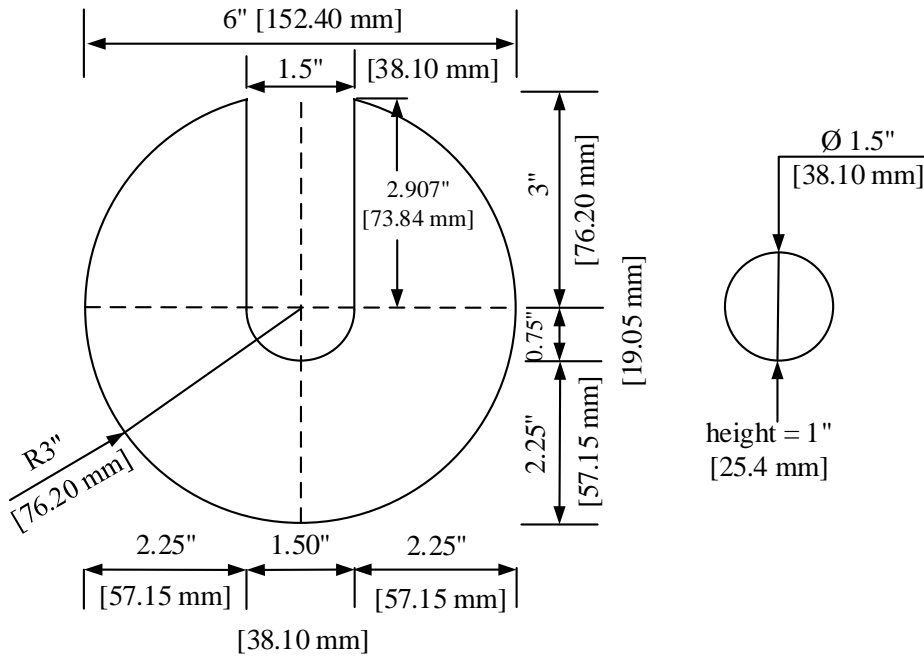


128

129

130

Figure 6-1: Typical Double-Punch Test Arrangement



131

132

Figure 6-2: Dimensions of Centering Disk and Steel Punch

133 **7. Specimens**

134 7.1 Specimens shall be prepared by saw cutting molded concrete cylinders having a nominal
135 diameter of 6 in. (152.4 mm) and a nominal height of 12 in. (305 mm), into two cylinders, each
136 having a nominal diameter of 6 in. (152.4 mm) and a nominal height of 6 in. (152.4 mm). The
137 losses from saw kerf shall not be more than 0.15 in. [4 mm].

138 7.2 The top or bottom 6 × 6 in. (152.4 × 152.4 mm) portion can be used for testing. However,
139 generally, specimens obtained from the bottom portion have a greater fiber density and distribution
140 than those from the top portion, due to segregation during casting. Therefore, the top portion shows
141 higher variations in the response parameters. Thus, top and bottom specimens should not be
142 compared directly. It has been shown that adding viscosity modifying agent to the FRC mixtures
143 is able to minimize that difference between the top and bottom portions. It is recommended that
144 the COV in the peak load in the bottom and the top portion should be less than 20% in order to
145 consider both top and bottom samples for average computation. It is also suggested six 6 × 6 in.
146 (152.4 × 152.4 mm) specimens be used for the evaluation.

147 7.3 Specimen surfaces shall be smoothed so that the steel punches make uniform (flat) contact
148 with the top and bottom faces of the specimen. Smooth contact surfaces can be obtained by
149 grinding the ends of the cylinder using a milling machine such that the ends do not depart from
150 perpendicularity to the axis by more than 0.5° (approximately equivalent to 1 mm in 100 mm [0.05
151 in. in 5 in.]). The ends of the cylinders shall be ground plane to within 0.050 mm [0.002 in.].

152 **8. Procedure**

153 8.1 Using a punch centering disk (or masking tape), place steel punches concentrically at the
154 top and bottom of the specimen. To avoid eccentricity of load, the centroid of each steel punch

155 should align with the centroid of the cylinder surface within ± 0.1 in. [± 2.5 mm]. A plywood
156 dimensional guide may be used to help ensure this.

157 8.2 Place the specimen concentrically in the testing machine.

158 8.3 Loading can be applied by either load control or displacement control. However a
159 displacement-controlled testing generally provide stable response especially at the post-cracking
160 and the descending curve. Displacement-controlled testing is generally preferred.

161 8.4 Load the specimen using the following sequence if load-controlled testing machine is used:

162 8.4.1 *Shakedown (Initial Loading and Unloading to Seat Punches and possible unevenness of the*
163 *surfaces of the specimen)* – Load the specimen at a rate of 100 lb/sec (445 N/sec) \pm 25 lb/sec (\pm
164 111 N/sec) up to a load of approximately 2 kips (8.9 kN). Unload the specimen at a rate between
165 100 and 300 lb/sec (445 and 1334 N/sec) to a load between 100 lb (445 N) and 200 lb (890 N).
166 The deflection at that final load is termed the “initial deformation offset.”

167 8.4.2 *Reloading* – Load the specimen at a rate of 100 lb/sec (445 N/sec) \pm 25 lb/sec (\pm 111
168 N/sec). Load at this rate until the first radial crack appears in the top or bottom face of the
169 specimen. The load can be increased to 300 lb/sec (1335 N/sec) \pm 25 lb/sec (\pm 111 N/sec) in the
170 post-cracking stage.

171 8.5 Load the specimen using the following sequence if displacement-controlled testing
172 machine is used:

173 8.5.1 *Shakedown (Initial Loading and Unloading to Seat Punches and possible unevenness of the*
174 *surfaces of the specimen)* – Load the specimen at a rate of 0.04 in./min (1.02 mm/min) \pm 0.005
175 in./min (\pm 0.13 mm/sec) up to a load of approximately 2 kips (8.9 kN). Unload the specimen at a

176 rate 0.04 in./min (1.02 mm/min) to a load of 0.5 kips (2.2 kN). The deflection at that final load is
177 termed the “initial deformation offset.”

178 8.5.2 *Reloading* – Load the specimen at a rate of 0.04 in./min (1.02 mm/min) \pm 0.005 in./min
179 (\pm 0.13 mm/sec). The testing can be typically completed within 12-15 minutes if an ultimate
180 deformation of 0.3 in. (7.6 mm) is reached.

181 8.6 *Data Recording* – Record the applied load and the deformation of the loading head at 1-
182 second time intervals. The typical maximum load for FRC is about 35-40 kips [156-178 kN] and
183 UHP-FRC about is about 120 kips [534 kN].

184 **9. Evaluation and Reporting of Results**

185 9.1 Subtract the initial deformation offset from each deformation reading during the reloading
186 phase. The resulting deformations are termed “corrected deformations.”

187 9.2 Using the recorded loads and the corrected deformations, calculate and report the initial
188 slope, maximum load, and residual load, as follows:

189 9.2.1 Evaluate the initial slope as the slope between applied loads of approximately 5 kips (22 kN) and
190 15 kips (67 kN).

191 9.2.2 Evaluate the maximum load directly. Evaluate the residual load, $P_{P+0.1}$, at a corrected
192 deformation at $\delta_{0+0.1}$, which is the average number from the two LVDTs.

193

TYPICAL DPT PERFORMANCE CURVE
KEY TEST PARAMETERS

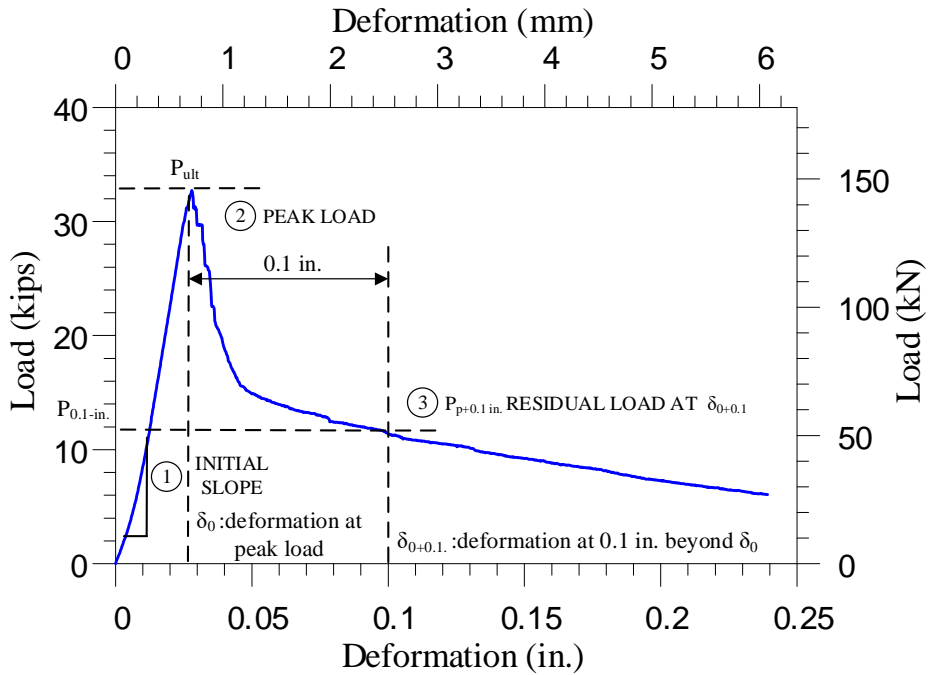


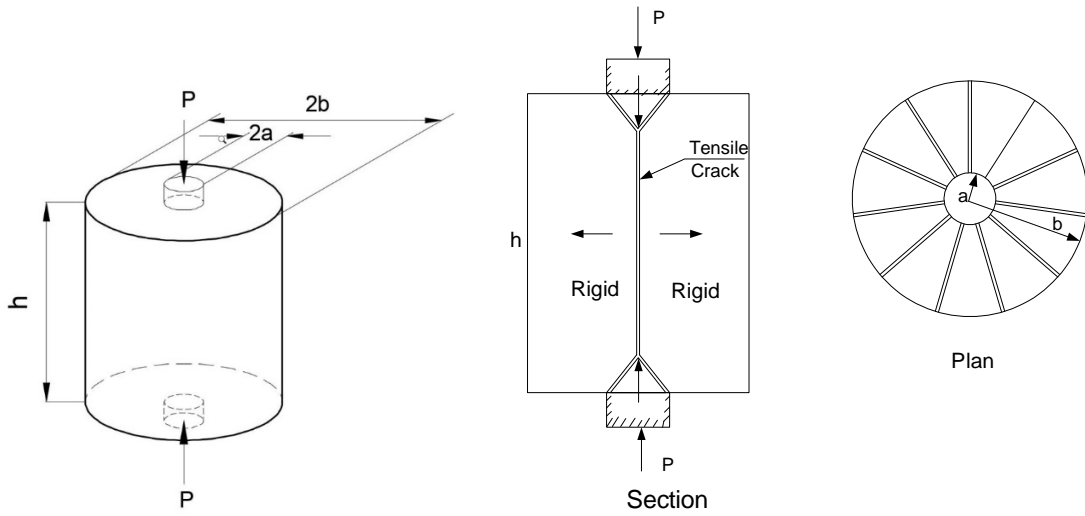
Figure 9-1: Typical Double-Punch Test (DPT) Load versus Deformation Plot (Performance Curve) showing Key Test Parameters

194
195
196
197

198 9.2.3 Evaluate the equivalent tensile stress versus strain response. Theoretically, by applying
199 a compressive load through the punches, uniform tensile stresses are generated over diametric
200 planes, and tensile cracks occur along these diametric planes. The equivalent tensile stress, derived
201 from the assumptions of plastic material and multiple tension cracking failure mechanisms, is
202 calculated as:³

$$f_t = \frac{0.75 \times P}{\pi(1.2bh - a^2)} \quad (1)$$

204 where f_t is equivalent tensile stress, P is applied load, b is radius of cylinder, h is height of cylinder,
205 and a is radius of punches.



206

207

208

Figure 9-2: Definitions of the Parameters used in Equation 1

209

9.2.4 The equivalent circumferential tensile strain (ϵ_P) can be calculated using Equation (3)

210

at specified post-peak deformation (δ_P) obtained using Equation (2).

211

$$\delta_P = \delta - \delta_0 \quad (2)$$

212

where, δ_0 = deformation at peak load, in. [mm]

213

δ = total vertical deformation from beginning of test, in. [mm]

214

δ_P = post peak deformation, in. [mm]

215

ϵ_P = circumferential strain after peak

216

$$\delta_P = \alpha \epsilon_P \quad (3)$$

217

where, $\alpha = 5$ (for FRC)

218

$\alpha = 4$ (for UHP-FRC)

219

220

221

222

223

224

225

226

227

228 9.2.5 Count the number of cracks (N). The cracks that started radially from the center and
 229 propagated at least up to the mid-height of the specimen shall be considered. Calculate average
 230 crack width at specified post using the following formulas:

231
$$CW = \frac{\pi D_0 \times \delta_p}{\alpha N}$$

232 For typical DPT, with $D_0 = 6$ in. [152.4 mm] and substituting α as given in section 9.2.4.

233
$$CW = \frac{3.78\delta_p}{N} \quad (\text{for FRC})$$

234
$$CW = \frac{4.72\delta_p}{N} \quad (\text{for UHP-FRC})$$

235 where, δ_p = post-peak deformation, in.

236 9.2.6 Calculate maximum crack width at specified post-peak deformation using the following
 237 formulas:

238
$$C_{\max} = 1.78\delta_p^{1.5} \quad (\text{median value for FRC})$$

239
$$C_{\max} = 1.78\delta_p^{1.2} \quad (\text{upper bound value for FRC})$$

240
$$C_{\max} = 1.14\delta_p^{1.41} \quad (\text{for UHP-FRC with steel fibers})$$

241
$$C_{\max} = 5.61\delta_p^{2.2} \quad (\text{for UHP-FRC with PE fibers})$$

242 where, δ_p = post-peak deformation, in.

243



244
245
246

Figure 9-3: Multiple Tensile Cracks Occur Along Diametric Planes of Typical FRC Specimens



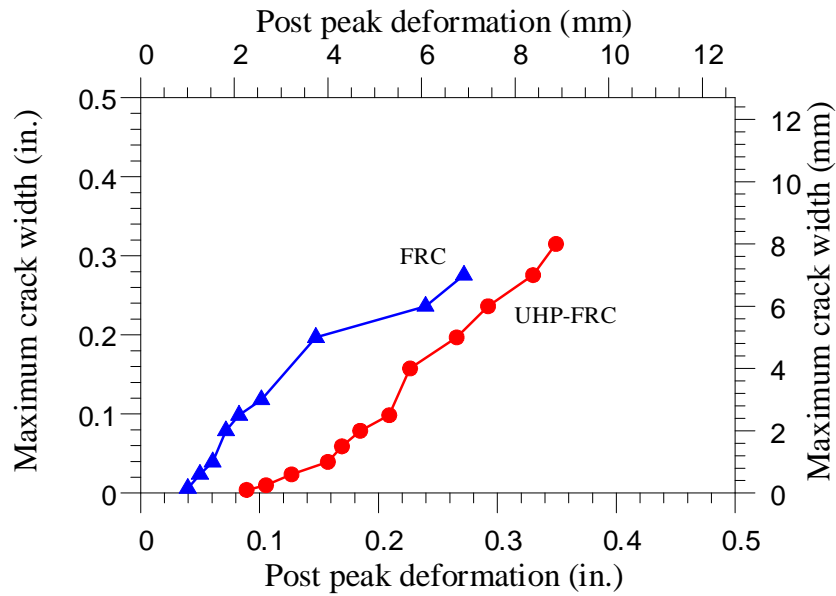
247
248

Figure 9-4: Cracks that do not grow up to mid height does not count.



249
250
251

Figure 9-5: Cracks that grow at least up to mid height or full height counts



252
253
254
255 **Figure 9-6: Deformation versus measured Maximum crack widths of FRC and UHP-FRC**
256 **DPT specimens (Sample)**

257
258 **10. Precision and Bias**

259 10.1 Because the specific testing protocol of this standard is relatively new, limited inter-
260 laboratory study of this test method has been performed to quantify its precision and bias.
261 Available research data, indicates that the within-batch, intra-laboratory coefficients of variation
262 for key test parameters is generally low and comparable to other current test methods for FRC: ±
263 10% Initial Slope; ± 5% Peak Load; and ± 20% Residual Strength at $\delta_{0+0.1}$ deformation. A
264 precision and bias statement will be prepared as more data becomes available.

265 **11. Keywords**

266 double-punch test; cylindrical concrete specimens; fiber-reinforced concrete; peak tensile
267 strength; residual strength; toughness

References

- ACI Committee 544R-88, American Concrete Institute, Farmington Hill, MI, 1998.
- AFGC (2013), "Béton fibrés à ultra-hautes performances, (Ultra high performance fiber-reinforced concretes)", recommendations, France.
- Aghdasi, P.; Palacios, G.; Heid, A.E.; and Chao, S.-H. (2015), 'Mechanical properties of a highly flowable ultra-high-performance fiber-reinforced concrete mixture considering large-size effects,' High Performance Fiber Reinforced Cement Composites (HPFRCC 7), International Workshop, Stuttgart, Germany.
- Aghdasi, P., "Development of Ultra-High-Performance Fiber-Reinforced Concrete (UHP-FRC) for Large-Scale Casting," University of Texas at Arlington, Arlington, Texas, Master's thesis, 2013, 84 pp.
- Aire, C., Carmona, S., Aguado, A., and Molins, C. (2015). "Double-punch test of fiber-reinforced concrete: Effect of specimen origin and size." *ACI Materials Journal*, 112(2), pp. 327 – 340.
- ASTM C39 / C39M-17b "Standard Test Method for Compressive Strength of Cylindrical Concrete Specimens," ASTM International, West Conshohocken, PA, 2017.
- ASTM C496/C496M-17 "Standard Test Method for Splitting Tensile Strength of Cylindrical Concrete Specimens," ASTM International, West Conshohocken, PA 2017.
- ASTM C1550-12a, "Standard Test method for Flexural Toughness of Fiber Reinforced Concrete (Using Centrally Loaded Round Panel)," ASTM International, West Conshohocken, PA, 2012.
- ASTM C1609/C1609M-12, "Standard Test method for Flexural Performance of Fiber-Reinforced Concrete (Using Beam with Third-Point Loading)," ASTM International, West Conshohocken, PA, 2012.

- Bentur, A, and Mindness, S. "Fiber Reinforced Cementitious Composites," 2nd edition published 2007 by Taylor and Francis 2 Park Square, Milton Park, Abingdon, Oxon, OX 14 4RN
- Blanco, A., Cavalaro, S., Galcote, F., and A.Aguado (2015). "Assessment of constitutive model for ultra-high performance fiber reinforced cement composites using the barcelona test." A: International RILEM Workshop on High Performance Fiber Reinforced Cement Composites. 7th RILEM workshop on High Performance Fiber Reinforced Cement Composites: HPRCC-7: Stuttgart, Germany, June 1-3, 2015, pp. 129 – 136.
- Blanco, A., Pujadas, P., Cavalaro, S., de la Fuente, A., and Aguado, A. (2014). "Constitutive model for fibre reinforced concrete based on the barcelona test." *Cement and Concrete Composites*, 53(Supplement C), pp. 327 – 340.
- Bortolotti, L., "Double Punch Test for Tensile and Compressive Strength in Concrete," *IACI Materials Journal*, Vol, 85-M4, Jan.- Feb., 1988 pp. 26-32
- Carmona Malatesta, S., Aguado de Cea, A., and Molins Borrell, C. (2012). "Generalization of the barcelona test for the toughness control of FRC." *Materials and Structures*, 45(7), pp. 1053–1069.
- Chao, S.H., Cho, J.-S., Karki, N. B., Sahoo, D. R., and Yazdani, N. (2011). "FRC performance comparison: Uniaxial direct tensile test, third-point bending test, and round panel test." *Special Publication*, 276, pp. 327 – 340.
- Chao, S.H., Karki, N. B., Cho, J. S., and Waweru, R. N. (2012). *Use of Double Punch Test to Evaluate the Mechanical Performance of Fiber Reinforced Concrete*. Springer Netherlands, Dordrecht, pp. 27–34.

- Chen, W. F., "Double Punch Test for Tensile Strength of Concrete," *ACI Materials Journal*, 1970, pp. 993–995
- Chen, W. F., "Limit Analysis and Soil Plasticity," Elsevier Scientific Publishing Company, Amsterdam, Oxford, New York, 1975, Chapter 11, pp. 501-541.
- Chen, W. F., M. ASCE and Yuan R. L., "Tensile strength of concrete: Double-Punch Test," *Journal of Structural Division*, *Proceeding of American Society of Engineers*, Vol. 106, No ST8, August, 1980 pp.1673-169.
- Federal Highway Administration (FHWA), "Ultra-High Performance Concrete: A State-of-the-Art Report for the Bridge Community," Publication Number: FHWA-HRT-13-060, June 2013.
- Fehling, E.; Bunje, K.; and Leutbecher, T. (2004), "Design relevant properties of hardened Ultra High Performance Concrete," *Proceedings of the International Symposium on Ultra High Performance Concrete*, University of Kassel, pp. 327-338, Kassel, Germany.
- Galeote, E., Blanco, A., Cavalaro, S. H., and de la Fuente, A. (2017). "Correlation between the barcelona test and the bending test in fibre reinforced concrete." *Construction and Building Materials*, 152(Supplement C), pp. 529 – 538.
- Graybeal, B. A., and Davis, M. (2008), "Cylinder or Cube: Strength Testing of 80 to 200 MPa (11.6 to 29 ksi) Ultra-High Performance Fiber-Reinforced Concrete," *ACI Materials Journal*, V. 105, No. 6, pp. 603-609.
- Graybeal, B. A. (2014). "Tensile mechanical response of ultra-high-performance concrete." *Advances in Civil Engineering Materials*, Vol. 4 No.2, pp. 62 – 74.

- Kim, J., Lee, G.-P., and Moon, D. Y. (2015). "Evaluation of mechanical properties of steel-fibre-reinforced concrete exposed to high temperatures by double-punch test." *Construction and Building Materials*, 79(Supplement C), pp. 182 – 191.
- Marti, P., "Size Effect in Double-Punch Test on Concrete Cylinders," *ACI Materials Journal*, Vol. 86 No. 6, Nov.-Dec. 1989, pp. 597-601.
- Mindess, S., Young, J. F., and Darwin, D., *Concrete*, 2nd Edition, Prentice Hall, Upper Saddle River, NJ, 2003, 644 pp
- Pros, A., Diez P. and Molins, C., "Model Validations of Numerical Simulation of Double Punch Test," ECCM 2010, IV European Conference on Computational Mechanics, Paris, France May 16-21, 2010.
- Molins, C., Aguado, A., and Saludes, S. (2009). "Double punch test to control the energy dissipation in tension of FRC (Barcelona Test)." *Materials and Structures*, Vol. 42(4), pp. 415–425.
- Pujadas, P., Blanco, A., Cavalaro, S., de la Fuente, A., and Aguado, A. (2013). "New analytical model to generalize the barcelona test using axial displacement." *Journal of Civil Engineering and Management*, Vol. 19(2), pp. 259–271.
- Pujadas, P., Blanco, A., Cavalaro, S., de la Fuente, A., and Aguado, A. (2014). "Multidirectional double punch test to assess the post-cracking behaviour and fibre orientation of frc." *Construction and Building Materials*, Vol. 58(Supplement C), pp. 214 – 224.
- Ranade, R.; Li, V.C.; Stults, M.D.; Heard, W.F.; and Rushing, T.S. (2013), "Composite Properties of High-Strength, High-Ductility Concrete," *ACI Materials Journal*, V. 110, No. 4, pp. 413-422.
- Richard, P.; and Cheyrezy, M. (1995), "Composition of Reactive Powder Concretes," *Cement and Concrete Research*, V. 25, No. 7, Oct., pp. 1501-1511.

- Tue, N. V.; Simsch, G.; Schneider, H.; Schmidt, D. (2004), "Bearing Capacity of Stub Columns made of NSC, HSC and UHPC confined by a Steel Tube," Proceedings of the International Symposium on Ultra High Performance Concrete, University of Kassel, pp. 339-350, Kassel, Germany, September.
- Wille, K.; Naaman, A.E., and El-Tawil, S. (2011), "Optimizing Ultra-High-Performance Fiber-Reinforced Concrete: Mixtures with Twisted Fibers Exhibit Record Performance under Tensile Loading," Concrete International, V. 33, No. 9, pp.35-41.
- Wille, K.; Naaman, A.E.; El-Tawil, S.; and Parra-Montesinos, G.J., (2012), "Ultra-High Performance Concrete and Fiber Reinforced Concrete: Achieving Strength and Ductility without Heat Treatment," Materials and Structures, V. 45, No. 3, pp. 309-324.
- Woods, A. P., Klingner, R., Jirsa, J., Chao, S.-H., Karki, N., and Bayrak, O. Evaluating concrete with high-performance steel fibers using double-punch testing.

Biographical Information

Shuveksha Tuladhar graduated from Tribhuvan University, Kathmandu, Nepal in 2012 with Bachelor's degree in Civil Engineering. After completing her undergraduate study, she worked as Civil Structural Engineer at R&R Engineering Consultancy Pvt. Ltd. and CEAD (Consulting, Engineers, Architect, and Designers) in Nepal. She was responsible for performing structural analysis and design of seismic resistant high-rise buildings, the design of bridges and seismic retrofitting of various buildings in the Kathmandu valley. She started her Masters of Science program in Civil Engineering (Concentration: Structural Engineering) at The University of Texas at Arlington (UTA) in August 2015. During her graduate program, she worked as a Graduate Research Assistant under the supervision of Dr. Shih-Ho Chao. She was awarded ACI Katherine and Bryant Mather Scholarship (2016-2017) by American Concrete Institute (ACI) Foundation; Civil Engineering Outstanding Graduate Student Award (2016-2017); and Civil Engineering Graduate Scholarship (2015-2016) from UTA. Her research interest includes fiber reinforced concrete (FRC), ultra-high performance fiber reinforced concrete (UHP-FRC), earthquake engineering and seismic behavior of structural systems.